ISSN 0915-633X

NATIONAL INSTITUTE FOR FUSION SCIENCE

Dynamos and MHD Theory of Turbulence Suppression

A. Yoshizawa, S.-I. Itoh, K. Itoh and N. Yokoi

(Received - Nov. 14, 2003)

NIFS-788 Dec. 2003

RESEARCH REPORT
NIFS Series

TOKI, JAPAN

Dynamos and MHD theory of turbulence suppression

Akira Yoshizawa[1,2], Sanae-I Itoh[3], Kimitaka Itoh[2] and Nobumitsu Yokoi[1]

[1] Institute of Industrial Science, University of Tokyo, Komaba, Meguro-ku, Tokyo 153-8505, Japan

[2] National Institute for Fusion Science, Toki, Gifu 509-5292, Japan

[3] Research Institute for Applied Mechanics, Kyushu University, 87, Kasuga 810-8580, Japan

Abstract

Characteristics of electrically-conducting media are reviewed from the macroscopic viewpoint based on the mean-field magnetohydrodynamics, while being compared with the methodology and knowledge in fluid mechanics. The themes covered in this review range from the generation mechanism of stellar magnetic fields (dynamo) to transport properties in fusion. The primary concern here is to see the characteristics common to these apparently different phenomena, within the framework of the mean-field theory. Owing to the intrinsic limitation of the approach, the present discussions are limited more or less to specific aspects of phenomena. They are supplemented with the reference to theoretical, numerical, and observational approaches intrinsic to each theme. In the description of dynamo phenomena, an emphasis is put on the cross-helicity dynamo. Features common to the stellar magnetic-field generation and the rotational-motion drive in toroidal plasmas are illustrated on this basis.

Keywords:
Dynamo, stellar magnetic field, stellar jet, accretion disk, turbulence suppression, mean-field MHD, turbulence, renormalization, structure formation, helicity, cross-helicity

Contents

1. Introduction

A variety of characteristics are observed in laminar, turbulent, and transient states of electrically-nonconducting fluid flows. Those characteristics may be explained systematically on the basis of the hydrodynamic equations, except some special cases such as the inside and close vicinity of a shock wave. The advance of computer capability is highly advantageous to numerical methods. For geometrically simple flows, they may often provide the information that is difficult to be detected by observations. Such typical instances are the turbulence properties near a solid wall, the pressure-related correlation functions, etc.

An entirely different situation is encountered in electrically-conducting media. One of the primary ingredients causing the difference is a magnetic field. A charged particle is trapped around a magnetic field line, while moving freely along it. This property persists partially in the aggregation of charged particles. The gas of charged particles is subject to a larger resistive force for the motion normal to magnetic field lines, compared with the parallel direction. The degree of persistence of the microscopic effects differs at observed spatial scales. Then the motion of electrically-conducting media shows highly different appearances in accordance to spatial scales. It is quite difficult to cope with all the states of motion, with the use of a single system of equations, resulting in the necessity of the hierarchy of systems of equations. The number of necessary systems is dependent on the phenomenon to be explored.

In the study of electrically-conducting media, attention is usually focused on a specific phenomenon, and its characteristics have been explored for a wide range of scales, with the use of the hierarchy of systems of equations. Such a typical instance is hot plasmas in nuclear fusion. Many efforts have been made towards understanding of the turbulent-transport and structure-formation processes. These achievements have come to some level of maturity, and quite a few characteristic features of nonlinear dynamics far from the thermal equilibrium have been captured there. On the other hand, so much attention has not always been paid to understanding of the properties common to entirely different phenomena, with resort to a single system of equations. This is due to the situation that an emphasis has been put on the elucidation of each phenomenon. A related but other area whose physics has shown a prosperous evolution is the stellar dynamo and has a striking analogy to the study of confined plasmas. The integration of laboratory-plasma and stellar-dynamo theories might be a source of future progress in the research of plasmas.

In this topical review, we describe the physics of stellar dynamo by using the mean-field magnetohydrodynamic (MHD) theory. We focus attention on delving into the properties common to phenomena that seem entirely different in their appearance. By this

approach, we attempt to understand, in a systematic manner, some macroscopic properties of stellar magnetic fields, astronomical jets, tokamak's plasmas, etc. The characteristics captured here are limited aspects of each phenomenon, but to discuss the common properties in a variety of phenomena is interesting from the viewpoint of exploring the essence of the macroscopic motion in electrically-conducting media.

We put an emphasis on the mutual interaction between the flow and magnetic-field generation. There are couple of motivations for this approach. First, the flow generation process in toroidal plasmas has a deep similarity to the stellar dynamo. Second, the response of plasma properties arising from the interaction between flow and magnetic field is common to plasma physics. Third, the structure formation in stellar magnetic fields is understandable through the simultaneous investigation into the flow and magnetic field.

From these motivations, the importance of the cross-helicity mechanism of dynamo is stressed. This review provides an account complementary to those already published on fusion and stellar dynamo with much emphasis on the helicity mechanism, and attention is focused on the structure formation of flow and magnetic field. Their temporal evolution is beyond the scope, and the quantitative discussion about turbulent transport coefficients is not covered.

The present review is organized as follows. In § 2, phenomena explored in light of the stellar dynamo are surveyed. The similarity to fusion plasmas is mentioned from a viewpoint of seeking common aspects. In § 3, the basic equations are explained. In § 4, the mean-filed MHD equations are given. The details of the deduction of the correlation functions is summarized in Appendix A. The basic concepts of the α, β and γ effects are explained. Throughout this review, β denotes the turbulence resistivity, but not the plasma pressure normalized by the magnetic pressure (the difference of convention is explained when necessary). The spherical-shell dynamo is explained in § 5. The difference between the geodynamo and solar dynamo is discussed in detail. In § 6, the generation of electromagnetic flow is discussed with accretion disks as an example. There the relationship with the flow-generation problem in tokamaks is also mentioned. In § 7, feedback effects of the generated field on transport coefficients are illuminated, and turbulence suppression processes in electrically-conducting media are explored. The summary is given in § 8.

2. Explored Phenomena and Mean-Field Approach

2.1. Planetary magnetic fields

A variety of interesting phenomena are observed in electrically-conducting media. One long-quested theme of them is magnetic dynamo or the generation mechanism of planetary magnetic fields such as geomagnetic, solar, galactic fields, etc. Their reviews and surveys are given in [2/1-2/9].

Geomagnetic and solar fields are similar in the geometrical context that both emerge from the motion of electrically-conducting media in a spherical-shell region. Their properties, however, are very different each other, as will be explained below. To clarify the difference is expected to contribute to understanding of the essence of the spherical-shell dynamo. Here attention will be focused on the global properties of those fields.

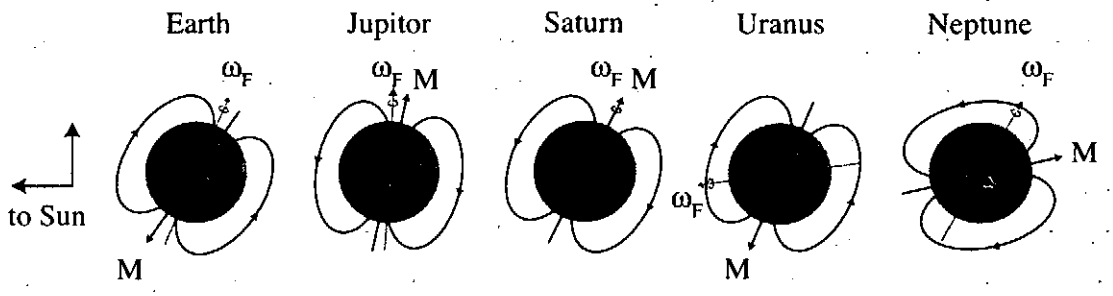

Fig. 2.1. Dipole magnetic fields of planets.

2.1.1. Dipole fields of planets

It is known well that many planets are accompanied by magnetic fields. The magnetic field of a large planet is characterized by distinct spatial structures represented by the dipole field. Figure 2.1 illustrates the relationship between the rotation axis and magnetic dipole moment in the earth, Jupiter, Saturn, Uranus and Neptune, respectively [2/10, 2/11]. Mercury has also a noticeable dipole magnetic field, but the magnetic fields of Venus and Mars are weak. The center of magnetic moment is often close to the center of mass of a planet. In some cases, however, there is a large deviation between these two centers [2/12].

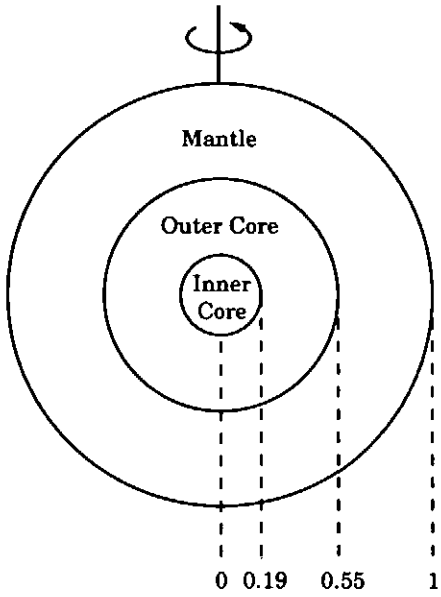

Fig. 2.2. Interior of the earth.

The spatial structure of the geomagnetic field is prototypical for those of other planets. The interior of the earth is roughly divided into three regions, the inner core (solid iron), the outer core (melted iron), and the mantle (silicon), as is depicted in Fig. 2.2 (the radius is about 6300 km). The geomagnetic field arises from the motion of melted iron in the outer core [2/13, 2/14]. For the motion, two driving forces are considered. One is the thermal buoyancy force due to the temperature difference between the inner core and the mantle. The other is the compositional buoyancy force due to the mass difference between the melted iron and the silicon in it.

The toroidal component (the component in the azimuthal direction around the rotation axis) of the geomagnetic field is not observable at the surface, owing to the electrically-nonconducting mantle. The primary part of the poloidal field observable is the dipole component, whose present axis is nearly antiparallel to the direction of the earth's rotation axis. Its strength is a few gauss (G) at the surface. The toroidal field is inferred to be $O(10)$ times the dipole field from other observational data.

The polarity of the dipole field changes in a nonperiodic manner. The change of the magnetic polarity is much faster, compared with the staying time in the quasi-stationary state. The period of the same polarity persists for $O(10^4)-O(10^6)$ years [2/14]. In the study of geodynamo, the earth's polarity change has attracted much attention for this strange behavior.

2.1.2. Solar magnetic field

The sun consists of hydrogen (90 %) and helium (10 %), and its interior is divided into the core, the radiative zone, and the convective zone, as in Fig. 2.3 (the solar radius is about 700000 km). The solar magnetic field is generated in the convective zone, and the energy source is the thermonuclear fusion in the core [2/15-2/17]. The convective zone is the outermost region. As a result, the solar magnetic properties ranging from global to fine scales are observable, and the observational information on the field is much richer, compared with the geomagnetic field.

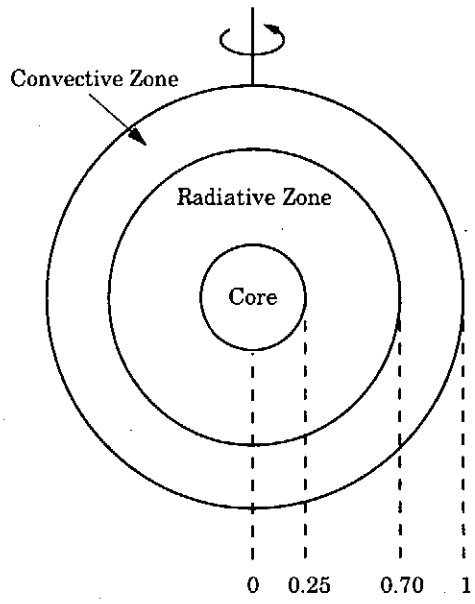

Fig. 2.3. Interior of the sun.

The primary global component of the solar magnetic field is the toroidal field. Its evidence is sunspots, which are illustrated in Fig. 2.4. Their origin is the magnetic-flux tube that is generated in the convective zone. The tube rises up owing to the magnetic buoyancy force and breaks through the photosphere adjacent to the outer surface of the convective zone. Sunspots represent the cross sections of the tube and are observed in pairs of different magnetic polarity, as in Fig. 2.4. The intensity of a large-sunspot field is a few kG, and the toroidal field with the intensity stronger by one order is inferred to be generated at the bottom of the convective zone. The poloidal component is much weaker, compared with the toroidal component. Specifically, it is a few G in the pole region. The striking difference between the toroidal- and poloidal-component relationship of geomagnetic and solar fields is considered to be linked with the essence of the spherical-shell dynamo.

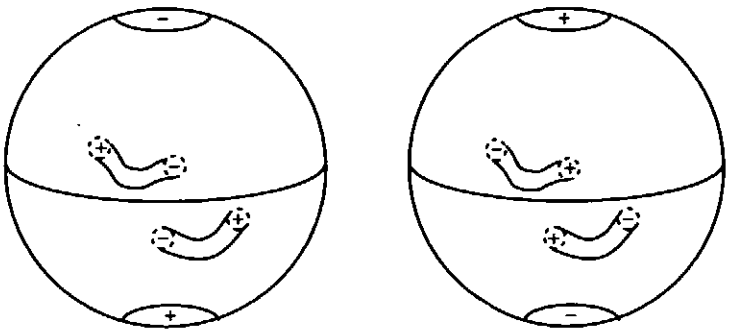

Fig. 2.4. Sunspot and their polarity rule.

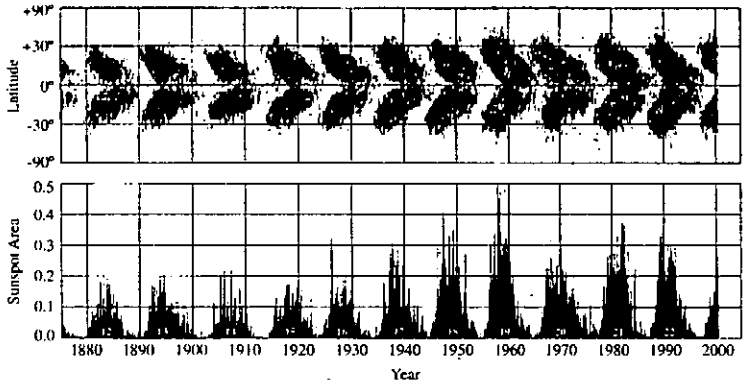

Fig. 2.5. Changes of latitude (upper) and number (lower) of sunspots [2/18].

The spatial shape of the observed solar magnetic field seems complicated and random, but the temporal evolution of global properties makes an ordered variation (see Fig. 2.5). The sunspots occur in the low- to middle-latitude region, and their number is a representative indicator of the solar-activity strength. The solar magnetic polarity varies so regularly, namely, in about 11 years, for instance, from the left to right in Fig. 2.4 [2/15] (as a whole, the solar magnetic field has the period of about 22 years). The polarity and resulting sunspot-number changes indicate the variation of solar magnetic activity, exerting a big influence on the earth. Concerning the polarity change, the sun makes a sharp contrast with the earth.

2.1.3. Comparison of geomagnetic field and solar magnetic field

The difference among stellar magnetic fields should have an origin in those of the structures and dynamics of planets. As a representative case, the earth and the sun are compared in Table 2.1.

Table 2.1. Characteristics of the earth and the sun. In the outer core, 1 G corresponds to 10^{-3} m s^{-1} [see Eq. (5.19)].

	Earth	**Sun**
Radius	$r_E = 6\times10^6$ m	$r_S = 7\times10^8$ m
Rotation period	1 day	26 days
Rotation velocity at the equator	4×10^2 m s^{-1}	2×10^3 m s^{-1}
Typical differential velocity	$O(10^{-4})$ m s^{-1}	$O(10^2)$ m s^{-1}
Typical length scale of differential motion	$O(10^{-1})\, r_E$	$O(10^{-1})\, r_S$
Typical turnover time of differential motion (t_{turnover})	$O(10^2)$ years	$O(1)$ days
Typical period of polarity variation (t_{polarity})	$O(10^4) - O(10^6)$ years	22 years
$t_{\text{polarity}} / t_{\text{turnover}}$	$O(10^2) - O(10^4)$	$O(10^3)$
Poloidal magnetic field	$O(1)$ G	$O(1)$ G
Toroidal magnetic field	$O(10) - O(10^2)$ G	$O(1) - O(10)$ kG

The prominent geometrical difference is the relative magnitude of the fluid region generating a magnetic field to the inner region without a fluid flow. In the earth, the ratio of the outer-core width to the inner-core radius is about 2, whereas the solar counterpart is about 0.4. The outer core of the earth is a thick shell, while the convective zone of the sun is a thin shell.

Observations show that the temporal changes of the geomagnetic and solar magnetic field are entirely different. One of the characteristic time scales in stellar objects is the inverse of the angular velocity of rotation. The time scale of the rotation of the earth and the sun, however, is not helpful to understanding of the polarity change, as is mentioned below. A strong similarity between them may be seen in the eddy turnover time of an electrically-conducting fluid.

The earth rotates once in about one day, whereas the sun does in about 26 days. The rotation time scale is shorter in the earth. The relative magnitude of the foregoing same-polarity period is in a situation opposite to the angular velocity. In this context, the geomagnetic profile may be regarded as much more stable than the solar counterpart.

The fluid velocity in the outer core of the earth is inferred to be $O(10^{-4})$ m s^{-1} [2/13, 2/14]. The solar counterpart in the convective zone is estimated from the velocity related to the differential angular velocity. At the solar equatorial plane, the angular velocity at the bottom of the convective zone is smaller by about 10 percent than the upper-surface counterpart [2/18, 2/19]. This difference corresponds to 200 m s^{-1}. With each shell width as a reference length, the time scale related to the fluid motion in the earth is $O(10^4)$ times its solar counterpart. Such a situation is consistent with the difference between the polarity-reversal time scales of the earth and the sun.

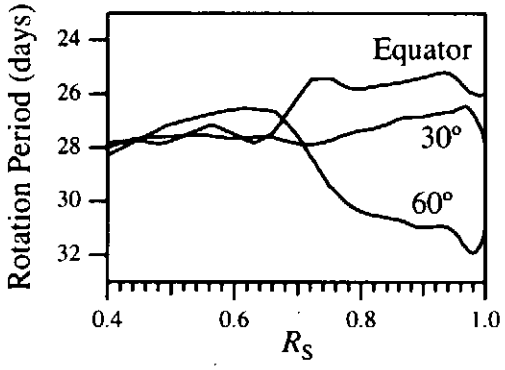

Fig. 2.6. Solar rotation rate [2/18].

2.2. Spontaneous magnetic-field generation in toroidal plasmas

In reversed-field pinches of plasmas (RFPs) [2/20, 2/21], the poloidal magnetic field B_P is nearly comparable to the toroidal field B_T. The RFP state is characterized by

$$q << 1 , \tag{2.1}$$

where the safety factor q is defined by

$$q = \frac{a}{R} \frac{B_T}{B_P} , \tag{2.2}$$

where R and a are the major and minor radii, respectively (see Fig. 2.7). The direction of the toroidal magnetic field is opposite at the center and edge. The reversal of the

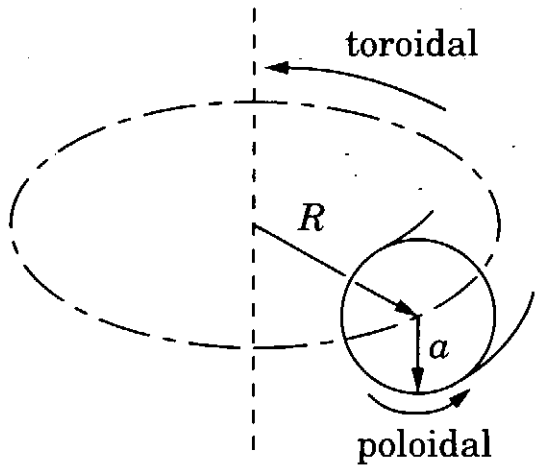

Fig. 2.7. Toroidal and poloidal directions in a torus.

toroidal magnetic field is realized as a result of the evolution of large-scale MHD turbulence owing to a large current density.

In tokamaks, their magnetic properties are characterized by the safety factor [2/22, 2/23]

$$q > 1 \ . \tag{2.3}$$

The spontaneous generation of the poloidal magnetic field occurs owing to the diffusion driven current called the bootstrap current [2/24, 2/25]. In this case, turbulence plays no important role, and the microscopic length governing the diffusion process is related to the banana width.

2.3. Electromagnetic flow generation and accretion disks

In addition to the generation of magnetic fields by turbulence, the flow can also be generated by them. In general, magnetic fields and flow must be investigated simultaneously. Under these circumstances, the so-called kinematic approach [2/26, 2/27] to the study of the generation of magnetic fields under a prescribed velocity field ceases to be valid. An entirely different viewpoint for the magnetic-field generation mechanism is necessary. Such a new viewpoint has emerged in relation to the study of accretion disks. The importance of the flow generation has also been recognized strongly in toroidal plasmas.

2.3.1. Accretion disk

Astronomical high-mass objects such as active galactic nuclei, protostar, cataclysmic

variables, neutron stars, etc. are surrounded by gases in the form of a disk [2/28-2/30] (see Fig. 2.8). In such circumstances, the magnetic field may be observed, as in Fig. 2.9 [2/31, 2/32]. The gases accrete onto the central object, while rotating. The release of the gravitational energy provides the source for the activities of the object.

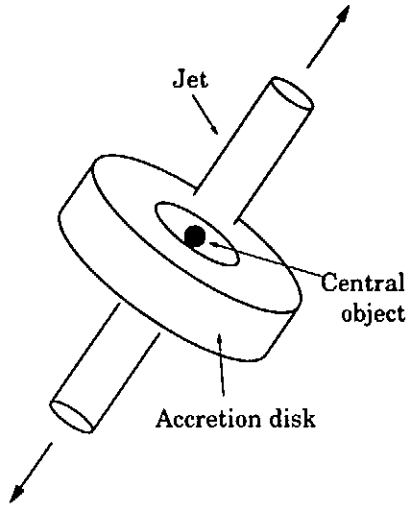

Fig. 2.8. Accretion disk and bipolar jets.

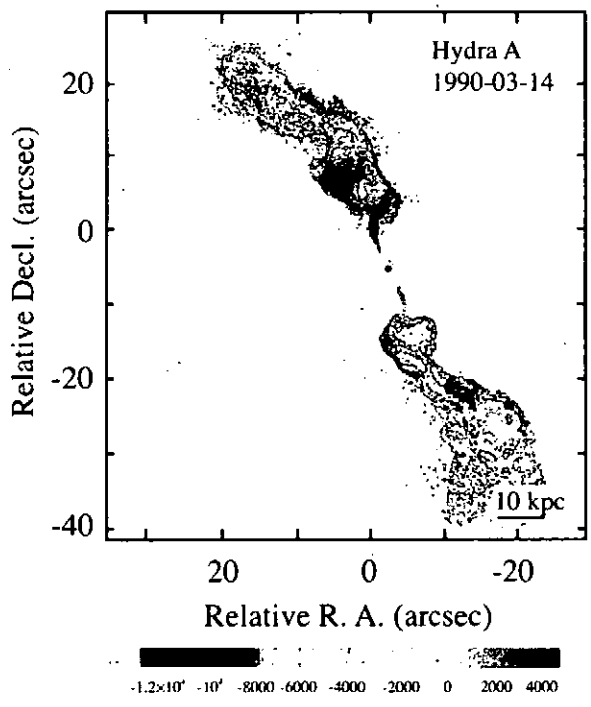

Fig. 2.9. Magnetic fields of Hydra A cluster by Faraday rotation measurement [2/32]: Magnetic field derived from the Faraday rotation is 33 mG with total energy $O(10^6)$ ergs.

The angular momentum of gases needs to be released for the continuation of gas accretion leading to the reduction in the total gravitational potential energy. At present, two mechanisms are presented for the angular-momentum release [2/28-2/30, 2/33-2/35]. One is the transport by turbulent motion towards the outer part of the disk through enhanced viscous diffusion. The other is the release by the bipolar jets that are observed ubiquitously around high-mass objects. Such jets may carry away the angular momentum from the disk as long as they are swirling jets, that is, they perform a helical motion. In either event, the magnetic field is generated together with the global flow.

The driving force for the jets is under an intensive study. One of the most promising candidates is the magnetic force arising from the Lorentz force. There attention is focused on the generation of flow by the distortion of magnetic field lines. In this sense, the mechanism may be called the flow dynamo in contrast to the magnetic dynamo with a primary attention placed on the magnetic-field generation by flow.

A prominent feature of bipolar jets is the high collimation [2/28, 2/33]. They keep a straight shape in a long distance with an extremely small growth of jet width. A candidate of the high-collimation mechanism is the confinement of ionized gases by a magnetic field, specifically, its toroidal component. The jet speed is $O(10) \sim O(10^2)$ km s^{-1} for protostars and several ten percent of the light speed for active galactic nuclei. In the latter, relativistic effects are essential, which are beyond the scope of this review.

Table 2.2. Some analogy between accretion disk and toroidal plasmas.

	Accretion disk	**RFP**	**Tokamak**
Spontaneous current generation mechanism	Turbulent dynamo	←	Diffusion-driven (bootstrap) current
Characteristic length	Turbulence correlation length	←	Banana width
Transportation of magnetic flux	Energy-containing turbulent motion	←	Diffusion
Resulting global structure	Axial jet (ejection by magnetic pressure)	Reversal of toroidal field	Current depletion near axis (e.g., current hole)
Relevant turbulence -related parameters	Coefficients α, β and γ in Eq. (2.11)	←	Turbulent transport coefficients ν_T and χ_T in Eqs. (2.12) and (2.13)

The spontaneous generation of a toroidal magnetic field in an accretion disk leads to the formation of a distinct structure. The occurrence of a characteristic structure due to the spontaneous poloidal magnetic field may be observed in tokamaks. Some analogy in light of the role of a spontaneous magnetic field is illustrated in Table 2.2.

2.3.2. Transport barriers in tokamaks

The generation of flow is an important theme in nuclear fusion. The discovery of high-confinement (H) modes [2/36] has opened a new area of the study of plasma turbulence and structure formation. In the H modes, the transports of heat and particles are suppressed in a thin region near the plasma edge, i.e., at an edge transport barrier. This barrier region is characterized by the simultaneous occurrence of the radial electric field (E_r) and the poloidal plasma rotation [2/37-2/40].

H modes were followed by the improved-confinement modes that have different transport barriers. There the transport barriers of heat and particles are formed in the core and are named internal transport barriers [2/41]. Examples include the reversed-shear (RS), negative-central-shear, enhanced-reversed-shear modes, etc. [2/42, 2/43] (hereafter these shear-related modes will be generally called RS modes). The barriers are also characterized by the radial electric field and the poloidal plasma rotation. In addition to these characteristics, RS modes are often associated with the minimum of the safety factor q off the axis [2/44]. Readers may consult [2/8, 2/37, 2/41, 2/45-2/48] for a comprehensive review of theories for the improved confinement.

To clarify the driving mechanism of the poloidal plasma rotation is indispensable for understanding of the barrier formation in RS modes as well as H modes. A mechanism of plasma flow driven in tokamaks may be also called the flow dynamo, as in the case of bipolar jets. Readers may consult [2/49] for the detailed review of zonal flows in toroidal plasmas. The occurrence of a radial electric field and plasma rotation is one central theme in the study of tokamaks. At the same time, how they affect and suppress the transports of heat and particles is the other important theme. The relationship of the turbulent transports with the radial electric field and the plasma rotation is now under an intensive study.

2.4. Stellar dynamo and structure formation in toroidal plasmas

The foregoing surveys show a remarkable analogy between the dynamo in stars and the flow generation mechanism in toroidal plasmas. The further resemblance may be seen between them and some problems in fluid dynamics and plasma physics. Common features are stated as follows.

Table 2.3. Comparison between dynamo, electromagnetic (EM) flow generation and flow structure formation (Navier-Stokes equation is abbreviated as NS eq.).

Name of Concept	Name	Main small-scale fluctuations	Generated global structure	Examples	Equations in fluid limit and fundamental drive	Coverage by this review
Magnetic dynamo	Dynamo	Fluid motion (thermal convection)	Magnetic field	Geodynamo Solar dynamo	MHD eq. Thermal convection Coriolis force	Yes
	Magnetic structure formation	Magnetic fluctuations (kink, tearing)	Magnetic field	RFP torus	MHD eq. External toroidal current	Yes
Electro-magnetic flow dynamo	MHD flow dynamo	EM and flow fluctuations	Magnetized flow	Bipolar jets	MHD eq. Gravitational force Coriolis force	Yes
	$E \times B$ flow dynamo	EM and pressure fluctuations (drift waves)	$E \times B$ flow	Zonal flow in toroidal plasmas	MHD eq. Plasma response Pressure gradient	Partly
Flow dynamo	Neutral flow dynamo	Small-scale thermal convection	Zonal flow	Jobian spot Tidal current Jet stream, etc.	Navier-Stokes eq. Thermal convection Coriolis force	No
	Flow structure formation	Small-scale convection	Structured flow	Swirling flow, Asymmetry in pipe flow	Navier-Stokes eq. Drive of axial flow	No

First, in both cases, large-scale axial vector fields such as the magnetic field $\mathbf{B}$ and the vorticity $\boldsymbol{\omega}$ ($= \nabla \times \mathbf{u}$) are sustained against the dissipation ($\mathbf{u}$ is the velocity). The energy source is the inhomogeneity of a scalar field. One representative example is the temperature gradient in stellar dynamo and toroidal plasmas, and the other is the gradient of the gravitational potential in accretion disks.

Second, turbulence plays a central role. When the symmetry of field holds and no microscale length exists, the flow of a vector field cannot be driven by the gradient of a scalar field (Curie's principle). In the context of stellar dynamo, Cowling's anti-dynamo theorem is famous. In the dynamo, turbulence induces the transport of magnetic flux that generates the magnetic field. It is also known that the fluxes of momentum and angular momentum are induced by turbulence, establishing a large-scale vortex. The correspondence between

$$\mathbf{A} \leftrightarrow \mathbf{u}, \quad \mathbf{B} \leftrightarrow \boldsymbol{\omega} \tag{2.4}$$

might hold in the magnetic and flow dynamos, where $\mathbf{A}$ is the vector potential.

Third, a generated field has a definite feedback effect on the turbulence that induces the magnetic and flow dynamos. Fourth, turbulence in some circumstances has a long correlation length that is comparable to the system size. These analogies are summarized in Table 2.3. The areas covered by this topical review are also indicated there.

2.5. Mean-field magnetohydrodynamic approach

Attempts to understand the macroscopic aspects of magnetic dynamo, flow dynamo, and turbulent transports have been developed on the basis of the mean-field MHD. As was described above, the dynamics at a large scale is governed by the presence of micro turbulence. We denote the former scale length by ℓ_{macroo} and the latter by ℓ_{micro}, and assume the intermediate length for averaging or coarse graining, ℓ_{av}, that obeys

$$\ell_{\mathrm{micro}} << \ell_{\mathrm{av}} << \ell_{\mathrm{macroo}}. \tag{2.5}$$

In the thermodynamical equilibrium, the fluctuations are in the range of micro-molecular dissipation length. Ohm's law and the heat-flux equation for macroscopic phenomena in classical thermodynamics are written as [2/50]

$$\mathbf{E}+\mathbf{u}\times\mathbf{B}=\eta\mathbf{j}+a\nabla\theta+R\mathbf{B}\times\mathbf{j}+N\mathbf{B}\times\nabla\theta, \tag{2.6}$$

$$\mathbf{q}-\phi\mathbf{j}=a\theta\mathbf{j}-\kappa\nabla\theta+N\theta\mathbf{B}\times\mathbf{j}+L\mathbf{B}\times\nabla\theta, \tag{2.7}$$

where $\mathbf{E}$ is the electric field, θ is the temperature, and $\mathbf{q}$ is the heat flux. Some fluxes are perpendicular to the magnetic field and the temperature gradient. The term $R\mathbf{B}\times\mathbf{j}$ is called the Hall term, $N\mathbf{B}\times\nabla\theta$ is the Nernst effect, $N\theta\mathbf{B}\times\mathbf{j}$ is the Ettingshausen effect, and $L\mathbf{B}\times\nabla\theta$ is the Leduc-Righi effect. Effects of microscopic thermal fluctuations are included in the transport coefficients. The common coefficients a and N in Eqs. (2.6) and (2.7) reflect the Onsager symmetry of transport matrix.

In the study of dynamo, ℓ_{micro} is taken in the range of plasma turbulence. We denote the averaging over the scale ℓ_{av} by the overbar or $\langle\cdot\rangle$. The mean-field version of the one-fluid constant-density MHD equations is as follows. The equation of motion is

$$\frac{\partial\overline{u}_i}{\partial t}+\frac{\partial}{\partial x_j}\overline{u}_i\overline{u}_j=-\frac{\partial}{\partial x_i}\left(\overline{p}+\left\langle\frac{\mathbf{B}'^2}{2}\right\rangle\right)+\left(\overline{\mathbf{j}}\times\overline{\mathbf{B}}\right)_i+\frac{\partial}{\partial x_j}\left(-R_{ij}\right)+\nu\nabla^2\overline{u}_i, \tag{2.8}$$

the magnetic-field counterpart of Eq. (2.8) is

$$\frac{\partial\overline{\mathbf{B}}}{\partial t}=-\nabla\times\left(\overline{\mathbf{u}}\times\overline{\mathbf{B}}+\mathbf{E}_T\right)-\nabla\times\left\langle\eta\mathbf{j}+a\nabla\theta+R\mathbf{B}\times\mathbf{j}+N\mathbf{B}\times\nabla\theta\right\rangle, \tag{2.9}$$

and the energy equation is

$$\frac{D\overline{\theta}}{Dt} = \nabla\cdot\left(-\mathbf{H}_\theta\right) + \chi_\theta\nabla^2\overline{\theta}. \tag{2.10}$$

In the one-fluid description, the last term on the right hand side of Eq. (2.9) is usually replaced by $\eta\nabla^2\overline{\mathbf{B}}$. The turbulent electromotive force $\mathbf{E}_T$, the Reynolds stress of MHD flow, R_{ij}, and the turbulent heat flux $\mathbf{H}_\theta$ are written as [2/8]

$$\mathbf{E}_T \equiv \langle \mathbf{u}' \times \mathbf{B}' \rangle = \alpha\overline{\mathbf{B}} - \beta\overline{\mathbf{j}} + \gamma\overline{\boldsymbol{\omega}}, \tag{2.11}$$

$$R_{ij} \equiv \left\langle u_i' u_j' \right\rangle - \left\langle B_i' B_j' \right\rangle = \frac{2}{3}K_R\delta_{ij} - \nu_T\overline{s}_{ij} + \nu_M\overline{M}_{ij}, \tag{2.12}$$

$$\mathbf{H}_\theta \equiv \langle \theta' \mathbf{u}' \rangle = -\chi_T\nabla\overline{\theta}, \tag{2.13}$$

with $(\nu_T, \nu_M) = (7/5)(\beta, \gamma)$, where primed quantities denote fluctuations, and $\overline{s}_{ij}$ and $\overline{M}_{ij}$ are the mean velocity- and magnetic-strain tensors, respectively [see Eqs. (4.13) and (4.40)].

The terms with coefficients α, β and γ are called α, β and γ effects, respectively. Coefficients α, β, γ, K_R, ν_T and ν_M are related to fluctuation amplitudes. The mean-field approach is to investigate into the structures of the coarse-grained magnetic field and flow by solving Eqs. (2.8)-(2.10) with the help of a turbulence theory that determines α, β, γ, etc.

The detailed explanation of the foregoing mean-field MHD system of equations is given in § 4. There the system is also compared with the so-called kinematic dynamo theory. In the history of the magnetic-dynamo study, much attention has been paid to the generation of magnetic fields by fluid motion. In reality, the study started from the kinematic approach [2/26, 2/27]. There the generation mechanism is sought under a prescribed velocity field. At present, it is keenly recognized that the self-consistent determination of magnetic field and flow is necessary for understanding of stellar and flow dynamos. The deduction of structures in the magnetic field and flow based on Eqs. (2.8)-(2.13) is reviewed in the following sections.

In this article, special attention will be paid to the turbulent cross helicity or the correlation function between magnetic and velocity fluctuations, whose effects occur through the coefficients γ and ν_M. The introduction of this concept will be shown to pave the way for a systematic description of various dynamo phenomena. The essence of those results is summarized in Table 2.4, whose physical implications will be clarified in subsequent explanations.

Many important properties of hot plasmas linked with fusion are beyond the scope of the MHD approach. The turbulent transports of heat and particles, however, are often caused by energetic fluctuations or the energy-containing fluctuations. Then the mean-field approach may be expected to shed light on macroscopic properties responsible for the transports that are common to a variety of phenomena in electrically-conducting media. In the following accounts, attention will be paid to the theoretical (analytical) understanding of phenomena. It will be supplemented with the findings by computer simulations and observations, although their coverage is limited.

Table 2.4. Comparison of structures in stellar magnetic field

	Earth	Sun	Accretion disk	
			Disk	Jet
$\lvert\gamma/\beta\rvert$	$\lvert\gamma/\beta\rvert \ll 1$	$\lvert\gamma/\beta\rvert < 1$	$\lvert\gamma/\beta\rvert < 1$	$\lvert\gamma/\beta\rvert < 1$
Magnetic- field equation	$\nabla\times\overline{\mathbf{B}} - (\alpha/\beta)\overline{\mathbf{B}} = 2(\gamma/\beta)\boldsymbol{\omega}_F$	$\nabla\times\overline{\mathbf{B}} = (\gamma/\beta)(\overline{\boldsymbol{\omega}} + 2\boldsymbol{\omega}_F)$	←	$\nabla\times\overline{\mathbf{B}} = \left(1-(\gamma/\beta)^2\right)^{-1}(\alpha/\beta)\overline{\mathbf{B}}$
Magnetic field	$\overline{\mathbf{B}}_{\text{dipole}} = \langle\alpha/\gamma\rangle\boldsymbol{\omega}_F$, Superposition of Taylor field	$\overline{\mathbf{B}} = (\gamma/\beta)(\overline{\mathbf{u}} + \boldsymbol{\omega}_F\times\mathbf{r})$	←	Taylor field
Magnetic field structure	Distinct dipole field	Distinct toroidal field	Toroidal and vertical field	Toroidal and vertical field
Differential velocity	$\overline{\mathbf{u}} = (\gamma/\beta)\overline{\mathbf{B}}$			$\overline{\mathbf{u}} = (\gamma/\beta)\overline{\mathbf{B}}$ Taylor field
Partition $r_E = \dfrac{\overline{\mathbf{B}}^2/2}{\overline{\mathbf{u}}^2/2}$	$(\beta/\gamma)^2$	$(\gamma/\beta)^2$	$(\gamma/\beta)^2$	$(\beta/\gamma)^2$
$\dfrac{\text{differential velocity}}{\text{mean rotational velocity}}$	$\ll\ll 1$	< 1	< 1	~ 1
Solid body rotation	Dominantly important	Important	←	Not dominant

3. Magnetohydrodynamic Equations

We start from the magnetohydrodynamic equations for ion and electron gases, and give their simplified version.

3.1. Two-fluid equations

Subscript S denotes I (ion) or E (electron). The equations for the number density and the momentum are [2/22]

$$\frac{\partial n_S}{\partial t} + \nabla \cdot \left(n_S \mathbf{v}_S \right) = 0, \tag{3.1}$$

$$\frac{\partial}{\partial t} n_S m_S v_{Si} + \frac{\partial}{\partial x_j} n_S m_S v_{Sj} v_{Si} = -\frac{\partial p_{Sij}}{\partial x_j} + n_S e_S \left(\mathbf{E} + \mathbf{v}_S \times \mathbf{B} \right)_i + F_{cSi}, \tag{3.2}$$

where n_S is the number density, m_S is the mass, $\mathbf{v}_S$ is the gas velocity, $\mathbf{E}$ is the electric field, $\mathbf{B}$ is the magnetic field, and e_S is the electric charge given by

$$e_E = -e, \quad e_I = Ze \tag{3.3}$$

(Z is the charge number). In Eq. (3.2), p_{Sij} expresses the stress arising from the collision among ions or electrons themselves and is decomposed into the isotropic (pressure) and anisotropic (viscosity) parts,

$$p_{Sij} = -p_S \delta_{ij} + \Pi_{Sij}. \tag{3.4}$$

For the pressure p_S, we adopt the perfect-gas relation

$$p_S = k_B n_S \theta_S, \tag{3.5}$$

where k_B is the Boltzmann constant, and θ_S is the temperature. The last term $\mathbf{F}_{cS}$ in Eq. (3.2) is the force arising from the collision between electron and ion, which is written as

$$\mathbf{F}_{cE} = -\mathbf{F}_{cI} = -n_E m_E \nu_c \left(\mathbf{v}_E - \mathbf{v}_I \right), \tag{3.6}$$

with ν_c as the collision frequency.

The equations for the electric and magnetic fields are

$$\nabla \times \mathbf{B} = \mu_0 \mathbf{j} + \frac{1}{c^2} \frac{\partial \mathbf{E}}{\partial t}, \tag{3.7}$$

$$\nabla \times \mathbf{E} = -\frac{\partial \mathbf{B}}{\partial t}, \tag{3.8}$$

$$\nabla \cdot \mathbf{B} = 0, \tag{3.9}$$

$$\nabla \cdot \mathbf{E} = \frac{\rho_c}{\varepsilon_0}, \tag{3.10}$$

where μ_0 is the magnetic permeability, ε_0 is the dielectric constant, $c\ (= 1/\sqrt{\varepsilon_0 \mu_0})$ is the light speed, and ρ_c is the net charge density given by

$$\rho_c = e(Zn_I - n_E). \tag{3.11}$$

For closing the above fluid and electromagnetic system of equations, we need the equations for the thermal energy or θ_S, which is omitted here.

3.2. One-fluid equations

3.2.1. Variable-density flow

We introduce the mass density ρ, the velocity $\mathbf{u}$, and the pressure p as

$$\rho = n_E m_E + n_I m_I, \tag{3.12}$$

$$\mathbf{u} = \frac{n_E m_E \mathbf{v}_E + n_I m_I \mathbf{v}_I}{\rho}, \tag{3.13}$$

$$p = p_E + p_I. \tag{3.14}$$

We assume the electrical neutrality

$$\rho_c = 0. \tag{3.15}$$

From Eqs. (3.1), (3.2), and (3.15), we have

$$\frac{\partial \rho}{\partial t} + \nabla \cdot (\rho \mathbf{u}) = 0, \tag{3.16}$$

$$\frac{\partial}{\partial t} \rho u_i + \frac{\partial}{\partial x_j} \rho u_i u_j = -\frac{\partial p}{\partial x_i} + (\mathbf{j} \times \mathbf{B})_i + \frac{\partial}{\partial x_j} \mu s_{ij}, \tag{3.17}$$

where

$$\mathbf{j} = n_E e(\mathbf{v}_I - \mathbf{v}_E), \tag{3.18}$$

$$s_{ij} = \frac{\partial u_j}{\partial x_i} + \frac{\partial u_i}{\partial x_j} \tag{3.19}$$

and the simplest representation based on the isotropic viscosity μ was adopted for Π_{lij}.

For a perfect gas, p and internal energy ζ are given as

$$p = (\gamma - 1)\rho\zeta, \quad \zeta = C_V\theta, \tag{3.20}$$

where γ is the ratio of the specific heat at constant pressure, C_P, to its constant-volume counterpart C_V.

Under Eq. (3.15), Eq. (3.2) with $S = E$ results in Ohm's law

$$\mathbf{j} = \sigma_0(\mathbf{E} + \mathbf{u} \times \mathbf{B}) \ , \tag{3.21}$$

with the Hall and ∇p_E-related terms discarded, where the electric conductivity is given by

$$\sigma_0 = \frac{n_E e^2}{m_E \nu_C}. \tag{3.22}$$

We combine Eq. (3.21) and the Ampere law

$$\nabla \times \mathbf{B} = \mu_0 \mathbf{j} \tag{3.23}$$

with Eq. (3.8), and have

$$\frac{\partial \mathbf{B}}{\partial t} = \nabla \times (\mathbf{u} \times \mathbf{B}) + \eta \nabla^2 \mathbf{B}, \tag{3.24}$$

where the magnetic diffusivity η is given by

$$\eta = \frac{1}{\sigma_0 \mu_0}. \tag{3.25}$$

The internal energy ζ obeys

$$\frac{\partial}{\partial t}\rho\zeta + \nabla \cdot (\rho\zeta\mathbf{u}) = \nabla \cdot (\kappa \nabla\theta) - p\nabla \cdot \mathbf{u} + \phi_D, \tag{3.26}$$

where ϕ_D is the dissipation function expressing the conversion of kinetic and magnetic to thermal energies, and is written as

$$\phi_D = \mu s_{ij} \frac{\partial u_j}{\partial x_i} + \frac{1}{\sigma_0}\mathbf{j}^2. \tag{3.27}$$

Equations (3.16), (3.17), (3.24), and (3.26) constitute the one-fluid MHD system of equations. In the study of stellar magnetic fields, this system is supplemented by the Coriolis force, the buoyancy force, etc., providing a useful mathematical tool. In fusion plasmas, however, the one-fluid MHD system is quite limited [2/22, 3/1]. First, the dynamical characteristics of electron and ion differ, owing to the large mass difference. Many important characteristics arising from this difference are lost in the reduction to the one-fluid system. Second, charged particles behave entirely differently in the directions normal and parallel to a magnetic field. This feature is excluded from the isotropic representation for Π_{ij} leading to the last term on the right-hand side of Eq. (3.17). Third, the assumption about the electrical neutrality, Eq. (3.15), expels the explicit treatment of $\mathbf{E}$. At the transport barriers in tokamaks, however, the radial electric field is tightly linked with the suppression of the heat and particle transports, as was mentioned in § 2.3.2, and its explicit treatment is indispensable for the study of their suppression mechanism.

3.2.2. Constant-density flow

In the study of stellar magnetic-field generation and flow drive, the variation of the mass density ρ becomes important in relation to self-gravity and buoyancy effects. Some important processes of magnetic-field generation are often examined under the assumption of constant density, except the inclusion of the buoyancy force due to the Boussinesq approximation. This point is related to the fact that the magnetic induction equation (3.24) is not dependent explicitly on ρ. The assumption about the constancy of ρ greatly alleviates the mathematical complexity in the investigation into dynamo effects by turbulence theories.

In the case of constant fluid density, the use of Alfven-velocity units leads to a concise form of fundamental equations. In the units, $\mathbf{B}/\sqrt{\rho\mu_0}$ has the dimension of velocity. We make use of this fact and make the replacement

$$\frac{\mathbf{B}}{\sqrt{\rho\mu_0}} \to \mathbf{B}, \quad \frac{\mathbf{j}}{\sqrt{\rho/\mu_0}} \to \mathbf{j}, \quad \frac{\mathbf{E}}{\sqrt{\rho\mu_0}} \to \mathbf{E}, \quad \frac{p}{\rho} \to p. \tag{3.28}$$

Under this replacement, Eq. (3.17) is rewritten as

$$\frac{\partial u_i}{\partial t} + \frac{\partial}{\partial x_j} u_j u_i = \left(\frac{\partial}{\partial t} + \mathbf{u}\cdot\nabla\right) u_i = -\frac{\partial p}{\partial x_i} + (\mathbf{j}\times\mathbf{B})_i + \nu\nabla^2 u_i, \tag{3.29}$$

with the solenoidal condition $\nabla\cdot\mathbf{u} = 0$, where $\nu\ (= \mu/\rho)$ is the kinematic viscosity. In this case, Eq. (3.26) is reduced to the equation for the temperature,

$$\frac{\partial \theta}{\partial t} + \nabla \cdot (\theta \mathbf{u}) = \chi_\theta \nabla^2 \theta, \tag{3.30}$$

where χ_θ [$= \kappa/(C_P \rho)$] is the thermal diffusivity.

3.3. Electrohydrodynamics

In the one-fluid MHD equations, the electric field $\mathbf{E}$ occurs implicitly through the Ohm's law, Eq. (3.21). As was noted in § 2.3.2, $\mathbf{E}$ is one of the key quantities characterizing the transport barriers in tokamaks. For treating $\mathbf{E}$ explicitly, we need to abandon the Ohm's law based on Eq. (3.15). This situation makes the simultaneous treatment of both $\mathbf{E}$ and $\mathbf{B}$ effects quite complicated.

In the context of the transport barriers in tokamaks, we retain the variable-density and $\mathbf{E}$ or nonvanishing ρ_c effects and write

$$\frac{\partial}{\partial t} \rho u_i + \frac{\partial}{\partial x_j} \rho u_i u_j = -\frac{\partial p}{\partial x_i} + \rho_c E_i + \frac{\partial}{\partial x_j} \mu s_{ij}, \tag{3.31}$$

in place of Eq. (3.17). The pressure p obeys

$$\frac{\partial p}{\partial t} + \nabla \cdot (p \mathbf{u}) = -(\gamma - 1) p \nabla \cdot \mathbf{u} + \nabla \cdot \left(\kappa \nabla \frac{p}{C_V \rho} \right), \tag{3.32}$$

from Eqs. (3.20) and (3.26), where ϕ_D was discarded.

The relation between ρ_c and $\mathbf{E}$ is given by Eq. (3.10). In order to close this system, we need the equation for ρ_c, which is given by

$$\frac{\partial \rho_c}{\partial t} + \nabla \cdot (\rho_c \mathbf{u}) = \nabla \cdot \mathbf{s}_c, \tag{3.33}$$

from Eqs. (3.1) and (3.11), where $\mathbf{s}_c$ is defined by

$$\mathbf{s}_c = \frac{e n_E n_I (m_I - Z m_E)(\mathbf{v}_E - \mathbf{v}_I)}{\rho}. \tag{3.34}$$

The advection term on the left-hand side of Eq. (3.33) may generate $\mathbf{E}$ effects on the transport of heat, through the evolution of ρ_c. The right-hand side represents the evolution due to the velocity difference between ion and electron gases, which is beyond the scope of the one-fluid system. Hereafter, attention will be focused on the advection term.

4. Mean-Field Magnetohydrodynamics

The primary concern of this review is a turbulent state of electrically-conducting fluids. A theoretical method for investigating into global properties of such a state, specifically, the turbulent transports of momentum and scalars like heat is the mean-field MHD based on the ensemble-averaging procedure. We start from giving a brief explanation of the essence of the mean-field hydrodynamics and proceed to its MHD counterpart.

4.1. Constant-density hydrodynamic equations

As the simplest case, we consider the motion of a constant-density electrically-nonconducting fluid. From Eq. (3.17), the motion is described by

$$\frac{\partial u_i}{\partial t} + \frac{\partial}{\partial x_j} u_i u_j = -\frac{\partial p}{\partial x_i} + \nu \nabla^2 u_i, \tag{4.1}$$

with $\nabla \cdot \mathbf{u} = 0$. We use the ensemble averaging $\langle \cdot \rangle$ and make the decomposition

$$\mathbf{u} = \overline{\mathbf{u}} + \mathbf{u}', \ \overline{\mathbf{u}} = \langle \mathbf{u} \rangle; \quad p = \overline{p} + p', \ \overline{p} = \langle p \rangle. \tag{4.2}$$

The mean parts obey

$$\frac{D\overline{u}_i}{Dt} \equiv \left(\frac{\partial}{\partial t} + \overline{\mathbf{u}} \cdot \nabla \right) \overline{u}_i = -\frac{\partial \overline{p}}{\partial x_i} + \frac{\partial}{\partial x_j} \left(-R_{ij} \right) + \nu \nabla^2 \overline{u}_i, \tag{4.3}$$

where the Reynolds stress R_{ij} is given by

$$R_{ij} = \langle u_i' u_j' \rangle, \tag{4.4}$$

and expresses the transport of the momentum per unit mass by fluctuations.

4.1.1. Turbulent-viscosity representation

In order to close Eq. (4.3), we need to relate R_{ij} to the mean parts. The former is governed by [4/1]

$$\frac{DR_{ij}}{Dt} = -R_{j\ell} \frac{\partial \overline{u}_i}{\partial x_\ell} - R_{i\ell} \frac{\partial \overline{u}_j}{\partial x_\ell} + \left\langle p' \left(\frac{\partial u_j'}{\partial x_i} + \frac{\partial u_i'}{\partial x_j} \right) \right\rangle - 2\nu \left\langle \frac{\partial u_i'}{\partial x_\ell} \frac{\partial u_j'}{\partial x_\ell} \right\rangle$$

$$+ \frac{\partial}{\partial x_\ell} \left(-\langle u_i' u_j' u_\ell' \rangle + \langle p' u_i' \rangle \delta_{j\ell} + \langle p' u_j' \rangle \delta_{i\ell} + \nu \frac{\partial R_{ij}}{\partial x_\ell} \right). \tag{4.5}$$

A representative quantity characterizing the strength of velocity fluctuation is the turbulent energy

$$K = \left\langle \frac{1}{2}\mathbf{u}'^2 \right\rangle. \tag{4.6}$$

It obeys

$$\frac{DK}{Dt} = -R_{ij}\frac{\partial \overline{u}_j}{\partial x_i} - \nu\left\langle \left(\frac{\partial u_j'}{\partial x_i}\right)^2 \right\rangle + \nabla \cdot \left\langle -\left(\frac{1}{2}\mathbf{u}'^2 + p'\right)\mathbf{u}' + \nu \nabla K \right\rangle. \tag{4.7}$$

We integrate Eq. (4.7) over a whole fluid region V and have

$$\frac{\partial}{\partial t}\int_V K dV = \int_V \left(-R_{ij}\frac{\partial \overline{u}_j}{\partial x_i}\right) dV - \nu \int_V \left\langle \left(\frac{\partial u_j'}{\partial x_i}\right)^2 \right\rangle dV$$

$$+ \int_S \left(-K\overline{\mathbf{u}} + \left\langle -\left(\frac{1}{2}\mathbf{u}'^2 + p'\right)\mathbf{u}' + \nu \nabla K \right\rangle\right) \cdot \mathbf{n} dS, \tag{4.8}$$

where S is the surface of V, and $\mathbf{n}$ is the outward unit vector normal to S. The last part in Eq. (4.8) represents the energy flux across S. In the absence of such a flux, K inevitably decays so long as the shear of $\overline{\mathbf{u}}$ does not exist. Then the first term on the right-hand side of Eq. (4.7), that is,

$$P_K = -R_{ij}\frac{\partial \overline{u}_j}{\partial x_i}, \tag{4.9}$$

is called the production term and usually plays the role of generating or sustaining velocity fluctuation by draining the energy from $\overline{\mathbf{u}}$. As a result, the spatial profile of K may be estimated qualitatively from that of P_K [4/1, 4/2].

The mathematical resemblance exists between Eq. (4.5) and Eq. (4.7), except the third term on the right-hand side of the former. As a result, the situation quite similar to the relationship between K and P_K holds between R_{ij} and the first two terms in its equation. We denote the time scale characterizing the turbulent transport of momentum by τ_f, and write

$$R_{ij} = \frac{2}{3}K\delta_{ij} + C_R\tau_f\left[-R_{j\ell}\frac{\partial \overline{u}_i}{\partial x_\ell} - R_{i\ell}\frac{\partial \overline{u}_j}{\partial x_\ell}\right]_D, \tag{4.10}$$

where C_R is a positive constant, and

$$\left[A_{ij}\right]_D = A_{ij} - \frac{1}{3}A_{\ell\ell}\delta_{ij}. \tag{4.11}$$

In Eq. (4.10), we use the first or isotropic term and estimate the second term, having

$$R_{ij} = \frac{2}{3}K\delta_{ij} - C_1 K\tau_f \bar{s}_{ij}, \tag{4.12}$$

where C_1 is a positive constant, and $\bar{s}_{ij}$ is the mean velocity-strain tensor defined by

$$\bar{s}_{ij} = \frac{\partial \bar{u}_j}{\partial x_i} + \frac{\partial \bar{u}_i}{\partial x_j}. \tag{4.13}$$

Equation (4.12) is the well-known turbulent- or eddy-viscosity representation for the Reynolds stress, and the coefficient

$$\nu_T = C_1 K\tau_f \tag{4.14}$$

is the turbulent or eddy viscosity. It is reduced to a variety of expressions according to the choice of τ_f. Its simplest choice is

$$\tau_f = \frac{K}{\varepsilon}, \tag{4.15}$$

where ε is the dissipation rate of K that is given by the second term on the right-hand side of Eq. (4.7) or

$$\varepsilon = \nu\left\langle\left(\frac{\partial u_j'}{\partial x_i}\right)^2\right\rangle. \tag{4.16}$$

Equation (4.14) based on Eq. (4.15) results in the $K-\varepsilon$ model, which is the prototype of all the turbulence models used in the calculation of engineering turbulent flows [4/3-4/5].

4.1.2. Nonlinear algebraic representation

The turbulent-viscosity representation, Eq. (4.12), is useful in the study of enhanced diffusion effects by turbulence, but it often suffers from critical deficiencies. We consider the situation

$$\bar{\mathbf{u}} = \left(\bar{u}(y), 0, 0\right), \quad \mathbf{u}' = \left(u', v', w'\right), \tag{4.17}$$

as in a turbulent flow between two parallel walls parallel to the x axis. From Eq. (4.12), we have

$$R_{xx} = R_{yy} = R_{zz} = \frac{2}{3}K. \tag{4.18}$$

Experiments show that

$$R_{xx} > R_{zz} > R_{yy}. \tag{4.19}$$

Namely, the velocity fluctuation normal to the wall is highly suppressed. This property cannot be described by Eq. (4.12).

The foregoing deficiency arising from the intrinsic property of isotropic diffusion manifests itself more seriously in the treatment of the structure formation by turbulent flows. Its representative instance is a turbulent flow in a square duct. The most prominent property of the flow is the occurrence of secondary flows in the cross section, as in Fig. 4.1 (the x is along the axis of the duct) [4/6]. There we may write

$$\overline{\mathbf{u}} = \left(\overline{u}(y,z), \overline{v}(y,z), \overline{w}(y,z)\right). \tag{4.20}$$

From Eq. (4.12), we have

$$R_{yy} = R_{zz}. \tag{4.21}$$

It may be shown that the secondary flows are driven by the anisotropy of velocity fluctuations, that is,

$$R_{yy} - R_{zz} \neq 0. \tag{4.22}$$

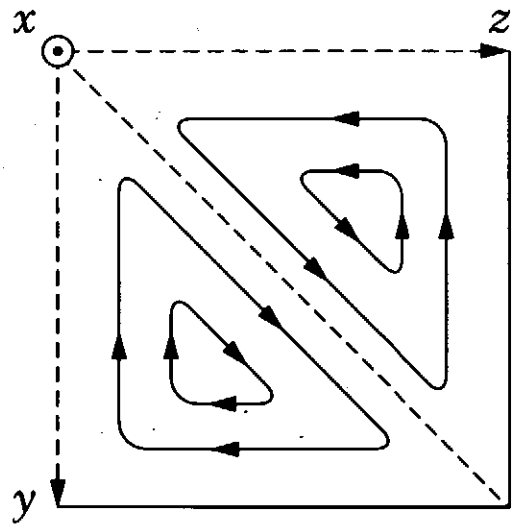

Fig. 4.1. Secondary flows in a turbulent square-duct flow (one-fourth of the cross section).

The occurrence of the foregoing secondary flows indicates that coherent structures may survive in turbulent motion, through the competition of diffusion and anti-diffusion effects. In order to seek the latter effect, we use Eq. (4.12) and estimate the second term in Eq. (4.10). We write

$$\frac{\partial \overline{u}_j}{\partial x_i} = \frac{1}{2}\left(\overline{s}_{ij} + \overline{\omega}_{ij}\right), \tag{4.23}$$

where the mean vorticity tensor $\overline{\omega}_{ij}$ is defined by

$$\overline{\omega}_{ij} = \frac{\partial \overline{u}_j}{\partial x_i} - \frac{\partial \overline{u}_i}{\partial x_j} \tag{4.24}$$

and is related to the mean vorticity $\overline{\boldsymbol{\omega}}\,(=\nabla\times\overline{\mathbf{u}})$ as

$$\overline{\omega}_{ij} = \varepsilon_{ij\ell}\overline{\omega}_\ell . \tag{4.25}$$

Then we have

$$R_{ij} = \frac{2}{3}K\delta_{ij} - C_1 K\tau_f \overline{s}_{ij} + C_{21}K\tau_f{}^2\overline{s}_{i\ell}\overline{s}_{\ell j} + C_{22}K\tau_f{}^2\left(\overline{s}_{i\ell}\overline{\omega}_{\ell j} + \overline{s}_{j\ell}\overline{\omega}_{\ell i}\right), \tag{4.26}$$

where C_{21} and C_{22} positive constants [4/5, 4/7, 4/8]. In this estimate, we have $C_{21} = 2C_{22}$, but this constraint is not necessary when the contribution from the third term on the right-hand side of Eq. (4.5) is taken into account. The third and fourth terms in Eq. (4.26) lead to Eq. (4.22). They compete the diffusion effect arising from the second term, resulting in the occurrence of the secondary flows in a square duct [4/8, 4/9].

4.1.3. Turbulent heat flux

The mean temperature obeys

$$\frac{D\overline{\theta}}{Dt} = \nabla\cdot\left(-\mathbf{H}_\theta\right) + \chi_\theta\nabla^2\overline{\theta}, \tag{4.27}$$

from Eq. (3.30), where $\mathbf{H}_\theta$ is the turbulent heat flux given by

$$\mathbf{H}_\theta = \langle\theta'\,\mathbf{u}'\rangle. \tag{4.28}$$

On the basis of the equation for $\mathbf{H}_\theta$, its algebraic expression may be derived in an entirely similar manner to the case of R_{ij}. Then we have [4/5, 4/10]

$$H_{\theta i} = -C_{\theta 1}K\tau_f\frac{\partial\overline{\theta}}{\partial x_i} + K\tau_f{}^2\left(C_{\theta 21}\overline{s}_{ij} + C_{\theta 22}\overline{\omega}_{ij}\right)\frac{\partial\overline{\theta}}{\partial x_j}, \tag{4.29}$$

where $C_{\theta 1}$, $C_{\theta 21}$, and $C_{\theta 22}$ are positive constants. The first term is the familiar turbulent-diffusivity representation.

We consider the heat diffusion in the mean flow with a nonvanishing shear,

$$\overline{\theta} = \overline{\theta}(x), \quad \overline{\mathbf{u}} = (0, \overline{v}(x), 0). \tag{4.30}$$

From Eq. (4.29), we have

$$H_{\theta x} = -C_{\theta 1} K \tau_C \frac{d\overline{\theta}}{dx}, \tag{4.31a}$$

$$H_{\theta y} = K \tau_C{}^2 (C_{\theta 21} - C_{\theta 22}) \frac{d\overline{v}}{dx} \frac{d\overline{\theta}}{dx}, \tag{4.31b}$$

$$H_{\theta z} = 0. \tag{4.31c}$$

We should note that the heat is transported in the direction normal to the mean temperature gradient, as is consistent with the observations [4/11]. This property is beyond the reach of the usual diffusivity representation.

4.2. One-fluid constant-density magnetohydrodynamic equations

We apply the ensemble averaging to Eq. (3.29) and have

$$\frac{\partial \overline{u}_i}{\partial t} + \frac{\partial}{\partial x_j} \overline{u}_i \overline{u}_j = -\frac{\partial}{\partial x_i} \left(\overline{p} + \left\langle \frac{\mathbf{B}'^2}{2} \right\rangle \right) + \left(\overline{\mathbf{j}} \times \overline{\mathbf{B}} \right)_i + \frac{\partial}{\partial x_j} \left(-R_{ij} \right) + \nu \nabla^2 \overline{u}_i, \tag{4.32}$$

where R_{ij} is the Reynolds stress of MHD flow defined by

$$R_{ij} = \left\langle u_i' u_j' \right\rangle - \left\langle B_i' B_j' \right\rangle. \tag{4.33}$$

Symbol R_{ij} has already been used in Eq. (4.4). We extend it to the MHD case and use the same symbol. The mean temperature $\overline{\theta}$ obeys the same equation as Eq. (4.27) with Eq. (4.28) as the turbulent heat flux $\mathbf{H}_\theta$.

The magnetic-field counterpart of Eqs. (4.32) is

$$\frac{\partial \overline{\mathbf{B}}}{\partial t} = \nabla \times \left(\overline{\mathbf{u}} \times \overline{\mathbf{B}} + \mathbf{E}_T \right) + \eta \nabla^2 \overline{\mathbf{B}}, \tag{4.34}$$

from Eq. (3.24), where $\mathbf{E}_T$ is called the turbulent electromotive force [2/1-2/6] and is defined by

$$\mathbf{E}_T = \langle \mathbf{u}' \times \mathbf{B}' \rangle. \tag{4.35}$$

The physical meaning of $\mathbf{E}_T$ becomes clear in light of Ohm's law. From Eq. (3.21) and replacement (3.28), we have

$$\bar{\mathbf{j}} = \frac{1}{\eta}\left(\overline{\mathbf{E}} + \mathbf{E}_T + \bar{\mathbf{u}} \times \overline{\mathbf{B}}\right). \tag{4.36}$$

Then $\mathbf{E}_T$ is the electric field generated by fluctuations, which has played a critical role in a long history of the investigation into stellar magnetic fields.

4.2.1. Algebraic representations for turbulent fluxes

In order to close Eqs. (4.32) and (4.34), we need to know the dependence of R_{ij} and $\mathbf{E}_T$ on the mean field. Their mathematical expressions may be obtained with resort to the procedures in § 4.1.1. In what follows, we give them in the same degree of approximation as the turbulent-viscosity representation, Eq. (4.12). The details of derivation are explained in Appendix A.1.

The turbulent fluxes are written as

$$\mathbf{E}_T = \alpha \overline{\mathbf{B}} - \beta \bar{\mathbf{j}} + \gamma \overline{\boldsymbol{\omega}}, \tag{4.37}$$

$$R_{ij} = \frac{2}{3} K_R \delta_{ij} - \nu_T \bar{s}_{ij} + \nu_M \overline{M}_{ij}, \tag{4.38}$$

with

$$K_R = \left\langle \frac{1}{2} \mathbf{u}'^2 \right\rangle - \left\langle \frac{1}{2} \mathbf{B}'^2 \right\rangle, \tag{4.39}$$

$$\overline{M}_{ij} = \frac{\partial \overline{B}_j}{\partial x_i} + \frac{\partial \overline{B}_i}{\partial x_j}, \tag{4.40}$$

and Eq. (4.13) as $\bar{s}_{ij}$ (K_R is named the turbulent residual energy). Dimensional coefficients α etc. are written as

$$\alpha = C_\alpha \tau_m H, \tag{4.41}$$

$$\beta = C_\beta \tau_m K, \tag{4.42}$$

$$\gamma = C_\gamma \tau_m W, \tag{4.43}$$

$$\nu_T = C_{\nu u} \beta, \tag{4.44}$$

$$\nu_M = C_{\nu B}\gamma, \tag{4.45}$$

in terms of the time scale characterizing the turbulent transport of momentum in MHD flow, τ_m, where C_α etc. are positive constants, and

$$H = -\langle \mathbf{u}' \cdot \boldsymbol{\omega}' \rangle + \langle \mathbf{B}' \cdot \mathbf{j}' \rangle, \tag{4.46}$$

$$K = \left\langle \frac{1}{2}\mathbf{u}'^2 \right\rangle + \left\langle \frac{1}{2}\mathbf{B}'^2 \right\rangle, \tag{4.47}$$

$$W = \langle \mathbf{u}' \cdot \mathbf{B}' \rangle. \tag{4.48}$$

Equations (4.46)-(4.48) are called the turbulent residual helicity, the turbulent MHD energy, and the turbulent cross helicity, respectively.

For the numerical coefficients, we may show

$$C_{\nu u} = C_{\nu B} = \frac{7}{5}, \tag{4.49a}$$

$$C_\beta \cong C_\gamma, \tag{4.49b}$$

by using an inhomogeneous-turbulence theory [4/12] and the numerical simulation [4/13], respectively.

The simplest choice of τ_m is

$$\tau_m = \frac{K}{\varepsilon}, \tag{4.50}$$

in correspondence to Eq. (4.15), where ε is the dissipation rate of K defined by

$$\varepsilon = \nu \left\langle \left(\frac{\partial u_j'}{\partial x_i} \right)^2 \right\rangle + \eta \left\langle \left(\frac{\partial B_j'}{\partial x_i} \right)^2 \right\rangle \tag{4.51}$$

[note that Eqs. (4.47) and (4.51) are the MHD extension of Eqs. (4.6) and (4.16), respectively].

The physical meaning of Eqs. (4.39) and (4.47) are clear. Specifically, the former represents the deviation from the equipartition of kinetic and magnetic energies. Equation (4.46) expresses the helical properties of flow and electric current, and Eq. (4.48) is an indicator of the degree of correlation between flow and magnetic field. We should note that the latter two are pseudoscalars.

The turbulent heat flux $\mathbf{H}_\theta$ is given by

$$\mathbf{H}_\theta = -C_{\theta 1}\tau_m(K+K_R)\nabla\bar{\theta}, \tag{4.52}$$

in the same degree of approximation as Eqs. (4.37) and (4.38), which corresponds to the first term in Eq. (4.29). No effect of the mean-magnetic field appears there. We include the terms corresponding to the second part in Eq. (4.29), and have

$$H_{\theta i} = -C_{\theta 1}\tau_m(K+K_R)\frac{\partial\bar{\theta}}{\partial x_i} + \tau_m{}^2(K+K_R)\left(C_{\theta 21}\bar{s}_{ij} + C_{\theta 22}\bar{\omega}_{ij}\right)\frac{\partial\bar{\theta}}{\partial x_j}$$

$$+\tau_m{}^2 W\left(D_{\theta 21}\bar{M}_{ij} + D_{\theta 22}\bar{J}_{ij}\right)\frac{\partial\bar{\theta}}{\partial x_j}, \tag{4.53}$$

where $D_{\theta 21}$ and $D_{\theta 22}$ are constants, and $\bar{J}_{ij}$ is the magnetic counterpart of $\bar{\omega}_{ij}$, which is defined by

$$\bar{J}_{ij} = \frac{\partial\bar{B}_j}{\partial x_i} - \frac{\partial\bar{B}_i}{\partial x_j} = \varepsilon_{ij\ell}\bar{j}_\ell. \tag{4.54}$$

We should note that the magnetic effects on $\mathbf{H}_\theta$ appear in the last part of Eq. (4.53).

4.2.2. Heuristic explanation for α, β and γ effects

The turbulent induction term or electromotive force $\mathbf{E}_T$ is written as Eq. (4.37). It is noticeable that it is linear with respect to $\bar{\mathbf{B}}$ and $\bar{\boldsymbol{\omega}}$. The nonlinear dependence on the latter may occur through coefficients α, β and γ.

A heuristic explanation about this apparent linearity may be explained as follows [2/9]. From Eq.(3.24), the fluctuation component of the magnetic field obeys

$$\frac{\partial\mathbf{B}'}{\partial t} = \nabla\times\left(\mathbf{u}'\times\bar{\mathbf{B}}\right) + \eta\nabla^2\mathbf{B}' + \mathbf{G}, \tag{4.55}$$

where

$$\mathbf{G} = \nabla\times\left(\mathbf{u}'\times\mathbf{B}' - \mathbf{E}_T\right), \tag{4.56}$$

in the absence of $\bar{\mathbf{u}}$. If the effect of $\mathbf{G}$ is negligible, $\mathbf{B}'$ is linear in $\bar{\mathbf{B}}$ for prescribed $\mathbf{u}'$. Then $\mathbf{E}_T$ is expanded as

$$E_{Ti} = \sum_j \alpha_{ij}\bar{B}_j + \sum_j \beta_{ij\ell}\frac{\partial\bar{B}_j}{\partial x_\ell} + \cdots. \tag{4.57}$$

When the turbulence spectrum is close to isotropic, we have

$$\mathbf{E}_T = \alpha\overline{\mathbf{B}} - \beta\nabla\times\overline{\mathbf{B}} + \cdots. \tag{4.58}$$

The current diffusion effect appears in the terms dependent on higher-order derivatives. Since the electric field and current density are polar vectors, whereas the magnetic field is an axial vector, Then α is a pseudo scalar, and β is a scalar.

This argument can be extended to the case in the presence of $\overline{\mathbf{u}}$. Neglecting $\mathbf{G}$ again, we have

$$\frac{\partial\mathbf{B}'}{\partial t} = \nabla\times(\overline{\mathbf{u}}\times\mathbf{B}') + \eta\nabla^2\mathbf{B}', \tag{4.59}$$

instead of Eq. (4.57). We use the formal solution of Eq. (4.59),

$$\mathbf{B}' = \left(\frac{\partial}{\partial t} - \eta\nabla^2\right)^{-1}\nabla\times(\overline{\mathbf{u}}\times\mathbf{B}'), \tag{4.60}$$

and have a formal expression

$$\mathbf{E}_T' = \left\langle \mathbf{u}'\times\left(\left(\frac{\partial}{\partial t} - \eta\nabla^2\right)^{-1}\nabla\times(\overline{\mathbf{u}}\times\mathbf{B}')\right)\right\rangle. \tag{4.61}$$

For prescribed $\mathbf{u}'$ and $\mathbf{B}'$, Eq. (4.61) is aslo linear in $\overline{\mathbf{u}}$ and is the origin of the γ effect.

4.2.3. Physical implications of turbulent-flux effects

The turbulence effect on the $\overline{\mathbf{B}}$ equation, $\mathbf{E}_T$, may be seen clearly in light of the mean Ohm's law, Eq. (4.36). From Eq. (4.37), it is written as

$$\overline{\mathbf{j}} = \frac{1}{\eta+\beta}\left(\mathbf{E} + \overline{\mathbf{u}}\times\overline{\mathbf{B}} + \alpha\overline{\mathbf{B}} + \gamma\overline{\boldsymbol{\omega}}\right). \tag{4.62}$$

From the combination $\eta+\beta$, the physical meaning of β [Eq. (4.42)] is clear. It is the magnetic counterpart of the turbulent viscosity ν_T and signifies the turbulent or anomalous magnetic diffusivity (simply called the turbulent resistivity) due to velocity and magnetic-field fluctuations [note on the dependence of β on K].

The α-related term is called the alpha effect or α dynamo [2/1-2/7], and its physical implication has been investigated in detail since the pioneering work by Parker [4/14]. The numerical analysis of Eq. (4.34) with the alpha and turbulent-resistivity effects embedded has been a central theme in the study of the kinematic dynamo.

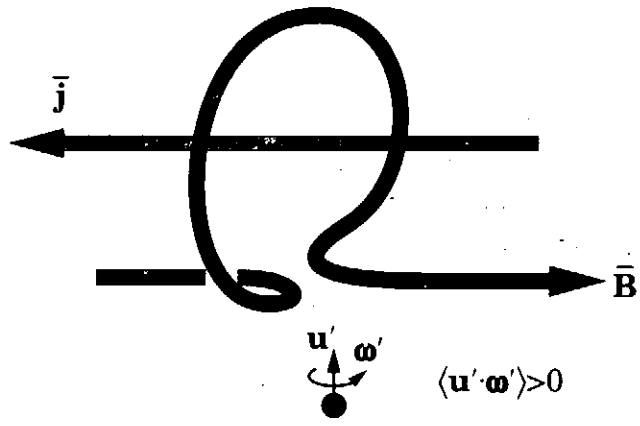

Fig. 4.2. Alpha or helicity dynamo.

From Eq. (4.62), the alpha effect generates $\bar{\mathbf{j}}$ aligned with $\bar{\mathbf{B}}$. This process makes a sharp contrast with the original process through $\bar{\mathbf{u}} \times \bar{\mathbf{B}}$ that results in $\bar{\mathbf{j}}$ perpendicular to $\bar{\mathbf{B}}$. The alpha effect arising from the turbulent kinetic helicity $\langle \mathbf{u}' \cdot \boldsymbol{\omega}' \rangle$ in H [Eq. (4.46)] is usually shown by Fig. 4.2. Such a simple illustrative explanation has not been given to the alpha effect by the turbulent current helicity $\langle \mathbf{B}' \cdot \mathbf{j}' \rangle$. The α dynamo consists of the contributions from these two helicities [4/15]. Which of these two helicity effects is dominant is highly dependent on phenomena concerned. In this context, we should recall the turbulent magnetic helicity $\langle \mathbf{A}' \cdot \mathbf{B}' \rangle$, that is, the other quantity expressing a helical property of magnetic fields, where the vector potential $\mathbf{A}'$ is related to $\mathbf{B}'$ as $\mathbf{B}' = \nabla \times \mathbf{A}'$.

The γ-related part in Eq. (4.62), which may be called the cross-helicity or γ dynamo, has been long missing in the dynamo study [2/8, 4/12, 4/16]. There $\bar{\mathbf{j}}$ aligned with $\bar{\boldsymbol{\omega}}$ occurs in the presence of W. This fact is equivalent to the occurrence of $\bar{\mathbf{B}}$ aligned with $\bar{\mathbf{u}}$ as long as the spatial variation of γ is neglected. The situation is illustrated in Fig. 4.3. In the transformation to the frame rotating with the angular velocity $\boldsymbol{\omega}_F$, $\bar{\boldsymbol{\omega}}$ is subject to the transformation

$$\bar{\boldsymbol{\omega}} \rightarrow \bar{\boldsymbol{\omega}} + 2\boldsymbol{\omega}_F, \tag{4.63}$$

which reduces Eq. (4.37) to

$$\mathbf{E}_T = \alpha \bar{\mathbf{B}} - \beta \bar{\mathbf{j}} + \gamma (\bar{\boldsymbol{\omega}} + 2\boldsymbol{\omega}_F). \tag{4.64}$$

Equation (4.64) indicates that the γ dynamo is sensitive to the frame rotation. In stellar magnetic fields, frame rotation is one of the ingredients strongly affecting their generation processes. In § 5.3.2.1, it will be discussed that this effect is closely related to the

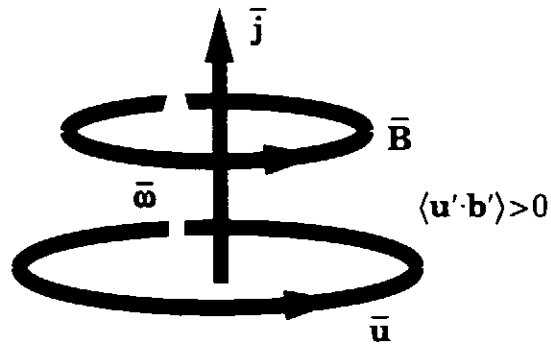

Fig. 4.3. Cross-helicity dynamo.

generation of the dipole component of the geomagnetic field aligned with the rotation axis. Then it is significant to pay attention to the effect.We substitute Eq. (4.38) into Eq. (4.32), and have

$$\frac{\partial \bar{u}_i}{\partial t} + \frac{\partial}{\partial x_j}\bar{u}_i\bar{u}_j = -\frac{\partial}{\partial x_i}\left(\bar{p} + \left\langle \frac{\mathbf{B}'^2}{2} \right\rangle + \frac{2}{3}K_R\right) + \left(\bar{\mathbf{j}} \times \bar{\mathbf{B}}\right)_i$$

$$+\frac{\partial}{\partial x_j}\left(\nu_T \bar{s}_{ij} - \nu_M \bar{M}_{ij}\right) + \nu \nabla^2 \bar{u}_i . \tag{4.65}$$

In order to grasp the essence of the turbulence effects on the mean MHD, we discard the spatial variation of ν_T and ν_M. Equation (4.65) is reduced to

$$\frac{\partial \bar{u}_i}{\partial t} + \frac{\partial}{\partial x_j}\bar{u}_i\bar{u}_j = -\frac{\partial}{\partial x_i}\left(\bar{p} + \left\langle \frac{\mathbf{B}'^2}{2} \right\rangle + \frac{2}{3}K_R\right) + \left(\bar{\mathbf{j}} \times \bar{\mathbf{B}}\right)_i$$

$$+\left(\nu + \nu_T\right)\nabla^2 \bar{u}_i - \nu_M \nabla^2 \bar{B}_i . \tag{4.66}$$

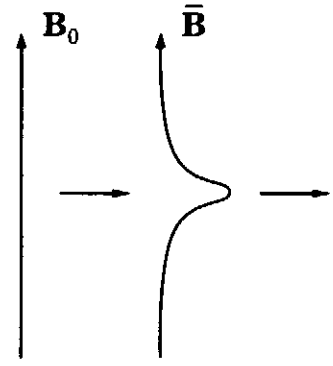

Fig. 4.4. Force by a distorted magnetic-field line.

In light of feedback effects of magnetic fields on fluid motion, we should note the following two points. One is that the alpha effect does not appear explicitly in $\bar{\mathbf{j}}\times\overline{\mathbf{B}}$. The cross-helicity term in $\bar{\mathbf{j}}$ may generate nonvanishing $\bar{\mathbf{j}}\times\overline{\mathbf{B}}$, as is clear from Eq. (4.62). The other is that the distortion of magnetic-field lines exerts force to the surrounding fluid through the last term related to the curvature of the lines. This situation is illustrated in Fig. 4.4. It suggests that the electric current with some specific spatial profile may drive plasmas from the relation

$$\nabla^2\overline{\mathbf{B}} = -\nabla\times\bar{\mathbf{j}}. \tag{4.67}$$

This point will be later discussed in light of the onset of the plasma rotation at an internal transport barrier that was referred to in § 2.3.2.

4.2.4. Turbulence equations for determining dynamo coefficients

In § 4.2.3, Eqs. (4.46)-(4.48) play an important role as the quantities characterizing a turbulent state of MHD flow. The last two, that is, K and W, obey the same form of equations

$$\frac{DZ}{Dt} = P_Z - \varepsilon_Z + \nabla\cdot\mathbf{T}_Z \quad (Z = K \text{ or } W), \tag{4.68}$$

where

$$P_K = -R_{ij}\frac{\partial\overline{u}_j}{\partial x_i} - \mathbf{E}_T\cdot\bar{\mathbf{j}}, \tag{4.69}$$

$$\varepsilon_K = \varepsilon, \tag{4.70}$$

$$\mathbf{T}_K = W\overline{\mathbf{B}} + \left\langle -\left(\frac{1}{2}\left(\mathbf{u}'^2+\mathbf{B}'^2\right)+\varpi'\right)\mathbf{u}' + (\mathbf{u}'\cdot\mathbf{B}')\mathbf{B}'\right\rangle$$

$$+\nu\nabla\left\langle\frac{\mathbf{u}'^2}{2}\right\rangle + \eta\nabla\left\langle\frac{\mathbf{B}'^2}{2}\right\rangle, \tag{4.71}$$

$$P_W = -R_{ij}\frac{\partial\overline{B}_j}{\partial x_i} - \mathbf{E}_T\cdot\overline{\boldsymbol{\omega}}, \tag{4.72}$$

$$\varepsilon_W = (\nu+\eta)\left\langle\frac{\partial u_j'}{\partial x_i}\frac{\partial B_j'}{\partial x_i}\right\rangle, \tag{4.73}$$

$$\mathbf{T}_W = K\overline{\mathbf{B}} + \left\langle -(\mathbf{u}'\cdot\mathbf{B}')\mathbf{u}' + \left(\frac{1}{2}\left(\mathbf{u}'^2+\mathbf{B}'^2\right)-\varpi'\right)\mathbf{B}'\right\rangle$$

$$+\nu\langle(\mathbf{B}'\cdot\nabla)\mathbf{u}'\rangle+\eta\langle(\mathbf{u}'\cdot\nabla)\mathbf{B}'\rangle, \tag{4.74}$$

with $\varpi = p+(\mathbf{B}^2/2)$. Here Eqs. (4.69) and (4.72) correspond to Eq. (4.9), and play the role of generating K and W by draining the energy and cross helicity from the mean field.

The turbulent residual helicity H does not obey a mathematically well-defined equation comparable to Eq. (4.68). This difference arises from the fact that the total amounts of MHD energy and cross helicity,

$$\int_V \frac{\mathbf{u}^2+\mathbf{B}^2}{2}dV,\ \int_V \mathbf{u}\cdot\mathbf{B}dV,$$

are conserved in the absence of molecular viscosity and resistivity, whereas the residual-helicity counterpart is not.

An important relationship between K and W is

$$\frac{|W|}{K}\le 1. \tag{4.75}$$

Here the left-hand side is proportional to $|\gamma|/\beta$ from Eqs. (4.42) and (4.43). This fact will later be quite instrumental to the estimate of the relative intensity of the generated magnetic field to the velocity of a flow.

4.2.5. Classification of mean-field dynamos

In the analytical investigation into the dynamo, statistical theories have been applied to the derivation of the turbulent electromotive force $\mathbf{E}_T$ [2/1, 2/3, 2/5, 2/6], unlike the heuristic method in § 4.2.1 and Appendix A.1, with little attention paid to the Reynolds stress R_{ij} [2/8, 4/3]. From the theoretical viewpoint, the magnetic dynamo may be classified into three categories, as in Table 4.1.

The mean-field dynamo started from the kinematic dynamo and still attracts much attention in the context of astronomical magnetic fields. There $\overline{\mathbf{u}}$ and the statistics of $\mathbf{u}'$ are prescribed, and generated $\mathbf{B}'$ gives rise to $\mathbf{E}_T$, on the basis of which the growth and sustainment of $\overline{\mathbf{B}}$ are examined. This approach will be explained in § 5.3.1.2.

In the counterkinematic dynamo, $\overline{\mathbf{B}}$ and the statistics of $\mathbf{B}'$ are prescribed. Resulting $\mathbf{u}'$ generates R_{ij}, determining $\overline{\mathbf{u}}$ through Eq. (4.32). Little attention, however, has been paid to such a process in the study of the mean-field dynamo. This dynamo is parts of the flow dynamo that will be discussed in § 6.

averaging procedure appropriate for the variable-density case is the mass-weighted or Favre averaging [4/17]. There the mean of a quantity f is defined by

$$\hat{f} = \frac{\langle \rho f \rangle}{\overline{\rho}} \equiv \{f\}_M, \quad f'' = f - \hat{f}. \tag{4.76}$$

We make the decomposition

$$\rho = \overline{\rho} + \rho', \quad \mathbf{u} = \hat{\mathbf{u}} + \mathbf{u}'', \quad p = \overline{p} + p'. \tag{4.77}$$

We perform the ensemble averaging of Eqs. (3.16) and (3.31)-(3.33), and have

$$\frac{\partial \overline{\rho}}{\partial t} + \frac{\partial}{\partial x_i}\overline{\rho}\hat{u}_i = 0, \tag{4.78}$$

$$\frac{\partial}{\partial t}\overline{\rho}\hat{u}_i + \frac{\partial}{\partial x_j}\overline{\rho}\hat{u}_i\hat{u}_j = -\frac{\partial \overline{p}}{\partial x_i} + \overline{\rho}_e\overline{E}_i + \frac{\partial}{\partial x_j}\left(-\overline{\rho}R_{Mij}\right) + \frac{\partial}{\partial x_j}\langle \mu s_{ij} \rangle, \tag{4.79}$$

$$\frac{\partial \overline{p}}{\partial t} + \frac{\partial}{\partial x_i}\overline{p}\hat{u}_i = \frac{\partial}{\partial x_i}\left(-P_i\right) - (\gamma - 1)\left\langle p\frac{\partial u_i}{\partial x_i}\right\rangle + \frac{\partial}{\partial x_i}\left\langle \kappa \frac{\partial}{\partial x_i}\frac{p}{C_V\rho}\right\rangle, \tag{4.80}$$

$$\frac{\partial}{\partial t}\overline{\rho}_e + \frac{\partial}{\partial x_i}\overline{\rho}_e\hat{u}_i = \frac{\partial}{\partial x_i}\left(-\Lambda_i\right), \tag{4.81}$$

with

$$R_{Mij} = \frac{\langle \rho u_i u_j \rangle - \overline{\rho}\hat{u}_i\hat{u}_j}{\overline{\rho}} = \frac{\langle \rho u_i'' u_j'' \rangle}{\overline{\rho}} \equiv \left\{u_i'' u_j''\right\}_M, \tag{4.82}$$

$$\mathbf{P} = \langle p\mathbf{u} \rangle - \overline{p}\hat{\mathbf{u}}, \tag{4.83}$$

$$\mathbf{\Lambda} = \langle \rho_e \mathbf{u} \rangle - \overline{\rho}_e\hat{\mathbf{u}}. \tag{4.84}$$

Here R_{Mij} is the mass-weighted Reynolds stress, and $\mathbf{P}$ is equivalent to the turbulent heat flux in the sense of mass-weighted averaging since

$$\mathbf{H}_{M\theta} = \{\theta''\mathbf{u}''\}_M = \frac{\mathbf{P}}{(\gamma - 1)C_V\overline{\rho}}, \tag{4.85}$$

from Eq. (3.20). In Eq. (4.81), we focused attention on the evolution of the charge density due to flow and discarded effects of the velocity difference between ion and electron gases.

Table 4.1. Classification of dynamos.

Typical dynamos	Physical processes
Kinematic dynamo	Given $\overline{\mathbf{B}}$ and $\mathbf{B}'$ $\Rightarrow$ $\mathbf{u}'$ $\Rightarrow$ R_{ij} $\Rightarrow$ $\overline{\mathbf{u}}$ through Eq. (4.32)
Counterkinematic dynamo	Given $\overline{\mathbf{B}}$ and $\mathbf{B}'$ $\Rightarrow$ $\mathbf{u}'$ $\Rightarrow$ R_{ij} $\Rightarrow$ $\overline{\mathbf{u}}$ through Eq. (4.32)
MHD dynamo	Given $\overline{\mathbf{u}}$, $\mathbf{u}'$, $\overline{\mathbf{B}}$, $\mathbf{B}'$ $\Rightarrow$ Feedback to $\mathbf{u}'$ and $\mathbf{B}'$ $\Rightarrow$ $\mathbf{E}_T$ and R_{ij} $\Rightarrow$ Feedback to $\overline{\mathbf{u}}$ and $\overline{\mathbf{B}}$ through Eqs. (4. 32) and (4.34) that affect the sustainment of a MHD turbulent state through Eq. (4.68)

The combination of the kinematic and counterkinematic dynamos leads to a closed loop of dynamo processes. The MHD dynamo corresponds to such combination and will be discussed in § 5.3.2. There Eq. (4.68) for the quantities characterizing MHD turbulence plays an important role.

4.3. Variable-density electrohydrodynamic equations

In the one-fluid MHD, the force due to the interaction between the magnetic field and the flow of charged particles was abstracted partially from the original two-fluid MHD. The electric field arising from the electrical nonneutrality is totally discarded there. In tokamaks, the electric field is linked with plasma rotation and plays a critical role in the suppression of heat and particle transports, as was noted in § 2.3.2. Then such an approximation is a big stumbling block in the study of transport barriers. The mass-density variation was also neglected in the one-fluid mean-field MHD given in § 4.2. In the confinement of fusion plasmas, however, the variation of mass density is closely associated with that of the pressure or the pressure gradient. The inclusion of mass-density variation is indispensable for the application of the mean-field method to the study of transport barriers.

4.3.1. Mass-weighted averaging

In order to supplement the one-fluid mean-field MHD, we consider the electrohydrodynamic (EHD) equations given in § 3.3. There electric-field and variable-density effects are explicitly taken into account, whereas magnetic-field effects are dropped. In a variable-density flow, the mean of the velocity $\mathbf{u}$ itself is physically less significant, and the momentum $\rho\mathbf{u}$ is a quantity much more intrinsic to fluid motion. The

As a quantity characterizing the intensity of turbulence, we consider the turbulent energy

$$K_M = \left\{ \frac{1}{2} \mathbf{u}''^2 \right\}_M . \tag{4.86}$$

It obeys

$$\frac{\partial}{\partial t} \bar{\rho} K_M + \frac{\partial}{\partial x_j} \bar{\rho} K_M \hat{u}_j = -\bar{\rho} R_{Mij} \frac{\partial \hat{u}_j}{\partial x_i} - \overline{u_i''} \frac{\partial \bar{p}}{\partial x_i} + \langle \rho_e' u_i'' \rangle \bar{E}_i$$

$$- \frac{\partial}{\partial x_i} \bar{\rho} \left\{ \frac{1}{2} \mathbf{u}''^2 u_i'' \right\}_M - \left\langle u_i'' \frac{\partial p'}{\partial x_i} \right\rangle . \tag{4.87}$$

Here the electric-field fluctuation and the molecular viscous effect were discarded since they are not necessary in subsequent discussions.

The primary difference between Eq. (4.87) and its constant-density counterpart, Eq. (4.7), lies in the second term on the right-hand side of the former. In the confinement of plasmas, the mean pressure gradient $\nabla \bar{p}$ is one of the key macroscopic quantities. Its effect on K_M occurs in the combination of $\overline{\mathbf{u}''}$, and the latter is a quantity intrinsic to a variable-density turbulent flow. Then the second term deserves special attention in light of the importance of the density and pressure gradients in tokamak plasmas.

4.3.2. Algebraic representations for turbulent fluxes

In the mean-field MHD, we derived the algebraic representations for some important turbulent fluxes by an intuitive approach, as in Appendix A.1. In the mean-field EHD, the turbulent fluxes are the third-order correlation function like Eq. (4.82) or are composed of two parts like Eqs. (4.83) and (4.84). As a result, such an intuitive approach is too complicated to abstract their expressions in a clear form. Then we derive algebraic representations for the turbulent fluxes with resort to a theory of inhomogeneous turbulence [4/18, 4/19]. Its procedures are given briefly in Appendix A.2.

We summarize the results used in subsequent discussions. They are given by

$$R_{Mij} = \frac{2}{3} K_M \delta_{ij} - C_{R1} \tau_e K_M \hat{s}_{ij} - C_{R2} \tau_e^2 \left(\bar{E}_i \frac{\partial \bar{\rho}_e}{\partial x_j} + \bar{E}_j \frac{\partial \bar{\rho}_e}{\partial x_i} \right), \tag{4.88}$$

$$P_i = -C_{P1} \tau_e K_M \nabla \bar{p} + C_{P2} \tau_e K_M \frac{\bar{p}}{\bar{\rho}} \nabla \bar{\rho} + C_{P3} \tau_e K_\rho \frac{\bar{p}}{\bar{\rho}^2} \frac{D\hat{\mathbf{u}}}{Dt}$$

$$+\tau_e^3 K_M\left(C_{P4}\frac{1}{\overline{\rho}}\frac{\partial\overline{p}}{\partial x_i}-C_{P5}\frac{\overline{p}}{\overline{\rho}^2}\frac{\partial\overline{\rho}}{\partial x_i}\right)\frac{\partial\overline{\rho}_e}{\partial x_i}\overline{\mathbf{E}}, \tag{4.89}$$

$$\overline{\mathbf{u}''}=C_{P2}\tau_e K_M\frac{1}{\overline{\rho}}\nabla\overline{\rho}+C_{P3}\tau_e K_\rho\frac{1}{\overline{\rho}^2}\frac{D\hat{\mathbf{u}}}{Dt}, \tag{4.90}$$

$$\langle\rho_e'\,\mathbf{u}''\rangle=-C_\Lambda\tau_e K_M\nabla\overline{\rho}_e, \tag{4.91}$$

where τ_e is the time scale characterizing the turbulent transports in EHD flow, K_ρ is the density variance

$$K_\rho=\langle\rho'^2\rangle, \tag{4.92}$$

and C_{R1} etc. are positive constants. Of these constants, we may show the relation

$$C_{P1}\cong C_{P2},\quad C_{P4}\cong C_{P5}. \tag{4.93}$$

From Eqs. (4.89) and (4.93), we may rewrite Eq. (4.85) as

$$\mathbf{H}_{M\theta}=-C_{P1}\tau_e K_M\nabla\hat{\theta}+C_{P3}\tau_e K_\rho\tau_e\frac{\hat{\theta}}{\overline{\rho}^2}\frac{D\hat{\mathbf{u}}}{Dt}+C_{P4}\tau_e^3 K_M\frac{1}{\overline{\rho}}\overline{\mathbf{E}}\frac{\partial\overline{\rho}_e}{\partial x_i}\frac{\partial\hat{\theta}}{\partial x_i}. \tag{4.94}$$

5. Spherical-Shell Dynamo

In a long history of dynamo study, the generation mechanism of magnetic fields in a spherical-shell region has been a central theme. Its typical instances are geomagnetic and solar fields. Both the fields occur through the motion of electrically-conducting fluids in a spherical-shell region, but their global behavior is quite different each other, as was noted in § 2.1.

5.1. One-fluid MHD model of stellar dynamo

The study of a spherical-shell dynamo started from the mean-field magnetic induction equation (4.34) under a prescribed velocity, which is combined with Eq. (4.37) (the cross-helicity effect is discarded). With the advance of a computer capability, the computer experiment based on the full one-fluid MHD equations has made a remarkable progress. Such an experiment was initiated for clarifying the characteristics of the solar magnetic field, as was represented by the works of Gilman [5/1, 5/2] and Glatzmaier [5/3]. Recently, much attention have been paid to understanding of the geodynamo since the works by Glatzmaier and Roberts [5/4, 5/5].

5.1.1. Fundamental equations

In the simulations of both the geodynamo and the solar dynamo, the thermal buoyancy force is a primary driver of the motion of fluids in the outer core and the convective zone. In the former, the temperature and velocity are much lower. In the current computer experiments mimicking the geodynamo, the buoyancy effect is often taken into account through the Boussinesq approximation (the density variation otherwise is neglected). This approximation is not sufficient for the simulation of the solar dynamo subject to large density and temperature changes.

The primary purpose of this section is to show some typical findings by the computer simulation of the geodynamo. We adopt the foregoing simplest approximation. Readers may consult the review by Roberts [5/6] for the works dealing with a non-Boussinesq approximation, a compositional buoyancy effect, a nonuniform heat-flux effect between the core and mantle, etc. The fundamental equations in the frame rotating with the angular velocity $\boldsymbol{\omega}_F$ are

$$\nabla \cdot \mathbf{u} = 0, \tag{5.1}$$

$$\frac{\partial u_i}{\partial t} + \frac{\partial}{\partial x_j} u_j u_i = -\frac{\partial p}{\partial x_i} + \nu \nabla^2 u_i + (\mathbf{j} \times \mathbf{B})_i + 2(\mathbf{u} \times \boldsymbol{\omega}_F)_i - \alpha_T (\theta - \theta_R) g_i, \tag{5.2}$$

$$\frac{\partial \theta}{\partial t} + \nabla \cdot (\theta \mathbf{u}) = \chi_\theta \nabla^2 \theta, \tag{5.3}$$

$$\frac{\partial \mathbf{B}}{\partial t} = \nabla \times (\mathbf{u} \times \mathbf{B}) + \eta \nabla^2 \mathbf{B}, \tag{5.4}$$

from Eqs. (3.24), (3.29), and (3.30). Here $\mathbf{u}$ denotes the velocity in the rotating frame and should be distinguished from $\mathbf{u}$ in the inertial frame. Moreover, p is the sum of the deviation from the static pressure and the centrifugal-force effect, α_T is the thermal-expansion coefficient, θ_R is the reference temperature, and $\mathbf{g}$ is the gravitational-acceleration vector.

5.1.2. Nondimensional parameters characterizing MHD flows

The importance of each term in Eqs. (5.2)-(5.4) changes greatly from one phenomenon to another. Various differences between the global properties of geomagnetic and solar fields arise from this situation. Representative nondimensional parameters are summarized in Table 5.1. There ℓ_R is the reference length, u_R is the reference velocity, $\Delta\theta_R$ is the reference temperature difference, and B_R is the reference magnetic field, respectively [2/14, 2/15, 5/7].

We are in a position to simply see the physical meanings of those nondimensional parameters. By $\{f\}_{\xi,\eta}$, we denote the magnitude of f that is estimated using quantities ξ and η. The Reynolds number signifies

Table 5.1 Nondimensional parameters

	Symbol	Definition
Reynolds number	R_e	$\ell_R u_R / \nu$
Taylor number	T_a	$(2\ell_R^2 \omega_F / \nu)^2$
Rayleigh number	R_a	$\alpha_T g \Delta\theta_R \ell_R^3 / (\nu\lambda_\theta)$
Prandtl number	P_r	ν / χ_θ
Magnetic Prandtl number	P_{rM}	ν / η
Magnetic Reynolds number	R_{eM}	$\ell_R u_R / \eta$
Peclet number	P_e	$\ell_R u_R / \chi_\theta$
Elsasser number	E_l	$B_R^2 / (2\ell_R u_R \omega_F)$

$$R_e = \frac{\{(\mathbf{u}\cdot\nabla)\mathbf{u}\}_{\ell_R,u_R}}{\{\nu\nabla^2\mathbf{u}\}_{\ell_R,u_R}}. \tag{5.5}$$

The Taylor number T_a comes from

$$T_a = \left(\frac{\{2\mathbf{u}\times\boldsymbol{\omega}_F\}_{u_R}}{\{\nu\nabla^2\mathbf{u}\}_{\ell_R,u_R}}\right)^2. \tag{5.6}$$

In short, it is the square of the Reynolds number based on velocity $\ell_R\omega_F$ and length ℓ_R.

The physical meaning of the Rayleigh number R_a may be explained as follows. We estimate the reference velocity u_R generated by the buoyancy force due to the temperature difference $\Delta\theta_R$ by

$$\{(\mathbf{u}\cdot\nabla)\mathbf{u}\}_{\ell_R,u_R} = \{\alpha_T(\theta-\theta_R)\mathbf{g}\}_{\Delta\theta_R}, \tag{5.7}$$

which gives

$$u_R = \sqrt{\alpha_T g\Delta\theta_R\ell_R}. \tag{5.8}$$

The Reynolds number related to this velocity is

$$R_e = \frac{\sqrt{\alpha_T g\Delta\theta_R\ell_R}\,\ell_R}{\nu}. \tag{5.9}$$

In the heat-transfer equation (5.3), the counterpart of R_e is called the Peclet number P_e, which is defined by

$$P_e = \frac{\{(\mathbf{u}\cdot\nabla)\theta\}_{\ell_R,u_R}}{\{\chi_\theta\nabla^2\theta\}_{\ell_R}}, \tag{5.10}$$

We may rewrite R_a as

$$R_a = R_eP_e = R_e{}^2P_r, \tag{5.11}$$

where P_r is the Prandtl number. In a flow subject to no thermal buoyancy force, the importance of the inertia term may be measured in the comparison with the viscous term. In a thermally buoyant flow, attention needs to be first paid to the temperature equation, where the relative importance of the inertia to diffusion terms is given by P_e. Afterwards, the relative importance of the inertia to viscous terms in the fluid equation is estimated by R_e. Their combination is expressed by the first relation in Eq. (5.11).

The magnetic Reynolds number R_{eM} and the Elsasser number E_f are defined by

$$R_{eM} = \frac{\{\nabla \times (\mathbf{u} \times \mathbf{B})\}_{f_R, u_R}}{\{\eta \nabla^2 \mathbf{B}\}_{f_R}} = R_e P_{rM}, \tag{5.12}$$

$$E_f = \frac{\{\mathbf{j} \times \mathbf{B}\}_{f_R, B_R}}{\{2\mathbf{u} \times \boldsymbol{\omega}_F\}_{u_R}}. \tag{5.13}$$

The importance of the magnetic Prandtl number P_{rM} will be discussed in light of the relative magnitude of the magnetic to kinetic energies in the geodynamo.

A nondimensional version of Eqs. (5.2)-(5.4) is helpful to understanding of the degree of importance of each term in various situations. It is given in Appendix B [see Eq. (B.4)].

For the outer core of the earth, we adopt [2/13]

$$\ell_R = O(10^6)\ \mathrm{m},\ \ \nu = O(10^{-6})\ \mathrm{m^2\ s^{-1}},\ \ u_R = O(10^{-4})\ \mathrm{m\ s^{-1}},$$

$$\lambda_\theta = O(10^{-6})\ \mathrm{m^2\ s^{-1}},\ \ \lambda_M = O(1)\ \mathrm{m^2\ s^{-1}}. \tag{5.14}$$

The nondimensional parameters corresponding to Eq. (5.14) are summarized in Table 5.2, with their counterparts for the sun.

Table 5.2. Magnitude of nondimensional parameters in the earth and sun.

	R_a	T_a	P_{rM}	R_e	P_r	R_{eM}
Earth	$O(10^{16})$	$O(10^{27})$	$O(10^{-6})$	$O(10^{8})$	$O(1)$	$O(10^{2})$
Sun	$O(10^{22})$	$O(10^{24})$	$O(10^{-4})$	$O(10^{10})$	$O(10^{2})$	$O(10^{6})$

From Table 5.2, the fluid motion in the outer core is highly turbulent, but the magnetic field is in a much more resistive state. From this fact, we are apt to consider that the energy of the magnetic field induced by the fluid motion is far smaller than the kinetic counterpart. Such a conjecture has been discussed in [5/8]. The real situation, however, is opposite, as may be seen from Table 2.1. This fact is one of the most mysterious properties of the geomagnetic field to be elucidated. Its understanding is one of the primary purposes in the present discussion about the geodynamo.

In the sun, the counterparts of Eq. (5.14) are highly dependent on a location in the convective zone and take a wide range of values. A typical set of parameters is shown in Table 5.2 [2/15, 5/9]. A prominent difference between the earth and sun indicates that the Coriolis force plays a much greater role in the motion of the earth's outer core.

5.1.3. Taylor-Proudman theorem and Busse column

When the Coriolis force is more influential than the thermal convection, there arises a characteristic structure. In Eq. (5.2), the dominance of $T_a^{1/2}$ over R_a leads to

$$2\mathbf{u} \times \boldsymbol{\omega}_F = \nabla p \tag{5.15}$$

[see Eq. (B.4)]. We take the curl of Eq. (5.15), and have

$$(\boldsymbol{\omega}_F \cdot \nabla)\mathbf{u} = 0. \tag{5.16}$$

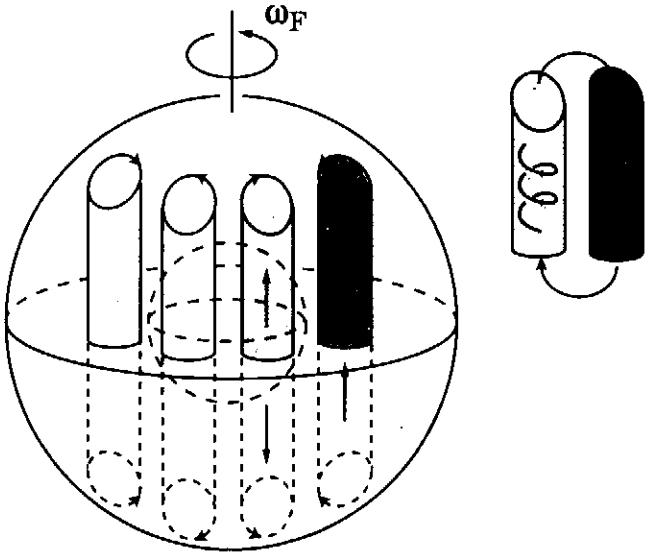

Fig. 5.1. Convection columns in a rotating spherical-shell region.

Equation (5.16) signifies that the fluid motion does not change along the axis of frame rotation. This finding is called the Taylor-Proudman theorem [5/7]. It brings quite interesting properties to the spherical-shell dynamo. There fluid is driven from the inner to outer parts of the outer core by the buoyancy force. From the theorem, a fluid blob rises or sinks along the rotation axis under the strong frame-rotation effect, as is illustrated in Fig. 5.1 (this point will be further referred to in § 5.2.2). Each vertical flow structure is called the convection column, and its formation mechanism has attracted much attention since the pioneering work by Busse [5/10] (see also [5/11] and the works cited therein).

5.2. Representative findings by computer experiments

The computer experiment of a spherical dynamo started for the solar magnetic field [5/1-5/3]. In subsequent works, however, more attention has been paid to the geodynamo, as was noted above [5/6, 5/12]. Then we shall mainly refer to some representative findings associated with the geodynamo.

5.2.1. Typical parameters for simulation

In the study of an electrically-nonconducting turbulent flow, the numerical simulation resolving all the spatial scales is named direct numerical simulation (DNS) [5/13, 5/14]. The finest scale in the constant-density case is the energy dissipation scale ℓ_D, which is related to the reference scale ℓ_R as [2/8, 4/4]

$$\frac{\ell_D}{\ell_R} = R_e^{-3/4}, \tag{5.17}$$

apart from a numerical factor, where R_e is defined in Table 5.1. For the DNS of a three-dimensional viscous flow, we need the number of grids

$$N = O\left(\left(\frac{\ell_R}{\ell_D}\right)^3\right) = O\left(R_e^{9/4}\right). \tag{5.18}$$

Then a flow with $R_e > O(10^5)$ is beyond the reach of a computer available at present even for geometrically simple flows such as channel turbulence.

In the strict sense of the DNS, R_e or R_a in the outer core is too large for the computer experiment. In the works done up to now, much smaller R_a and T_a are adopted with attention paid to their relative magnitude. The instances of R_a, T_a and P_{rM} are summarized in Table 5.3.

A prominent difference between the nondimensional parameters of the earth and those adopted in the geodynamo simulation lies in the magnetic Prandtl number P_{rM}, as is seen in Tables 5.2 and 5.3. The number in the outer core is far smaller than 1; namely, the magnetic field is much more diffusive than the momentum. In the geodynamo simulation, such small P_{rM} gives rise to a strong magnetic diffusion, and magnetic fields cannot be sustained stationarily.

The geodynamo simulation has been done with different sets of parameters, as is seen in Table 5.3. Then the details of findings differ from one to another, but some common features have been detected [5/6]. We shall mention some of such findings and discuss

Table 5.3. Magnitude of nondimensional parameters in computer experiments.

Authors	R_a	T_a	P_{rM}	Ref
Glatzmaier and Roberts	$O(10^7)$	$O(10^{12})$	500	[5/5]
Kageyama and Sato	$O(10^4)$	$O(10^6)$	$O(10) \sim O(10^2)$	[5/15]
Katayama *et al*	$O(10^3)$	$O(10^4)$	35	[5/16]
Olson *et al*	$O(10^2)$	$O(10^8)$	1 or 2	[5/17]
Ishihara and Kida	$O(10^4)$	$O(10^5)$	10	[5/18]

them from the viewpoint of the mean-field theory.

5.2.2. Convection column and magnetic field

One of the most prominent flow structures in a spherical-shell region is the occurrence of convection columns, as is depicted in Fig. 5.1. The number of columns is dependent on the nondimensional parameters adopted in the simulation. The columns occurs in pair. In one column, the fluid rotates in the same direction as the rotating shell and sinks from the column ends towards the equatorial plane. In the other, the fluid rises from the equatorial plane towards the ends, while rotating in the opposite direction. In both the columns, the kinetic helicity is negative in the northern hemisphere and positive in the southern hemisphere. Then the flow properties outside of the cylinder tangential to the inner core differ from those inside it. The poloidal field whose primary part is the dipole component is specifically strong near the location of each column. This fact indicates the close relationship between the helicity generation and the occurrence of the poloidal field aligned with the axis of the column in Fig. 5.1.

Here we should note the relationship of the convection columns with the mean-field theory. In the latter, we consider the quantities averaged in the ensemble sense, which are essentially equivalent to those averaged around the rotation axis. Then each column cannot be treated by the approach; namely, the motion related to each column is included in the velocity fluctuation $\mathbf{u}'$. What is really detectable by the theory is the resultant properties such as the turbulent helicity and the mean magnetic field. As has been confirmed by the computer simulation of the geomagnetic field, there is a high correlation between the poloidal field and the convection column. This fact indicates that the primary

component of the poloidal field, that is, the dipole field, can be abstracted through the averaging around the rotation axis.

The findings about the generation mechanism of the toroidal field are different among the computer experiments. The difference is highly dependent on the magnitude of T_a and R_a (for instance, see [5/17]). The former characterizing the occurrence of a column-like structure gives a preferred direction to a flow. The latter, on the other hand, is an indicator of the generation of velocity fluctuation. For increasing T_a with fixed R_a, the toroidal field tends to be generated by the convection columns. For decreasing T_a, it tends to arise from the poloidal field through the interaction with the axisymmetric differential rotation of flow.

5.2.3. Partition of energy

An interesting property common to almost all the geodynamo simulations is that the magnetic energy surpasses the kinetic energy of the fluid motion that is the generator of the former (see Table 2.1). This property is consistent with the geomagnetic field. In Alfven-velocity units, we have [2/13]

$$1 \text{ m s}^{-1} = 10^3 \text{ G}, \tag{5.19}$$

for the physical parameters

$$\rho = 0.8 \times 10^4 \text{ kg m}^{-3} \text{ (iron)}, \tag{5.20a}$$

$$\mu_0 = 1.3 \times 10^{-6} \text{ henry m}^{-1} \text{ (vacuum)}. \tag{5.20b}$$

The velocity in the outer core is inferred to be $O(10^{-4})$ m s^{-1}, which corresponds to $O(10^{-1})$ G. Then the energy of the toroidal magnetic field with the inferred strength $O(10)$ G is $O(10^4)$ times the kinetic energy of fluid motion.

The findings by the computer experiments about the energy ratio should be viewed with some caution. In the geomagnetic field, the magnetic Prandtl number P_{rM} is far smaller than 1, as in Table 5.2. Then the magnetic field is much more dissipative than the velocity. Nevertheless, the magnetic energy much larger than the kinetic energy is stored in the outer core. This situation is quite mysterious as well as the reversal of magnetic polarity, as was noted in § 5.1.2. In the computer experiments, P_{rM} needs to be larger than 1, for the sustainment of the generated magnetic field. For instance, the magnetic field grows for $P_{rM} > 10$ in [5/15]. Then the magnetic field is less dissipative (P_{rM} is smallest in [5/17]). In the present computer ability, we cannot adopt T_a so large to ensure the sustainment of magnetic field for $P_{rM} << 1$. Whether the foregoing conclusion about

the energy ratio is insensitive to the magnitude of P_{rM} or not is left for a very interesting future work.

5.2.4. Reversal of polarity

The reversal of magnetic polarity was first reproduced in the simulation by Glatzmaier and Roberts [5/4], followed by several studies such as [5/19]. Its occurrence is highly dependent on MHD models, the magnitude of nondimensional parameters, the heat flux imposed over the core-mantle boundary, etc. (for instance, see [5/20]). This theme is under an intensive study.

5.2.5. Other prominent features

As a mathematical property observable in various simulations, we may mention the relative magnitude of the Lorentz to Coriolis forces, which is called the local Elsasser number. In a spherical-shell region, the Coriolis force gives a preferred direction along the rotation axis to the flow. On the other hand, the Lorentz force arising from the generated field is not along this direction in general and tends to break the directional constraint due to the Coriolis force. In the actual simulations, the two forces often balance each other [5/6]. In other words, the magnetic and flow structures possessing the local Elsasser number close to one is stable in a MHD sense.

Th solar dynamo is the other representative spherical-shell dynamo, but its MHD computer experiments are much less, compared with the geodynamo (the simulation based on the mean-field dynamo will be mentioned later). In § 2.1, we have already noted that the prominent differences between the solar convective zone and the earth's outer core are the relative width of the shell to the inner zones as well as the magnitude of T_a and R_a. The relative width of the shell region is much narrower in the sun, suggesting the decrease in the importance of a convection-column flow structure. In addition, smaller $T_a^{1/2} / R_a$ enhances this situation.

A primary interest of the solar dynamo is the temporal behavior of the toroidal field that is the origin of sunspots, and the resulting magnetic-field cycle. Most of sunspots are confined to the belts between the equator and latitude $\pm 35^\circ$ [2/15]. In the polarity cycle, the number of sunspots decreases from the maximum to minimum, and then increases to the maximum. This temporal evolution constitutes the so-called butterfly diagram of sunspots, as is shown in Fig. 2.5 [2/18].

The pioneering computer experiments based on the MHD equations were made by Gilman [5/1, 5/2] and Glatzmaier [5/3]. These works clarified the important role of differential rotation around the rotation axis in the generation process of the toroidal

magnetic field and in the relationship with the solar cycle. The details of the magnetic field and flow are not in agreement with observations. The recent developments in the helioseismology provide a detailed information about the flow field such as the radial profile of the angular velocity [2/18, 2/19, 5/21], as is shown in Fig. 2.6. It is difficult to perform the computer experiment with large R_a and R_{eM} shown in Table 5.2 and reproduce the results consistent with those observations. This is considered to be one of the reasons why few computer experiments have recently been done for the solar dynamo in spite of the recent advance of a computable capability.

5.3. Mean-field dynamo

We are in a position to discuss on the relationship of the mean-field MHD with computer experiments and observations. The fundamental equations are given by Eqs. (4.34), (4.37), (4.38), and (4.66) (the spatial variation of the coefficients was discarded in the last). In the frame rotating with the angular velocity $\boldsymbol{\omega}_F$, they are written as

$$\frac{\partial \overline{\mathbf{B}}}{\partial t} = \nabla \times \left(\overline{\mathbf{u}} \times \overline{\mathbf{B}} + \alpha \overline{\mathbf{B}} - \beta \overline{\mathbf{j}} + \gamma \left(\overline{\boldsymbol{\omega}} + 2 \overline{\boldsymbol{\omega}}_F \right) \right), \tag{5.21}$$

$$\frac{\partial \overline{u}_i}{\partial t} + \frac{\partial}{\partial x_j} \overline{u}_i \overline{u}_j = -\frac{\partial}{\partial x_i} \left(\overline{p} + \left\langle \frac{\mathbf{B}'^2}{2} \right\rangle + \frac{2}{3} K_R \right)$$

$$+ 2 \left(\overline{\mathbf{u}} \times \boldsymbol{\omega}_F \right)_i + \left(\overline{\mathbf{j}} \times \overline{\mathbf{B}} \right)_i + \nu_T \nabla^2 \overline{u}_i - \nu_M \nabla^2 \overline{B}_i, \tag{5.22}$$

where the molecular viscous and resistive effects were dropped, and the centrifugal force was included in $\overline{p}$.

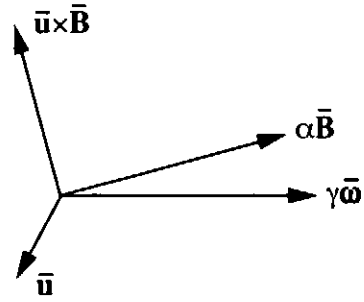

Fig. 5.2. Three terms of induction.

A global magnetic-field generation may be described by a stationary solution of Eqs. (5.21) and (5.22). The stationary balance in Eq. (5.21) may occur under

$$\beta \overline{\mathbf{j}} = \overline{\mathbf{u}} \times \overline{\mathbf{B}} + \alpha \overline{\mathbf{B}} + \gamma \left(\overline{\boldsymbol{\omega}} + 2 \boldsymbol{\omega}_F \right). \tag{5.23}$$

That is, the enhanced Ohmic dissipation term $\beta\bar{\mathbf{j}}$ balances with some or all of $\bar{\mathbf{u}}\times\bar{\mathbf{B}}$, $\alpha\bar{\mathbf{B}}$ and $\gamma(\bar{\boldsymbol{\omega}}+2\boldsymbol{\omega}_F)$. These induction terms are illustrated in Fig. 5.2.

The state where the Hall effect $\bar{\mathbf{u}}\times\bar{\mathbf{B}}$ is dominant has been studied in conjunction with the direct electricity conversion from plasma flow. The state with dominant $\alpha\bar{\mathbf{B}}$ is called the Woltejar state or Taylor state. The state with dominant $\gamma\bar{\boldsymbol{\omega}}$ may be called the rotation-dominant state. First, the former state will be explained under the name of alpha or α dynamo. The latter is then explained under the name of cross-helicity or γ dynamo. It is shown a posteriori that the $\bar{\mathbf{u}}\times\bar{\mathbf{B}}$ induction term is not effective in the steady-state solution of the mean-field MHD dynamo since there is a tendency for $\bar{\mathbf{B}}$ to be aligned with $\bar{\mathbf{u}}$.

5.3.1. Alpha dynamo

We neglect the cross-helicity effect in Eq. (5.21), and have

$$\frac{\partial\bar{\mathbf{B}}}{\partial t}=\nabla\times\left(\bar{\mathbf{u}}\times\bar{\mathbf{B}}+\alpha\bar{\mathbf{B}}-\beta\bar{\mathbf{j}}\right). \tag{5.24}$$

We consider the situation that the turbulent-helicity effect is so dominant to balance with the turbulent resistivity effect. There the quasi-stationary state of $\bar{\mathbf{B}}$ obeys

$$\bar{\mathbf{j}}=\frac{\alpha}{\beta}\bar{\mathbf{B}}. \tag{5.25}$$

This is a typical magnetic-field generation process of the α dynamo and is depicted schematically in Fig. 4.2.

5.3.1.1. Two typical dynamo processes

In the coordinate system illustrated in Fig. 5.3, we make the decomposition into the toroidal and poloidal components

$$\bar{\mathbf{u}}=\bar{u}_\phi\mathbf{e}_\phi+\bar{\mathbf{u}}_P\ , \tag{5.26}$$

$$\bar{\mathbf{B}}=\bar{B}_\phi\mathbf{e}_\phi+\bar{\mathbf{B}}_P, \tag{5.27}$$

with

$$\overline{\mathbf{u}}_P = \overline{u}_r \mathbf{e}_r + \overline{u}_\theta \mathbf{e}_\theta, \tag{5.28}$$

$$\overline{\mathbf{B}}_P = \overline{B}_r \mathbf{e}_r + \overline{B}_\phi \mathbf{e}_\phi = \nabla \times \left(\overline{A}_\phi \mathbf{e}_\phi \right), \tag{5.29}$$

where $\mathbf{e}_r$, $\mathbf{e}_\theta$, and $\mathbf{e}_\phi$ are three unit vectors in the spherical coordinates, and $\overline{A}_\phi$ is the toroidal component of the mean vector potential $\overline{\mathbf{A}}$.

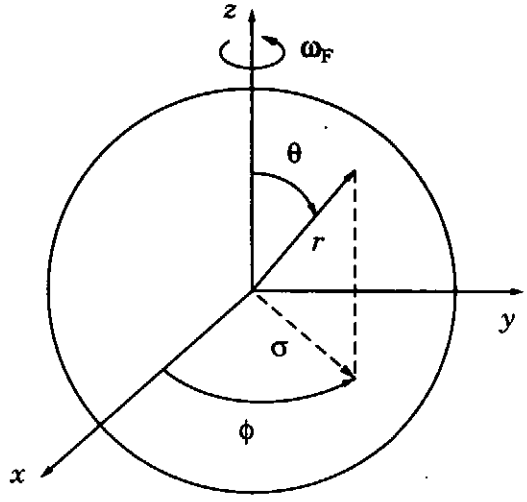

Fig. 5.3. Spherical and cylindrical coordinate systems.

From Eq. (5.24), we have [2/15]

$$\frac{\partial \overline{B}_\phi}{\partial t} + \sigma(\overline{\mathbf{u}}_P \cdot \nabla)\frac{\overline{B}_\phi}{\sigma} = \alpha\left(\nabla \times \overline{\mathbf{B}}_P\right)_\phi + \sigma\left(\overline{\mathbf{B}}_P \cdot \nabla\right)\frac{\overline{u}_\phi}{\sigma} + \beta\left(\nabla^2 - \frac{1}{\sigma^2}\right)\overline{B}_\phi, \tag{5.30}$$

$$\frac{\partial \overline{A}_\phi}{\partial t} + \frac{1}{\sigma}(\overline{\mathbf{u}}_P \cdot \nabla)(\sigma \overline{A}_\phi) = \alpha \overline{B}_\phi + \beta\left(\nabla^2 - \frac{1}{\sigma^2}\right)\overline{A}_\phi. \tag{5.31}$$

On the right-hand side of Eq. (5.30), we have two terms generating $\overline{B}_\phi$. The first term expresses the combination of the α dynamo and the Ampere law. In the second term, $\overline{u}_\phi / \sigma$ is the angular velocity. Then the term represents the generation of $\overline{B}_\phi$ from $\overline{\mathbf{B}}_P$, owing to the differential rotation or spatially varying $\overline{u}_\phi / \sigma$. In Eq. (5.31), the first term or the α dynamo on the right-hand side is the sole generator of $\overline{A}_\phi$, that is, $\overline{\mathbf{B}}_P$ [see Eq. (5.29)]. This fact confirms the computer-experiment result showing the close relationship between the poloidal field and a column-like structure generating helicity effects.

According to the relative importance of the two terms in Eq. (5.30), we have two typical magnetic-field generation mechanisms [2/1-2/6, 2/15]:

Alpha-Alpha (α^2) dynamo

$$\overline{\mathbf{B}}_P \rightarrow \overline{B}_\phi \text{ (Ampere law and alpha effect)}$$

$$\rightarrow \overline{\mathbf{B}}_P \text{ (alpha effect and Ampere law);} \tag{5.32}$$

Alpha-Omega ($\alpha - \omega$) dynamo

$$\overline{\mathbf{B}}_P \rightarrow \overline{B}_\phi \text{ (differential rotation)}$$

$$\rightarrow \overline{\mathbf{B}}_P \text{ (alpha effect and Ampere law);} \tag{5.33}$$

Equation (5.25) is the most typical manifestation of the α^2 dynamo.

5.3.1.2. Examination of kinematic dynamo

The approach based on Eq. (5.24) with prescribed $\overline{\mathbf{u}}$ is called the kinematic dynamo that was simply referred to in § 4.2.5. In the context of stellar dynamo, it was applied to the study of the solar cycle and the butterfly diagram of sunspots. Some of their primary characteristics were reproduced successfully with a proper choice of $\overline{\mathbf{u}}$ [2/26, 2/27].

In the computer experiments in § 5.2, increasing T_a with fixed R_a leads to a distinct column-like structure, signifying the increase in the importance of helicity effects. This situation corresponds to the dominance of the first over second terms on the right-hand side of Eq. (5.30). There the generation of global magnetic fields may be interpreted with the aid of the α^2 dynamo. On the other hand, with increasing R_a, the computer experiments suggest the increase in the importance of the differential rotation. Such a state is attributed to the $\alpha - \omega$ dynamo.

A shortfall of the kinematic dynamo is that the magnitude of $\overline{\mathbf{B}}$ cannot be determined within the framework of Eq. (5.24) linear in $\overline{\mathbf{B}}$. For resolving this shortfall, we have two approaches. One approach is the inclusion of a nonlinear effect on the α-dynamo coefficient so that

$$\alpha = \alpha\left(\overline{\mathbf{B}}\right) \rightarrow 0 \quad \text{as} \quad \left|\overline{\mathbf{B}}\right| \rightarrow \infty. \tag{5.34}$$

The effect is called the alpha quenching [5/22] (see § 7.1.1 for more details), and its theoretical derivation is one of the important themes in the study of kinematic dynamo [5/23-5/26]. To incorporate the Hall term proportional to $\mathbf{j} \times \mathbf{B}$ into Ohm's law was also proposed for bringing the nonlinearity to the magnetic-induction equation (3.24) [5/27].

The cross-helicity effect may be interpreted as the contribution of the mean velocity, specifically, its vorticity $\overline{\boldsymbol{\omega}}$, to $\mathbf{E}_T$ that cannot be described explicitly in terms of the alpha effect. The contribution of the mean velocity shear was also presented, and its effect on the instability of the mean field was examined [5/28].

The computer experiments mimicking the geodynamo show two typical features, as has already been noted. One is that the local Elsasser number or the ratio of the Lorentz to Coriolis forces is close to 1, and the other is that the energy of generated magnetic field is much larger than the kinetic energy. At present, it is not known whether the inclusion of the quenching effect really leads to the reproduction of these features, specifically, the former, since it is not dependent explicitly on the frame-rotation effect.

The other approach to the determination of the magnitude of $\overline{\mathbf{B}}$ is the combination with the mean-velocity equation (5.22) with the cross-helicity effect dropped. It is proper in light of discussing the relationship with the Elsasser number. The alpha effect is characterized by Eq. (5.25), which results in vanishing of the Lorentz force, namely,

$$\bar{\mathbf{j}} \times \overline{\mathbf{B}} = 0. \tag{5.35}$$

The field expressed by Eq. (5.25) is called the force-free field. It plays an important role in the study of relaxation processes of plasmas such as reversed-field pinches in fusion [2/20, 2/21, 5/29]. Owing to this property, the alpha effect on the mean-flow equation (5.22) is weak. Then to explain the finding by the computer experiments about the local Elsasser number is an important theme of the α dynamo.

5.3.2. Alpha/cross-helicity dynamo

We retain the cross-helicity effects in Eqs. (5.21) and (5.22), and discuss about the mean-field dynamo.

5.3.2.1. Relevance to geodynamo

5.3.2.1.A. Why is the primary poloidal field the dipole component?

With the stationary property of the geodynamo in mind, we examine Eq. (5.23). We pay attention to the finding by the computer experiments about the local Elsasser number, and consider that three effects, that is, the helicity, turbulent-resistivity, and cross-helicity effects, balance one another [2/8, 5/30]. Then a stationary state is attained by

$$\bar{\mathbf{j}} = \frac{\alpha}{\beta}\overline{\mathbf{B}} + \frac{\gamma}{\beta}\left(\overline{\boldsymbol{\omega}} + 2\boldsymbol{\omega}_F\right) \equiv \frac{\alpha}{\beta}\overline{\mathbf{B}} + 2\frac{\gamma}{\beta}\boldsymbol{\omega}_F \ . \tag{5.36}$$

Here we have attached more importance to the frame-rotation effect than to the mean vorticity. The drop of $\overline{\mathbf{u}} \times \overline{\mathbf{B}}$ will be guaranteed by the subsequent discussion. Equation (5.36) gives

$$\overline{\mathbf{j}} \times \overline{\mathbf{B}} = -2\frac{\gamma}{\beta}\overline{\mathbf{B}} \times \boldsymbol{\omega}_F. \tag{5.37}$$

We substitute Eq. (5.37) into Eq. (5.22), and have

$$\frac{\partial \overline{u}_i}{\partial t} + \frac{\partial}{\partial x_j}\overline{u}_i\overline{u}_j = -\frac{\partial}{\partial x_i}\left(\overline{p} + \left\langle \frac{\mathbf{B}'^2}{2} \right\rangle + \frac{2}{3}K_R\right)$$

$$+ 2\left(\overline{\mathbf{u}} \times \boldsymbol{\omega}_F\right)_i - 2\frac{\gamma}{\beta}\left(\overline{\mathbf{B}} \times \boldsymbol{\omega}_F\right)_i + \nu_T \nabla^2 \overline{u}_i - \nu_T \nabla^2\left(\frac{\gamma}{\beta}\overline{B}_i\right). \tag{5.38}$$

On the right-hand side, the third term comes from the Lorentz force or Eq. (5.37), and $\nu_T \nabla^2 \overline{\mathbf{u}}$ represents the enhancement of the momentum diffusion by fluctuations. Such diffusion is detrimental to the duration of an ordered structure of magnetic fields. Their tension of magnetic field lines tends to resist against the deformation by fluid motion, as is seen from Eq. (4.67). The last term corresponds to this action.

We consider that a specific ordered magnetic-field profile is sustained in a spherical-shell region. For the duration of this profile, the diffusion effect due to $\nu_T \nabla^2 \overline{\mathbf{u}}$ needs to be canceled out or weakened by some other effect. Its candidate is the last term in Eq. (5.38); namely, we put

$$\overline{\mathbf{B}} = \frac{\beta}{\gamma}\overline{\mathbf{u}}, \tag{5.39}$$

which guarantees vanishing of $\overline{\mathbf{u}} \times \overline{\mathbf{B}}$ dropped previously.

The curl of Eq. (5.38) gives

$$\frac{\partial \overline{\boldsymbol{\omega}}}{\partial t} = \nabla \times \left(2\left(\overline{\mathbf{u}} - \frac{\gamma}{\beta}\overline{\mathbf{B}}\right) \times \boldsymbol{\omega}_F + \nu_T \nabla^2\left(\overline{\mathbf{u}} - \frac{\gamma}{\beta}\overline{\mathbf{B}}\right)\right). \tag{5.40}$$

From Eq. (5.39), we have

$$\frac{\partial \overline{\boldsymbol{\omega}}}{\partial t} = 0, \tag{5.41}$$

which shows that the velocity field is also in the stationary state. Then Eq. (5.39) is a simple but relevant form of the stationary solution of the dynamical equation for the velocity field.

Equation (5.37) together with Eq. (5.39) gives an interesting suggestion to the structure of the geomagnetic field within the framework of the mean-field MHD. Equation (5.39) provides the relation $\overline{\boldsymbol{\omega}} = (\gamma/\beta)\overline{\mathbf{j}}$. From its combination with the first relation in Eq. (5.36), the equation that describes the magnetic field is expressed as

$$\left(1-\frac{\gamma^2}{\beta^2}\right)\nabla\times\overline{\mathbf{B}}-\frac{\alpha}{\beta}\overline{\mathbf{B}}=2\frac{\gamma}{\beta}\boldsymbol{\omega}_F. \tag{5.42}$$

Equation (5.42) shows that the strong solid-body rotation acts as a drive for the magnetic-field structure formation. There the magnetic field is apt to be aligned with $\boldsymbol{\omega}_F$. Coefficients α and γ are pseudo scalars. Then the main part of $\overline{\mathbf{B}}$ could have the same up-down symmetry with $\boldsymbol{\omega}_F$. Such symmetry property allows the occurrence of a dipole-field component. This result is an answer by the mean-field theory to the question: *Why is the primary poloidal field the dipole component?*

We should note that the coefficient $1-\gamma^2\beta^{-2}$ is positive definite since the inequality $|W|/K \le 1$ leads to $\gamma^2\beta^{-2} \le 1$ from Eqs. (4.42), (4.43) and (4.49b). In the case of $\gamma^2\beta^{-2} << 1$, Eq. (5.42) is simplified as

$$\nabla\times\overline{\mathbf{B}}-\frac{\alpha}{\beta}\overline{\mathbf{B}}=2\frac{\gamma}{\beta}\boldsymbol{\omega}_F. \tag{5.43}$$

Equation (5.43) shows that the sustained magnetic field is described by the superimposition of the inhomogeneous solution linearly dependent on $\boldsymbol{\omega}_F$ and a homogeneous solution. From Eqs. (5.39) and (5.43), we may perform an order estimate as

$$|\overline{\mathbf{B}}| = \frac{\ell_C}{\sqrt{1+\ell_C{}^2(\alpha/\beta)^2}}\left|\frac{\gamma}{\beta}\boldsymbol{\omega}_F\right|, \tag{5.44a}$$

$$|\overline{\mathbf{u}}| = \frac{\ell_C}{\sqrt{1+\ell_C{}^2(\alpha/\beta)^2}}\left|\left(\frac{\gamma}{\beta}\right)^2\boldsymbol{\omega}_F\right|, \tag{5.44b}$$

where ℓ_C is a characteristic length of fluctuations such as the radius of a convection column.

According to the balance of the left hand side of Eq. (5.43), we are led to an estimate of $\ell_C \cong |\beta/\alpha|$. The proposition that the differential flow velocity is much smaller than the solid-body rotation velocity, $|\bar{\mathbf{u}}| << |\ell_C \boldsymbol{\omega}_F|$, is attributed to the condition

$$\left(\frac{\gamma}{\beta}\right)^2 << 1. \tag{5.45}$$

For the dipole magnetic field, the inhomogeneous solution gives an estimate

$$|\bar{\mathbf{B}}_{\text{dipole}}| \cong \left|\left\langle\frac{\gamma}{\alpha}\right\rangle_{\text{outer}} \boldsymbol{\omega}_F\right|, \tag{5.46}$$

where $\langle\cdot\rangle_{\text{outer}}$ denote the volume average over the outer core.

The global value of $\langle\gamma/\alpha\rangle_{\text{outer}}$ is determined from turbulent fluctuations. Let us make a further conjecture about the relation between $\langle\gamma/\alpha\rangle_{\text{outer}}$ and the local value γ/α. We may consider that γ/α has a constant value in one column, but that it has a different constant value in the other column. The number of columns, N, are estimated as $N \cong (r_O/\ell_C)^2$, where r_O is the width of the outer core. In case that each column has a completely independent value of γ/α, the lower bound of $\langle\gamma/\alpha\rangle_{\text{outer}}$ for large N may be estimated as

$$\left\langle\frac{\gamma}{\alpha}\right\rangle_{\text{outer}} \cong \frac{1}{\sqrt{N}}\left|\frac{\gamma}{\alpha}\right|, \tag{5.47}$$

from the law of large numbers. This might provide a lower bound of the dipole magnetic field. At the present stage of geodynamo study, the relationship between N and the nondimensional parameters such as R_e and T_a is not known at all. Once this relationship is obtained, the foregoing finding paves the way for estimating the relationship between the dipole-field strength and the nondimensional parameters.

It is noteworthy that Eq. (5.39) shows the balance between the Coriolis and Lorentz forces in Eq. (5.38), that is,

$$\text{local } E_\ell \text{ (Elsasser number)} = 1. \tag{5.48}$$

This result is answer to the question presented by the computer experiments [5/6]: *Why do the Lorentz and Coriolis forces tend to balance each other?*

5.3.2.1.B. Why does the magnetic energy surpass the kinetic energy?

We are now in a position to refer to the other important finding by the computer experiments, that is, the ratio of the magnetic to kinetic energies. From Eqs. (4.42) and (4.43), we may write

$$r_E = \frac{\overline{\mathbf{B}}^2/2}{\overline{\mathbf{u}}^2/2} \cong \left(\frac{K}{W}\right)^2, \tag{5.49}$$

where use has been made of Eq. (5.39) as well as the estimate by the numerical simulation of the MHD equations that $C_\beta \cong C_\gamma$ [4/13].

For $|W|/K$, we have an important constraint, that is, inequality (4.75). This quantity is an indicator of the strength of the correlation between magnetic field and velocity. The inequality $|W|/K \leq 1$ gives

$$r_E \geq 1. \tag{5.50}$$

In the system of the alpha/cross-helicity or $\alpha - \gamma$ dynamo, the magnetic energy is predicted to be larger than the kinetic energy of fluid motion. For instance, we have

$$\frac{|W|}{K} = 0.1 \rightarrow r_E \cong 10^2. \tag{5.51}$$

In the outer core, the magnetic Prandtl number P_{rM} is far smaller than 1, as is shown in Table 5.2, suggesting that the correlation is not so strong. Then it is highly probable that r_E becomes much larger than 1, as is consistent with the computer experiments. This is an answer by the mean-field theory to the question: *Why does the magnetic energy surpass the kinetic energy?*

5.3.2.2. Relevance to solar dynamo

In light of the width relative to the inner region with no fluid motion, the solar convective zone is much narrower than the earth's outer core (see Figs. 2.2 and 2.3), leading to the decrease in the role of convection columns along the rotation axis. Moreover, $T_a^{1/2}/R_a$ is smaller in the zone, as is seen from Table 5.2 [see also Eq. (B.4)]. These two facts suggest a smaller role of helicity effects in the convective zone, compared with the outer core.

With these situations taken into account, we assume that the turbulent-resistivity and cross-helicity effects are dominant in Eq. (5.23), and also drop $\overline{\mathbf{u}} \times \overline{\mathbf{B}}$ (this point will be mentioned below) [2/8, 5/31]. Then we have

$$\overline{\mathbf{j}} = \frac{\gamma}{\beta}(\overline{\boldsymbol{\omega}} + 2\boldsymbol{\omega}_F), \tag{5.52}$$

According to the balance of the left hand side of Eq. (5.43), we are led to an estimate of $\ell_C \cong |\beta/\alpha|$. The proposition that the differential flow velocity is much smaller than the solid-body rotation velocity, $|\overline{\mathbf{u}}| << |\ell_C \boldsymbol{\omega}_F|$, is attributed to the condition

$$\left(\frac{\gamma}{\beta}\right)^2 << 1. \tag{5.45}$$

For the dipole magnetic field, the inhomogeneous solution gives an estimate

$$\left|\overline{\mathbf{B}}_{\text{dipole}}\right| \cong \left|\left\langle\frac{\gamma}{\alpha}\right\rangle_{\text{outer}} \boldsymbol{\omega}_F\right|, \tag{5.46}$$

where $\langle\cdot\rangle_{\text{outer}}$ denote the volume average over the outer core.

The global value of $\langle\gamma/\alpha\rangle_{\text{outer}}$ is determined from turbulent fluctuations. Let us make a further conjecture about the relation between $\langle\gamma/\alpha\rangle_{\text{outer}}$ and the local value γ/α. We may consider that γ/α has a constant value in one column, but that it has a different constant value in the other column. The number of columns, N, are estimated as $N \cong (r_O/\ell_C)^2$, where r_O is the width of the outer core. In case that each column has a completely independent value of γ/α, the lower bound of $\langle\gamma/\alpha\rangle_{\text{outer}}$ for large N may be estimated as

$$\left\langle\frac{\gamma}{\alpha}\right\rangle_{\text{outer}} \cong \frac{1}{\sqrt{N}}\left|\frac{\gamma}{\alpha}\right|, \tag{5.47}$$

from the law of large numbers. This might provide a lower bound of the dipole magnetic field. At the present stage of geodynamo study, the relationship between N and the nondimensional parameters such as R_e and T_u is not known at all. Once this relationship is obtained, the foregoing finding paves the way for estimating the relationship between the dipole-field strength and the nondimensional parameters.

It is noteworthy that Eq. (5.39) shows the balance between the Coriolis and Lorentz forces in Eq. (5.38), that is,

$$\text{local } E_\ell \text{ (Elsasser number)} = 1. \tag{5.48}$$

This result is answer to the question presented by the computer experiments [5/6]: *Why do the Lorentz and Coriolis forces tend to balance each other?*

5.3.2.1.B. Why does the magnetic energy surpass the kinetic energy?

$$n = \begin{cases} O\left(10^{32}\right) \text{ m}^{-3} \text{ in the core,} \\ O\left(10^{23}\right) \text{ m}^{-3} \text{ in the photosphere.} \end{cases} \tag{5.59}$$

The inequality (5.58) for the lower limit of plasma density is satisfied in the interior of the sun.

With $n = O(10^{32})$ m^{-3}, Eq. (5.57) requires $|W|/K \geq O(10^{-4})$. In the convective zone, hydrogen gases are highly ionized, and both the Reynolds and Magnetic Reynolds numbers are large. These circumstances indicate that the correlation between velocity and magnetic field is high. If we adopt an order estimate

$$\frac{|W|}{K} = O\left(10^{-1}\right), \tag{5.60}$$

Eq. (5.56) gives

$$n = O\left(10^{28}\right) \text{ m}^{-3}, \tag{5.61}$$

which is a reasonable estimate of the number density of hydrogen in the convective zone in light of Eq. (5.59).

In the above discussions, the bulk velocity plays a key role, and no explicit effect of the differential rotation occurs. This point seems to contradict the importance of the differential rotation in the solar dynamo. This is not the case. In the γ dynamo, W is critically important. Its sustainment or generation is made by the production term in Eq. (4.68), P_W, which is defined by Eq. (4.72). In the present case, it is given by

$$P_W = -R_{ij}\frac{\partial \overline{B}_j}{\partial x_i} - \mathbf{E}_T \cdot \left(\overline{\boldsymbol{\omega}} + 2\boldsymbol{\omega}_F\right). \tag{5.62}$$

Under Eq. (5.52) with the alpha effect dropped, $\mathbf{E}_T$ vanishes [see Eq. (4.64)], leading to

$$P_W = \frac{\gamma}{\beta}\nu_T\left(1 - \left(\frac{\gamma}{\beta}\right)^2\right)\left(\sigma\left(\frac{\partial}{\partial\sigma}\frac{\overline{u}_\phi}{\sigma}\right)^2\right) \cong \frac{\gamma}{\beta}\nu_T\left(\sigma\left(\frac{\partial}{\partial\sigma}\frac{\overline{u}_\phi}{\sigma}\right)^2\right), \tag{5.63}$$

from Eqs. (4.38) and (5.53). Equation (5.63) does not vanish in the presence of the differential rotation or nonvanishing $\partial(\overline{u}_\phi/\sigma)/\partial\sigma$. Namely the differential rotation is closely related to the generation of W. In short, the toroidal field in the γ dynamo is generated by the combination of the bulk and differential rotation. The relevance to the solar polarity change may be discussed with the aid of the $\alpha - \gamma$ dynamo [5/30].

5.3.2.3. Selection of structure

From the considerations on the geodynamo and the solar dynamo, the differences between established magnetic fields may be stated as follows. First of all, the solid-body rotation in the earth is dominant over the differential rotation. Then the uniform angular velocity $\boldsymbol{\omega}_F$ plays a distinctive role in sustaining the dipole magnetic field. In the sun, the differential velocity cannot be neglected, compared with the mean rotation velocity, and the dynamics of flow is not separable from $\boldsymbol{\omega}_F$. As a result, the local helical structures of the magnetic field and flow dominate, and the magnetic field does not simply point to the direction of $\boldsymbol{\omega}_F$.These results are summarized in Fig. 5.4.

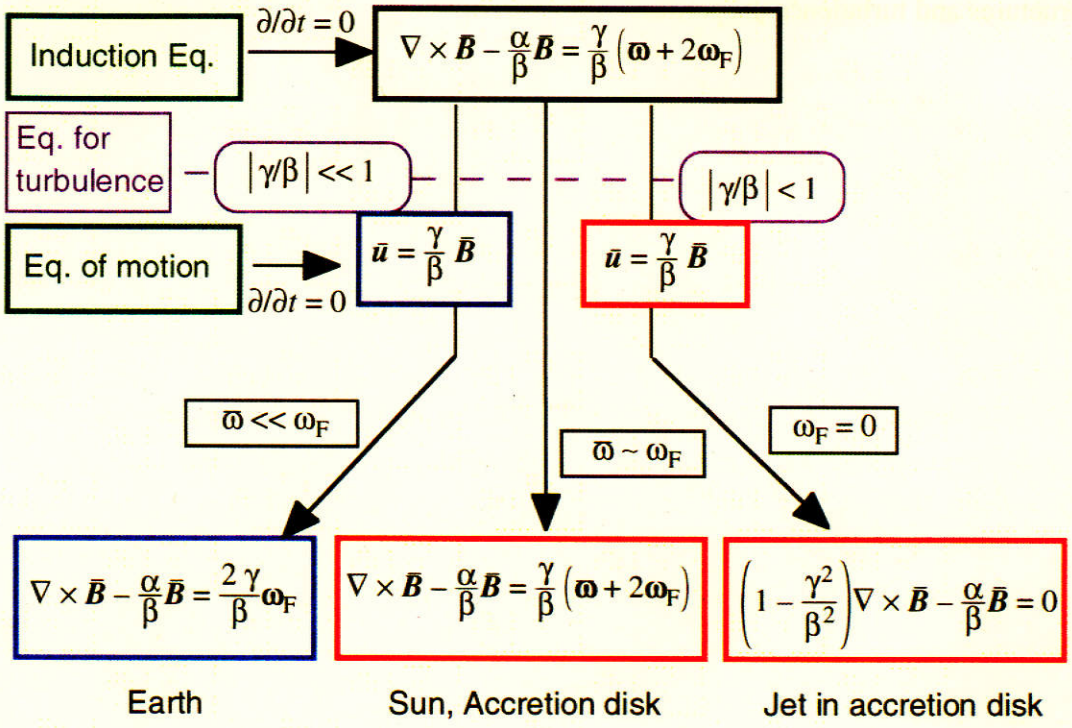

Fig. 5.4. Equations that describe the magnetic fields in the earth, sun and accretion disk (accretion disk is explained in § 6).

With the foregoing logic advanced one step further, the differential flow must be determined self-consistently within the framework of the mean-field theory. In this aspect, the governing parameter is the coefficient ratio γ/β. In the case of small γ/β, the differential-rotation velocity is much smaller than the solid-body counterpart. For γ/β closer to unity, on the other hand, the differential-rotation velocity is comparable to the mean velocity. The global structure of an established magnetic field is dictated by the ratio γ/β, which is nearly equal to W/K. These points are also shown in Table 2.4.

It is considered that a large difference between P_r and P_{rM} keep the magnetic-field and flow fluctuations, $\mathbf{B}'$ and $\mathbf{u}'$, from being in phase. Then the ratio W/K is considered to be small in the earth (see Table 5.2). In the sun, the difference between P_r and P_{rM} is about hundred times smaller than the difference in the earth, and hydrogen gases are highly ionized. This situation is favorable for a higher correlation between $\mathbf{B}'$ and $\mathbf{u}'$ or a larger value of W/K. This may give a partial answer to the question: *Why do the global properties of magnetic fields differ so much in the earth and the sun?*

A key factor in the quest for the structure formation in the magnetic dynamo is, as a whole, the mechanism that determines the ratio γ/β or W/K. This fact points to one direction of the future dynamo research: the simultaneous pursuit of magneto-flow structures and turbulence properties.

6. Flow Generation by Electromagnetic Effects

The primary interest in the dynamo study lies in clarifying how coherent magnetic-field structures are generated by turbulent motion, irrespective of the computer experiment based on the full MHD equations or the mean-field method. It is needles to say that the proper treatment of the mutual interaction between magnetic field and flow is necessary for understanding of the generation processes. In some phenomena, more attention is paid to how a coherent flow is driven by electromagnetic effects. The mechanism of flow generation may be called the flow dynamo in contrast to the magnetic dynamo or the dynamo with stress on the magnetic-field generation. In this section, we shall discuss about the former.

6.1. Accretion disks

In accretion disks, the magnetic dynamo plays multiple roles. The key issue in accretion disks is the transportation of angular momentum. If the angular momentum of a part of disk is conserved, this part continues to perform the Keplerian motion. There the gravitational potential is bounded by the lower and upper boundaries, depending on the initial condition of the orbit, and the gravitational potential cannot be released. When the angular momentum can be exchanged between different parts of the disk, the accretion is allowed to go on and the gravitational energy is released.

The angular momentum is considered to be transported in two ways. One is based on the anomalous viscosity. This makes the rotation closer to the rigid rotation, allowing a release of gravitational energy. In this process, the origin of turbulence that generates the anomalous viscosity is considered to be magneto-rotational instability [6/1, 6/2]. A brief account of the instability is given in Appendix C. In the other process, the angular momentum is lost through a formation of jet. The generation of the jet is due to the magnetic field at the disk. In either cases, magnetic and flow dynamos are the key for the evolution of an accretion disk.

We first survey the jet formation and then refer to the effect of anomalous viscosity.

6.1.1. Computer simulation of bipolar jets

The computer experiment of bipolar jets based on the full MHD equations was started from the pioneering works by Uchida and Shibata [6/3-6/6], being followed by the works with boundary conditions improved, resistivity effects explicitly included, etc. [6/6-6/9]. A comprehensive review about linear and nonlinear phenomena in accretion disks is given in [6/10].

A standard tool for the jet-formation mechanism is a system of compressible MHD equations,

$$\frac{\partial \rho}{\partial t} + \nabla \cdot (\rho \mathbf{u}) = 0, \tag{6.1}$$

$$\frac{\partial}{\partial t} \rho u_i + \frac{\partial}{\partial x_j} \rho u_i u_j = -\frac{\partial p}{\partial x_i} + (\mathbf{j} \times \mathbf{B})_i + \frac{\partial \Phi}{\partial x_i}, \tag{6.2}$$

$$\frac{\partial B}{\partial t} = \nabla \times (\mathbf{u} \times \mathbf{B}) + \eta \nabla^2 \mathbf{B}, \tag{6.3}$$

$$\frac{\partial}{\partial t} \rho \zeta + \nabla \cdot (\rho \zeta \mathbf{u}) = -p \nabla \cdot \mathbf{u} + \frac{1}{\sigma_0} \mathbf{j}^2, \tag{6.4}$$

where Φ is the gravitational potential

$$\Phi = -\frac{GM}{r} \tag{6.5}$$

(G and M are the gravitational constant and the mass of a central object, respectively), and the internal energy ζ is related to p as Eq. (3.20).

In most of the jet simulations, the viscosity is not included explicitly in Eq. (6.2), and its effects occur through the numerical dissipation in a computational scheme. On the other hand, more attention is paid to resistivity effects. This point is closely related to the reconnection of magnetic field lines that is a cause of the deriving force for jets, as will be later referred to. The jet simulation is computationally heavy. Then the dependence of a quantity on the azimuthal or ϕ coordinate (see Fig. 5.3) is often dropped, although the ϕ component of a vector is kept. Such a simulation is called a 2.5-dimensional simulation. An example of the computer simulation is given in Fig. 6.1.

The fundamental idea for the jet formation is the sweeping magnetic twist mechanism advocated by Uchida and Shibata [6/3- 6/5]. There the poloidal magnetic field threading through the equatorial plane of a disk is regarded as primordial. Under the gravitational force expressed by the last term in Eq. (6.2), gases accrete onto the central object, while rotating. Then magnetic field lines are carried into the inner part of the disk and, at the same time, are twisted owing to the differential rotation, leading to the generation of the toroidal component of the magnetic field. This process corresponds to the generation of the toroidal field in the $\alpha - \omega$ dynamo in § 5.3.1.1.

The reconnection of magnetic-field lines due to the differential rotation drives gases in the directions normal to the disk. This fact means that the magnitude of the resistivity has

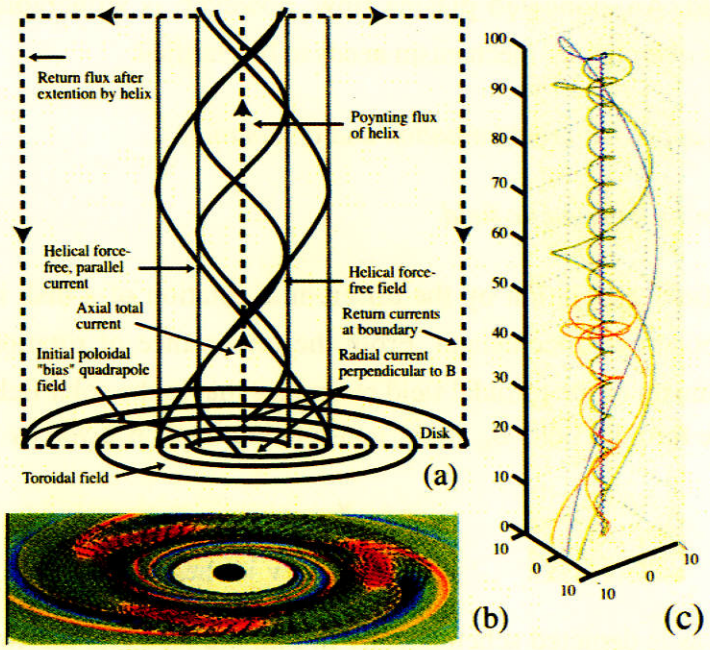

Fig. 6.1. Helix generated by the dynamo in the disk [2/31]: (a) Footprints of the external quadruple field lines; (b) Surface of the disk; (c) Force-free helix.

a big influence on the reconnection processes through the spatial scale of reconnection. It was confirmed by the simulation [6/11] that the jet occurrence is quasi-stationary at a low magnetic Reynolds number R_{eM}, but that it becomes intermittent with increasing R_{eM}. In the sweeping magnetic twist mechanism, the poloidal field generating the toroidal field through the reconnection is presumed to be primordial. It is interesting to clarify whether the primordial poloidal field is sufficient or the regeneration of the poloidal field is necessary for the continuation of jet formation.

In the current computer experiments, less attention is focused on the collimation of jets that is the other striking structural feature, compared with the jet formation. This situation is due to the shortage of the capability of a computer available now. We need a large computational domain for the simultaneous treatment of the near and far regions of a disk and the resulting long computing time. The current simulation indicates that the magnetic field of a helical profile exerts influence on the collimation of jets near the disk.

The jet-collimation mechanism has been long examined by analytical methods. Readers may consult [2/33] for a detailed survey of their developments. There much attention is not paid to turbulence effects enhancing the growth of jet width. One of the most familiar models for the collimation mechanism is the jet confinement by the global strong toroidal

or azimuthal field. An elongated plasma flow, however, is vulnerable to MHD kink instability, and its overcoming mechanism needs to be clarified.

6.1.2. Mean-field approach to jet formation and collimation

6.1.2.1. Accretion-disk magnetic field

The toroidal-field generation by the differential rotation of a disk is critical in the sweeping magnetic twist mechanism. From the importance of rotational motion, the generation mechanism of the toroidal field resembles that in the solar field discussed in § 5.3.2.2. There the toroidal field $\overline{B}_\phi$ in the non-rotating frame is given by

$$\overline{B}_\phi = \frac{\gamma}{\beta}\overline{u}_\phi, \tag{6.6}$$

from Eq. (5.53), as is depicted schematically in Fig. 6.2 (see Fig. 5.3 for the coordinate system). The disk is geometrically symmetric with respect to the equatorial plane. Then $\overline{B}_\phi$ is antisymmetric since the turbulent cross helicity W in γ is a pseudoscalar and antisymmetric.

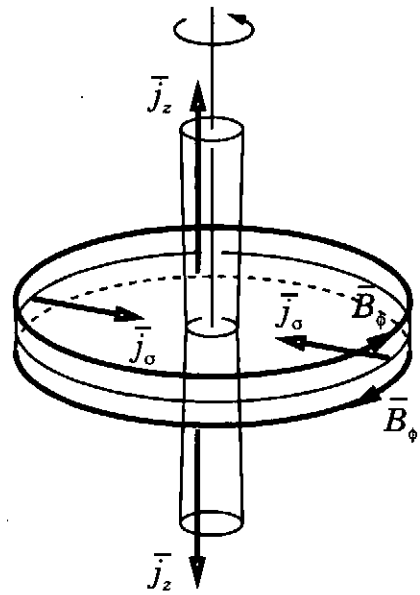

Fig. 6.2. Toroidal field and radial current in a disk.

6.1.2.2. Ejection of jets

We investigate a jet-occurrence mechanism on the basis of Eq. (6.6). Antisymmetric $\overline{B}_\phi$ generates the radial current $\overline{j}_\sigma$ towards the center of the disk. We denote the radius and width of the disk by R_D and h_D, respectively. From the Ampere law, we have

$$4\pi R_D \overline{B}_\phi(R_D) = J_D \equiv 2\pi R_D h_D \overline{j}_\sigma(R_D). \tag{6.7}$$

As long as this current goes near the center and then flows along the rotation axis, we have

$$2\pi\sigma\overline{B}_{\phi}(\sigma) = \frac{J_D}{2}, \tag{6.8}$$

at location σ, which results in

$$\frac{\overline{B}_{\phi}(\sigma)}{\overline{B}_{\phi}(R_D)} = \frac{R_D}{\sigma}. \tag{6.9}$$

Equation (6.9) signifies that $\overline{B}_{\phi}$ is highly enhanced near the center of the disk. In case that this magnetic energy is dominant over the gravitational energy, the gases may overcome the gravitational force and escape from the disk. The location at which two energies are balanced, σ_b, is determined by

$$\frac{1}{2}\overline{B}_{\phi}(\sigma_b)^2 = \Phi(\sigma_b). \tag{6.10}$$

The jet speed may be estimated on the basis of Eqs. (6.6), (6.9), and (6.10) [6/12, 6/13].

An elongated plasma flow such as a jet is vulnerable to MHD kink instability. The confinement mechanism of a jet was discussed in light of the suppression of the instability due to a small-scale toroidal field [6/14]. There the stress due to the tangled magnetic fields exerts an inward force, contributing to the jet confinement.

The recent observation [6/15] confirms that the magnetic field inside a jet is of a helical form, indicating that the jet itself is in helical motion, that is, it flows while rotating. In the sense of an elongated helical flow structure, the jet is quite similar to one of the convection columns in the outer core that have been examined in depth by the computer experiment of the geomagnetic field. In the column, the helicity effects become important in the poloidal-field generation, as was noted in § 5.2.2. This fact suggests the relevance of the poloidal field to the jet collimation.

We now refer to the jet-collimation mechanism from the mean-field viewpoint. There we put an emphasis on a poloidal field or the field along the jet [2/8, 6/16]. In the first relation of Eq. (5.36), we drop the $\boldsymbol{\omega}_F$-related term, and have

$$\overline{\mathbf{j}} = \frac{\alpha}{\beta}\overline{\mathbf{B}} + \frac{\gamma}{\beta}\overline{\boldsymbol{\omega}}. \tag{6.11}$$

Equation (6.11) is founded on vanishing of $\overline{\mathbf{u}} \times \overline{\mathbf{B}}$ that will be guaranteed later.

The equation of motion gives another relation that describes the state subject to the generated magnetic field. We rewrite Eq. (4.66) as

$$\frac{\partial \bar{\mathbf{u}}}{\partial t} = -\nabla\left(\bar{p} + \frac{1}{2}\bar{\mathbf{u}}^2 + \left\langle\frac{\mathbf{B}'^2}{2}\right\rangle + \frac{2}{3}K_R\right)$$

$$+\bar{\mathbf{u}}\times\bar{\boldsymbol{\omega}} + \bar{\mathbf{j}}\times\bar{\mathbf{B}} + \nu_T\nabla^2\bar{\mathbf{u}} - \nu_M\nabla^2\bar{\mathbf{B}}, \tag{6.12}$$

and substitute Eq. (6.11) into Eq. (6.12). We take the curl of the resulting equation, and have

$$\frac{\partial\bar{\boldsymbol{\omega}}}{\partial t} = \nabla\times\left(\left(\bar{\mathbf{u}} - \frac{\gamma}{\beta}\bar{\mathbf{B}}\right)\times\bar{\boldsymbol{\omega}}\right) + \nu_T\nabla\times\left(\nabla^2\bar{\mathbf{u}} - \nabla^2\left(\frac{\gamma}{\beta}\bar{\mathbf{B}}\right)\right). \tag{6.13}$$

The turbulent diffusion effect arising from the $\nabla^2\bar{\mathbf{u}}$-related part in Eq. (6.12) is a primary ingredient causing the growth of jet width. Its vanishing is necessary for the jet collimation. This condition on Eq. (6.13) is the same as Eq. (5.39), that is,

$$\bar{\mathbf{u}} = \frac{\gamma}{\beta}\bar{\mathbf{B}}, \tag{6.14}$$

which also guarantees vanishing of the first part on the right-hand side and $\bar{\mathbf{u}}\times\bar{\mathbf{B}}$, and leads to

$$\frac{\partial\bar{\boldsymbol{\omega}}}{\partial t} = 0. \tag{6.15}$$

Equation (6.14) together with Eq. (6.11) leads to a stationary state for both the magnetic field and vorticity.

We substitute Eq. (6.14) into Eq. (6.11), and have the screened-alpha dynamo

$$\bar{\mathbf{j}} = \frac{1}{1-(\gamma/\beta)^2}\frac{\alpha}{\beta}\bar{\mathbf{B}} \cong \frac{\alpha}{\beta}\bar{\mathbf{B}}. \tag{6.16}$$

An approximation

$$\bar{\mathbf{j}} = \frac{\alpha}{\beta}\bar{\mathbf{B}}$$

may be obtained from Eqs. (4.42) and (4.43) as well as $|W|/K < 1$. The solution of Eq. (6.16) in the cylindrical configuration is known well in the context of the RFP torus [2/20, 2/21]. Equation (6.16) with Eq. (6.14) constitutes a system of homogenous

differential equations. The magnitude of the magnetic field and flow is determined by external conditions such as the specified total angular-momentum and mass fluxes.

In short, the magnetic field and flow obeying Eqs. (6.14) and (6.16) are free from the diffusion effects in both the magnetic and flow equations. In the jet, the flow component along it is primary, although it is swirling. Equation (6.14) signifies that the poloidal field is the main component of the magnetic field inside the jet. This field resists against the bending of the jet and contributes to keeping a straight shape. These processes are an explanation of the jet-collimation mechanism by the $\alpha - \gamma$ dynamo and are summarized in Table 2.4.

The presence of a magnetic field allows instability to occur, as is explained in Appendix C. In light of the instability, the present picture signifies that the magneto-rotational instability and magnetic field in the accretion disk are self-sustaining. The disk subject to the Keplerian motion is stable against various kinds of hydrodynamic perturbations. Once the magnetic field exists, the magneto-rotational instability can grow, generating turbulence that is an origin of the dynamo. The disk magnetic field is sustained by the dynamo action. When the generated magnetic field becomes strong enough, plasmas are ejected in the direction of the rotation axis, resulting in bipolar jets. In the jets, the magnetic field together with the flow field obeys the structure described by the Taylor relaxation state.

6.1.3. Anomalous diffusion of angular momentum

The magnetic field due to the dynamo plays an important role in sustaining the turbulent viscosity that transports the angular momentum in the radial direction [2/35, 6/10, 6/17]. The research in this direction has been flourishing and is briefly surveyed [6/18].

By dimensional consideration, the turbulent viscosity was proposed by Shakura and Sunyaev [2/34] in the form

$$\nu_T = \alpha_{SS} \frac{{c_S}^2}{\varpi}, \tag{6.17}$$

where c_S is the sound speed, ϖ is the rotation frequency of the disk, and α_{SS} is a nondimensional coefficient. In the accretion disk, the motion in the equatorial plane is dominated by the centrifugal force, i.e., $c_S << \varpi\sigma$ (see Fig. 6.2 for the coordinate system). Equation (6.17) has a resemblance to the Bohm diffusion

$$\nu_{\text{Bohm}} = \frac{1}{16}\frac{c_S^2}{\omega_{CI}}, \tag{6.18}$$

where ω_{CI} is the ion cyclotron frequency in the presence of confining magnetic fields.

Once the turbulence viscosity is prescribed, the transport rate of angular momentum may be calculated. The time of angular-momentum loss, i.e., the confinement time of angular momentum, is evaluated as $\tau_{\text{am}}^{-1} \equiv \nu_T \sigma^{-2}$. By use of Eq. (6.17), we have

$$\tau_{\text{am}} \cong \frac{1}{\alpha_{SS}}\frac{\varpi\sigma^2}{c_S^2}. \tag{6.19}$$

The rotation number $\varpi\tau_{\text{am}}$, which denotes the number of rotation around the gravitational center before the accretion, is given by

$$\varpi\tau_{\text{am}} \cong \frac{1}{\alpha_{SS}}\frac{\varpi^2\sigma^2}{c_S^2}. \tag{6.20}$$

Then $\varpi\tau_{\text{am}} >> 1$ represents the situation that plasma elements circumnavigate the gravitational center many times before the accretion. We consider that the motion in a portion of disk is close to the Keplerian motion

$$\varpi \propto \sigma^{-3/2}. \tag{6.21}$$

Equation (6.20) gives $\varpi\tau_{\text{am}} \propto \sigma^{-1}$, which may becomes large with decreasing σ. At such σ, the gases are subject to a slow inward motion through the loss of angular momentum.

The shape of the disk is influenced by the anomalous viscosity and the generated magnetic field. We can evaluate the thickness (height) of the disk, h_D, on the basis of the pressure balance. In the vertical direction, the pressure gradient induces an expansion, whereas the generated magnetic fields induce a compression due to the Lorentz force. The acceleration from these two effects is given by

$$\frac{c_S^2}{h_D} - \frac{\overline{B}_\phi^2}{h_D}, \tag{6.22}$$

in the vertical direction. It is balanced with the contraction acceleration (the combination of gravitational and centrifugal forces) $(h_D/\sigma)\sigma\varpi^2$. From the relation

$$\overline{B}_\phi \cong \frac{\gamma}{\beta}\sigma\varpi$$

based on Eq. (6.6), the balance of these two accelerations gives the disk width at location σ,

$$h_D \cong \sqrt{\frac{{c_S}^2}{\varpi^2\sigma^2} - \frac{\gamma^2}{\beta^2}}\,\sigma. \tag{6.23}$$

6.2. Rotation drive of fusion plasmas

In highly-improved confinement modes of tokamaks, we have two types of transport barriers of heat and particles, as was noted in § 2.3.2. One is an edge transport barrier (ETB) observed in high-confinement (H) modes. The other is an internal transport barrier (ITB) in reversed-shear (RS) modes. The properties of these two transport barriers are reviewed in [2/37-2/39, 2/42, 2/48]. In what follows, we consider these barriers in light of flow dynamo. In this context, we express the cylindrical coordinates by (r,ϑ,z), unlike Fig. 5.3, where ϑ and z are the poloidal and toroidal coordinates, respectively.

H modes as well as RS modes are characterized by the concurrence of the radial electric field and plasma rotation. These two factors are connected each other through the momentum equation for ion gases. In Eq. (3.2), we keep only the pressure and Lorentz forces, and have

$$-\frac{1}{n_I e_I}\nabla p_I + \mathbf{E} + \mathbf{v}_I \times \mathbf{B} = 0. \tag{6.24}$$

From Eq. (6.24), we have

$$\mathbf{v}_I = \frac{1}{B^2}\mathbf{E}\times\mathbf{B} - \frac{1}{n_I e_I \mathbf{B}^2}\nabla p_I \times \mathbf{B} + \frac{\mathbf{B}\cdot\mathbf{v}_I}{\mathbf{B}^2}\mathbf{B}. \tag{6.25}$$

Here the retention of only the first term leads to the so-called $E\times B$ process, that is, the generation of the poloidal flow through the radial electric field and the toroidal magnetic field. In what follows, we shall adopt the cylindrical approximation to a torus.

The description of the bifurcation processes in toroidal plasmas is totally beyond the scope of the one-fluid MHD equations. The consideration of appropriate plasma responses is inevitable for it (the $E\times B$ zonal-flow dynamo is reviewed in detail in [2/49]). Nevertheless, the mean-field MHD approach can provide an illuminating understanding of the flow generation in toroidal plasmas. We here briefly link the flow-generation problems in plasmas with the mean-field MHD approach. Effects of the resultant radial electric field and plasma rotation on the turbulent transport of heat are discussed in § 7.

6.2.1. *Flows in H modes and plasma responses*

The transition from low-confinement (L) to H modes was pointed out to be a bifurcation process through the pioneering works by Itoh and Itoh [6/19] and by Shaing and Crume [6/20]. In the work by Itoh and Itoh, attention is focused on the bifurcation of E_r. It was investigated through the temporal-evolution equation for E_r,

$$\frac{\partial E_r}{\partial t} = -j_r. \tag{6.26}$$

The radial current j_r is related to effects of particle losses and nonlinearity in the loss of turbulence wave momentum across the plasma surface. This approach has recently been extended so as to include other effects such as the anomalous-viscosity current, the neoclassical bulk-viscosity current, etc. [6/21].

In the approach by Shaing and Crume, the poloidal plasma velocity u_P was chosen as the fundamental variable (note that the ion velocity is essentially the same as the plasma velocity, owing to the mass difference between ion and electron). The bifurcation of u_P was examined through the poloidal momentum balance equation,

$$\frac{\partial}{\partial t}\rho\langle B_P u_P\rangle + \frac{\partial}{\partial x_j}\rho\langle B_P u_P u_j\rangle = \Psi, \tag{6.27}$$

where the bracket denotes the flux-surface average. Equivalence of Eqs. (6.26) and (6.27) is explained in [2/40]. Effects of the particle flux due to the ion orbit loss, the loss of turbulence wave momentum across the plasma surface, the poloidal viscosity, etc. are incorporated into Ψ.

The poloidal-rotation generation was studied by Hinton *et al.* [6/22] using the neoclassical theory. There the theory was extended to include the orbit-squeezing effect that gives rise to the reduction of the ion banana width, leading to the estimate of the ion poloidal flow [2/37, 2/40].

6.2.2. *Mean-field MHD picture*

6.2.2.1. *Zonal flow of semi-micro scales*

The drive of plasma rotation by turbulence is an important phenomenon in light of structure formation. In § 4.1.2, it was mentioned that the vortical flow in the cross section of a square duct is induced by the anisotropy of the Reynolds stress. A generation mechanism of the poloidal rotation due to electromagnetic effects was sought by Diamond

and Kim [6/23] and was applied to the discussion on the L- to H-mode transition [6/24, 6/25]. There the poloidal plasma flow obeys

$$\frac{\partial \overline{u}_\vartheta}{\partial t} = -\frac{\partial}{\partial \sigma}\left\langle u_\vartheta' u_\sigma' \right\rangle. \tag{6.28}$$

Here the Reynolds stress $\left\langle u_\vartheta' u_\sigma' \right\rangle$ is calculated in terms of the drift waves arising from the number-density and electron-temperature gradients. This effect is fed back to the calculation of the drift waves.

The analysis of $\left\langle u_\vartheta' u_\sigma' \right\rangle$ shows that the turbulent viscosity ν_T could be negative when the plasma response is included. The conditions on $\nu_T < 0$ is discussed in [6/25]. For $\nu_T < 0$, this mechanism is called the zonal-flow drive. In the mean-field MHD picture, such a mechanism may be discussed on the basis of the vorticity equation (6.13), that is,

$$\frac{\partial \overline{\boldsymbol{\omega}}}{\partial t} = \nabla \times \left(\left(\overline{\mathbf{u}} - \frac{\gamma}{\beta} \overline{\mathbf{B}} \right) \times \overline{\boldsymbol{\omega}} \right) + \nu_T \nabla^2 \overline{\boldsymbol{\omega}} - \nu_M \nabla^2 \overline{\mathbf{j}}. \tag{6.29}$$

Here the spatial dependence of ν_T and ν_M is neglected for the transparency of argument.

6.2.2.2. Interference of flow with magnetic field

One of the advantages of the mean-field approach is a systematic deduction of turbulence properties, allowing the study of various kinds of interference. We shall discuss the generation of the poloidal plasma rotation by the concave plasma current [2/8, 6/27].

Equation (6.29) is suitable for the study about effects of magnetic-field structure on the poloidal flow. With attention focused on the last or current term, it is rewritten as

$$\frac{\partial \overline{\omega}_z}{\partial t} = -\frac{5C_\gamma}{7} \tau_M W \nabla^2 \bar{j}_z + R_{\omega 1}, \tag{6.30}$$

where $R_{\omega 1}$ denotes the remaining contribution. In Eq. (6.30), ν_M was expressed in terms of W by use of Eq. (4.43).

The equation for W is given by Eq. (4.68). Specifically, W is generated by P_W [Eq. (4.72)]. We retain the $\bar{j}_z$-related term in Eqs. (4.37) and (4.72), and have

$$\frac{\partial W}{\partial t} = \beta \bar{j}_z \overline{\omega}_z + R_W = C_\beta \tau_M K \bar{j}_z \overline{\omega}_z + R_W, \tag{6.31}$$

in correspondence to Eq. (6.30), where Eq. (4.42) was used. We eliminate W from Eqs. (6.30) and (6.31). Here we focus attention on the temporal growth of W, and neglect the temporal change of $\bar{j}_z$, K, and τ_M. As a result, we have

$$\frac{\partial^2 \overline{\omega}_z}{\partial t^2} - \left(-\frac{5C_\beta C_\gamma}{7} \tau_M K \bar{j}_z \nabla^2 \bar{j}_z \right) \overline{\omega}_z = R_{\omega 2}, \tag{6.32}$$

where $R_{\omega 2}$ expresses all the remaining contributions not discussed here. Equation (6.32) indicates that $\overline{\omega}_z$ may grow through the interference with the magnetic field under the condition

$$\Omega^2 = -\frac{5C_\beta C_\gamma}{7} \tau_M K \bar{j}_z \nabla^2 \bar{j}_z > 0. \tag{6.33}$$

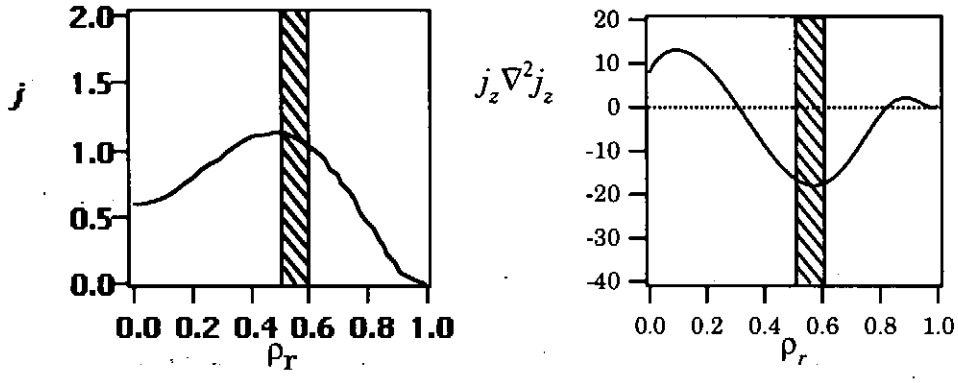

Fig. 6.3. Current density in the RS mode of JT-60U (units: j, MA m^{-2}) (left), and $j_z \nabla^2 j_z$ (right).

Let us see where Ω is real and largest, that is, where the poloidal rotation or $\overline{\omega}_z$ is expected to start. The plasma-current profile is hollow, as is reported in experiments [2/33, 6/28]. Its corresponding profile of $\bar{j}_z \nabla^2 \bar{j}_z$ is shown in Fig. 6.3. Large negative $\bar{j}_z \nabla^2 \bar{j}_z$ lies just at the location of minimum q or at $\rho_r \cong 0.6$ with the normalized minor radius $\rho_r = r/a$. As a result, the poloidal rotation is likely to occur at the minimum region of the q value, which corresponds to the location of ITB that is hatched in Fig. 6.3.

7. Electromagnetic Effects on Turbulent Transports: Towards Consistency

An accurate estimate of the heat transfer is one of the central themes in the study of electrically-nonconducting turbulent flows in engineering and meteorological fields. In magnetic and flow dynamos, transport coefficients α, β, γ, ν_T, etc. need to be determined simultaneously with the established magnetic field and plasma flow, $\overline{\mathbf{B}}$ and $\overline{\mathbf{u}}$. The influences of the generated structures of $\overline{\mathbf{B}}$ and $\overline{\mathbf{u}}$ on the transport coefficients must be clarified for their self-consistent determination. In this section, those feedback effects of the generated structures are discussed.

7.1. Effects of generated magnetic field on dynamo coefficients

The effects of the magnetic field on the coefficient α were mentioned in § 5.3.1.2. These effects are considered to arise from a modification of the time scale if α, β and γ are affected in a similar way. If some of them may be selectively influenced, the feedback process is decisively important for the selection of a dynamo mechanism in the process of structure formation. Such a research is on-going, and there are a couple of disputes. Some of the central issues are illustrated here with special reference to [2/9].

7.1.1. Suppression of α by generated magnetic field

The coefficient α may deviate from the estimate by the kinematic approach with the statistics of $\mathbf{u}'$ and the correlation time prescribed. We introduces a characteristic value of the magnetic field, B_{eq}, which obeys the equipartition of the energy, $B_{eq}{}^2 \equiv \overline{\mathbf{u}}^2$. The effect of the generated field $\overline{\mathbf{B}}$ on α may be expressed as a function of $(\overline{\mathbf{B}}/B_{eq})^2$. The quadratic dependence comes from the fact that the sign of the field does not affect the quench, based on the symmetry consideration. Then the effect is postulated as

$$\alpha = \frac{\alpha_0}{1 + R_{eM}{}^m \left(\overline{\mathbf{B}}/B_{eq}\right)^2}, \tag{7.1}$$

where α_0 is the estimate by the kinematic approach in the presence of a weak mean magnetic field, R_{eM} is the magnetic Reynolds number, and the power index m denotes the strength of suppression. Some theories support $m << 1$, whereas other theories and direct numerical simulations support $m \cong 1$. It is likely that the suppression with $m \cong 1$ is applicable in wider circumstances, although the further confirmation is necessary (see [2/9] and references therein).

The mechanism that gives $m \cong 1$ is considered to be the memory effect due to the generated magnetic field. The turbulent velocity and vorticity become more and more out

of phase so as to reduce α. Gruzinov and Diamond [5/22, 7/1] discussed the conservation property of magnetic helicity in the three-dimensional (3-D) case. There α in the high-conductivity limit is given by

$$\alpha = -\eta \frac{\langle \mathbf{B}' \cdot \mathbf{j}' \rangle}{\overline{\mathbf{B}}^2}, \tag{7.2}$$

where $\mathbf{B}'$ and $\mathbf{j}'$ include the entire small-scale fields, that is, both the prescribed turbulent fluctuations and small-scale dynamo fields. This is a large-R_{eM} limit of Eq. (7.1) with $m = 1$.

7.1.2. Suppression of β by generated magnetic field

The reduction of the coefficient β was clarified within the framework of a 2-D MHD theory. The squared magnetic potential

$$H_A = \int \mathbf{A}^2 dV \tag{7.3}$$

is conserved in the ideal limit. In the high-conductivity limit, it is quasi-conserved. This property yields the relation

$$\frac{\beta}{\eta} = \frac{\langle \mathbf{B}^2 \rangle}{\langle \mathbf{B} \rangle^2} \tag{7.4}$$

(Zeldovich theorem [7/2]). Along this line of thought, we have

$$\beta = \frac{\beta_0}{1 + R_{eM} \left(\overline{\mathbf{B}} / B_{eq} \right)^2}, \tag{7.5}$$

where β_0 is the value obtained from the kinematic approach.

In a 3-D MHD flow, it is shown that the relation $\beta \cong \beta_0$ holds in the case that an applied magnetic field is weak [5/22]. In the ideal limit, what is conserved is the magnetic helicity

$$H_m = \int \mathbf{A} \cdot \mathbf{B} dV, \tag{7.6}$$

but not H_A. Then H_m is quasi-conserved in the high-conductivity limit. Moreover α is a pseudoscalar, unlike β. These differences were pointed out as a possible cause of the disparity between α and β [2/9]. To what extent the relation $\beta \cong \beta_0$ holds is yet an open question, and an intensive study is on-going.

Equations (7.2) and (7.4) denote the balance between the average flux $\langle \mathbf{u}' \cdot \mathbf{B}' \rangle$ and the dissipation. It is worth while noting that such balance holds in the wide area of plasma dynamics. For instance, the cross-field plasma transport shows the balance of the cross-field flux and the Ohmic dissipation [2/40, 2/49].

7.1.3. Note on γ dynamo

The suppression due to feedback effects, if it applies selectively to α, leads to the increase in the importance of the γ-dynamo process in the generation of magnetic fields. So far, no clear assessment has been made on the suppression of the coefficient γ by the generated magnetic field. A few comment could be noted here. The cross helicity

$$H_C = \int \mathbf{u} \cdot \mathbf{B} dV \tag{7.7}$$

is conserved in the ideal MHD case. Then H_C is quasi-conserved in a weakly dissipative system. This situation implies that the γ dynamo is weakened by the generated magnetic field, as is in the suppression of α and β. There could be, however, a difference. The dynamo coefficient γ is given in terms of the correlation of the perturbed magnetic field and velocity field, $\langle \mathbf{u}' \cdot \mathbf{B}' \rangle$. Alfven effects occur when electromagnetic effects become important in magnetized plasmas. There perturbed magnetic and velocity fields tend to be aligned each other. Then a different dependence of γ on the generated magnetic field is possible. This point will be a key issue for the structure formation of magnetic fields and demands a future study.

7.2. Suppression of turbulent transport by generated flows

The primary concern in fusion is to suppress heat and particle transports and keep plasma in a high-temperature state. There the suppression of heat and particles by a radial electric field and a plasma flow has been discussed through the concept of turbulent diffusivity. In this approach, attention is focused on a diffusivity-type representation for a turbulent flux.

7.2.1. Increase in nonlinear damping by sheared flow

In the study of transport suppression, much attention has been focused on shear effects of radial electric field (E_r) and poloidal velocity (u_ϑ). These two quantities are tightly linked with each other through the $E \times B$ mechanism. It is widely accepted that the $E \times B$ shear suppresses both the turbulence and transports of heat and particles. Observational results about the shear effects are reviewed in [2/38, 2/39, 2/45]. In this section, the cylindrical coordinates are also written as (r, ϑ, z).

We now refer to the basic concepts in some theoretical works (readers may consult [2/37, 2/40, 7/3] for their more comprehensive survey). A fundamental concept for suppressing the transports is the destruction of coherent structures of plasma turbulence. In the work by Biglari *et al.* [7/4], the two-point correlation function

$$C_\xi(\mathbf{r}) = \langle \xi(\mathbf{x})\xi(\mathbf{x}+\mathbf{r}) \rangle \tag{7.8}$$

was introduced, and the relationship between the characteristic correlation length ℓ_ξ and the poloidal-velocity shear du_ϑ / dr was examined, where ξ is a fluctuation such as temperature fluctuation. The decrease in ℓ_ξ due to du_ϑ / dr, that is, the decorrelation, signifies the destruction of large energetic fluctuations governing the turbulent transport of ξ, resulting in the transport suppression.

A more direct linkage between the radial electric field and diffusivities was sought in the works by Itoh *et al.* [2/8, 7/5] and Ware *et al.* [7/6]. In the former, the renormalized diffusivities of heat and current was investigated for current diffusive ballooning modes. Those diffusivities are written in the form

$$\frac{D}{D_0} = \frac{1}{1 + G_1 \omega_{E1}{}^2 + G_2 \omega_{E2}{}^2}. \tag{7.9}$$

In Eq. (7.9), D_0 is the diffusivity in L modes, G_1 and G_2 are nondimensional coefficients, and ω_{E1} and ω_{E2} are related to the shear and curvature of E_r, respectively, as

$$\omega_{E1} = \frac{\tau_{AP}}{srB_z} \frac{dE_r}{dr}, \tag{7.10a}$$

$$\omega_{E2} = \frac{a\tau_{AP}}{s^2 B_z} \frac{d^2 E_r}{dr^2}, \tag{7.10b}$$

where τ_{AP} is the Alfven-velocity time based on B_ϑ, and s is the magnetic shear defined by

$$s = \frac{r}{q} \frac{dq}{dr}. \tag{7.11}$$

In the absence of E_r, D tends to the diffusivity in L modes, D_0. The transition to H modes is characterized by the magnitude of ω_{E1} and ω_{E2}.

In the work by Ware *et al.*, the electric-field shear was dealt with through the $E \times B$ shear. With its effect on nonlinear phase shifts in mind, the turbulent transports due to the

resistive pressure-gradient driven turbulence were examined on the basis of a two-field model for the density and vorticity fluctuations. In the case of a weak shear, the turbulent diffusivity for the density is expressed in the form

$$\frac{D}{D_0} = 1 - \frac{C_D}{\gamma_0^{\,2}}\left(W_0 \frac{dk_y}{dr}\frac{du_\vartheta}{dr}\right)^2, \tag{7.12}$$

where D_0 is the diffusivity in the absence of the shear, k_y is the poloidal-mode wavenumber, γ_0 is the linear growth rate, W_0 is the radial-mode width in the absence of the shear, and C_D is a numerical factor. Equation (7.12) shows the close relationship of the transport suppression with the radial shear, as is similar to Eq. (7.9).

7.2.2. Reduction of turbulence production within the framework of mean-field MHD

Some influences of a generated flow on the turbulent transport can be described within the framework of the mean-field MHD equations [7/7, 7/8]. These processes are briefly explained. We keep the ETB or ITB of tokamaks in mind, and write

$$\hat{\mathbf{u}} = \left(0, \hat{u}_\vartheta(r), 0\right), \quad \overline{\mathbf{E}} = \left(\overline{E}_r(r), 0, E_0\right), \tag{7.13}$$

under the cylindrical approximation (E_0 is constant).

7.2.2.1. Suppression of velocity fluctuations

The intensity of turbulence is determined by the balance between the pump and the nonlinear damping. The intensity in a turbulent variable-density flow is expressed by the turbulent energy K_M [Eq. (4.86)], which obeys Eq. (4.87). On the right-hand side of Eq. (4.87), the first three terms dependent on the mean field may be called the production terms, which play the role of transferring the kinetic energy between the mean and fluctuating parts, as was noted in § 4.1.1. Of the terms, the first is the same as its counterpart on the right-hand side of Eq. (4.7). The second is the effect intrinsic to a variable-density flow, owing to the occurrence of $\overline{\mathbf{u}''}$. We have already referred to the importance of this term in light of the combination with $\nabla\overline{p}$ (note that $\overline{p}$ is a primary parameter in the plasma confinement). The third is the direct effect of $\overline{\mathbf{E}}$ that is combined with the plasma nonneutrality. The effects of $\overline{\mathbf{E}}$ and plasma rotation on the production term may be studied on the basis of the results in § 4.3.2.

From Eq. (7.13), the three terms may be rewritten as

$$P_{K1} = -\overline{\rho} R_{Mij}\frac{\partial \hat{u}_j}{\partial x_i} = C_{vv1}\overline{\rho}\left(r\frac{d}{dr}\frac{\hat{u}_\vartheta}{r}\right)^2 = C_{vv1}\overline{\rho}r^2\left(\frac{1}{r}\frac{d\hat{u}_\vartheta}{dr} - \frac{\hat{u}_\vartheta}{r^2}\right)^2, \tag{7.14}$$

$$P_{K2} = -\overline{u_i''}\frac{\partial \overline{p}}{\partial x_i} = -C_{\rho v1}\frac{1}{\overline{\rho}}\frac{d\overline{\rho}}{dr}\frac{d\overline{p}}{dr} + C_{\rho v2}\frac{1}{\overline{\rho}^2}\frac{\hat{u}_\vartheta{}^2}{r}\frac{d\overline{p}}{dr}, \tag{7.15}$$

$$P_{K3} = \langle \rho_e' u_i'' \rangle \overline{E}_i = -C_{ev}\varepsilon_0 \Gamma, \tag{7.16}$$

with

$$\Gamma \equiv \frac{1}{\varepsilon_0}\overline{E}_r\frac{d\overline{\rho}_e}{dr} = \overline{E}_r\frac{d^2\overline{E}_r}{dr^2} + \frac{2}{r}\overline{E}_r\frac{d\overline{E}_r}{dr} - \frac{2}{r^2}\overline{E}_r{}^2, \tag{7.17}$$

where use has been made of Eqs. (4.90) and (4.91), and the relation

$$\left(\frac{D\hat{\mathbf{u}}}{Dt}\right)_r = -\frac{\hat{u}_\vartheta{}^2}{r}. \tag{7.18}$$

The contribution by $D\hat{\mathbf{u}}/Dt$ effects does not occur in a slab model that is frequently used in the study of plasma properties in tokamaks.

In Equation (7.15), both the terms are negative. Specifically, the plasma rotation contributes to negative P_{K2}, that is, the suppression of velocity fluctuation. From the observations of $\overline{E}_r$ in H modes, the second and third terms on the right-hand side of Eq. (7.17) may be confirmed to be negligibly small, compared with the first term. In the case of JFT-2M tokamaks, Γ becomes negative in the region near the edge ($\rho_r > 0.95$) and reaches -10^4 $V\,\mathrm{cm}^{-3}$. That is, we may see

$$P_{K3} < 0, \tag{7.19}$$

in the edge region, also contributing to the suppression of velocity fluctuation. These facts signify that the curvature of $\overline{E}_r$ as well as its magnitude is associated with the suppression.

We should stress that the foregoing findings based on the mean-field MHD do not lower the importance of the results in the current works of tokamaks about the $E \times B$ shear effects. They provide a complementary understanding. The arguments in § 7.2.1 were developed under the situation that the coherence length of turbulence is much shorter than the system size, while the present MHD modelling is useful in the case that the coherence length is comparable. It was reported [7/9] that drift- and flute-mode instabilities in the GAMMA 10 tandem mirror are dependent on both the shear and magnitude of the radial electric field. With fixed $|\overline{E}_r|$, the increase in $|d^2\overline{E}_r/dr^2|$ leads to that in $|d\overline{E}_r/dr|$. In the study on mirror plasmas [7/10], fluctuations with long radial correlation lengths were investigated. The narrowness of the region with large $\overline{E}_r$ is

reflected on $d^2\overline{E}_r/dr^2$ but not on $d\overline{E}_r/dr$. The curvature effect on turbulent diffusivities has already been pointed out by Itoh *et al.* [7/5] in Eq. (7.9). It is significant to further investigate into each role of $\overline{E}_r$, $d\overline{E}_r/dr$ and $d^2\overline{E}_r/dr^2$ and clarify the degree of contribution to the transport suppression.

7.2.2.2. Heat-flux suppression and countergradient diffusion

Under Eq. (7.13), we may rewrite Eq. (4.94) as

$$H_{Mr} = -C_{P1}\frac{d\hat{\theta}}{dr} - C_{P3}\frac{\hat{\theta}}{\overline{\rho}^2}\frac{\hat{u}_\vartheta{}^2}{r} + C_{P4}\frac{\varepsilon_0}{\overline{\rho}}\Gamma\frac{d\hat{\theta}}{dr}. \tag{7.20}$$

The first term is the familiar gradient diffusion effect and is positive due to $d\hat{\theta}/dr < 0$. It expresses the enhancement of heat transport towards the outer part of plasmas by turbulent motion. There the rise in the temperature contributes to a larger heat flux. The second term expresses the combination of centripetal-force and density-fluctuation effects, as is quite similar to the second term in the second relation of Eq. (7.15). It tends to cancel the first term. Originally, the centripetal force comes from $D\hat{\mathbf{u}}/Dt$. This fact suggests that the turbulent heat flux in one direction is sensitive to the acceleration of flow in the direction.

It is emphasized again that the mean-field MHD approach shows the reduction in the production term of turbulence by the radial electric field and plasma rotation. Both the enhanced nonlinear damping process in § 7.2.1 and the reduction in the production term contribute to the reduction in the turbulent energy transport.

As is seen from the discussion about Eq. (7.20), one of the great interests in fusion research is the reduction in the gradient diffusion of scalars such as heat and particles by turbulent motion. The extreme case of the gradient-diffusion suppression is countergradient diffusion in turbulent combustion. There scalars are transported by turbulence in the direction of the mean scalar gradient. This phenomenon seems curious to fusion researchers struggling for the suppression of gradient diffusion, but it is familiar to those of turbulent combustion [7/11].

It has recently been pointed out [7/12] that the countergradient diffusion is closely related to the acceleration effect arising from the thermal expansion by chemical reaction. This property is very similar to the acceleration effect represented by the second term in Eq. (7.20), and the physical resemblance may be observed between the transport suppression in fusion and the countergradient diffusion in turbulent combustion. A mechanism of the countergradient-diffusion is discussed briefly in Appendix D.

7.3. Magnetic-field effects on off-diagonal elements of heat-transport matrix

In engineering researches, the heat transport is intentionally enhanced for the rapid release of heat through the generation of turbulent motion. In § 4.1.3, we referred to the heat transport normal to the temperature gradient that is caused by a mean-velocity shear. Equation (4.31a) shows that no mean-flow effect appears on the heat flux in the x direction, whereas the heat flow in the mean-flow or y direction occurs newly, as is seen from Eq. (4.31b). A magnetic-field effect on the heat flux was discussed in § 4.2.1. There the heat flux is expressed by Eq. (4.53) with the turbulent-diffusivity representation as the leading part. With the heat transport in tokamaks in mind, we adopt the slab approximation, and denote the radial and poloidal directions by the x and y directions, respectively. In the slab geometry, we write

$$\bar{\theta} = \bar{\theta}(x), \quad \bar{\mathbf{u}} = 0, \quad \bar{\mathbf{B}} = \left(0, B_y(x), B_z(x)\right). \tag{7.21}$$

From Eq. (4.53), we have

$$H_{\theta x} = -C_{\theta 1}(K + K_R)\tau_m \frac{d\bar{\theta}}{dx}, \tag{7.22a}$$

$$H_{\theta y} = W\tau_m{}^2\left(D_{\theta 21} - D_{\theta 22}\right)\frac{d\bar{B}_y}{dx}\frac{d\bar{\theta}}{dx}, \tag{7.22b}$$

$$H_{\theta z} = W\tau_m{}^2\left(D_{\theta 21} - D_{\theta 22}\right)\frac{d\bar{B}_z}{dx}\frac{d\bar{\theta}}{dx}. \tag{7.22c}$$

Equation (7.22a) representing the radial transport is not affected explicitly by $\bar{\mathbf{B}}$. On the other hand, the heat flow normal to the temperature gradient may be induced by $\bar{\mathbf{B}}$, as in Eqs. (7.22b) and (7.22c). This result is essentially the same as the heat flux in an electrically-nonconducting flow with the mean-velocity shear, as is seen from Eqs. (4.30) and (4.31). Equations (7.22b) and (7.22c) represent the off-diagonal elements of the heat flux and are an extension of Eq. (2.7) to turbulent cases. Here the new term depends on the turbulent cross helicity W as well as the gradient of $\bar{\mathbf{B}}$.

7.4. On variational principles

A properly-constructed variational principle is a powerful method for investigating into structure formation. The governing equations of the magnetic and velocity fields, e.g., Eqs. (6.14) and (6.16), may reproduce structures that have been derived by the variational-principle approach to large-scale MHD turbulence. Here this issue is revisited in conjunction with dynamo problems.

The variational principle has been successful when the dissipation rates of two quantities have different time scales. For instance, the magnetic helicity defined by Eq. (7.6) and the flow helicity

$$H_u = \int \mathbf{u} \cdot \boldsymbol{\omega} dV, \tag{7.23}$$

are quasi-conserved in highly conducting media. The cross helicity defined by Eq. (7.7) is also quasi-conserved (see, e.g., [7/13]). On the other hand, the magnetic energy

$$K_m = \int \frac{\mathbf{B}^2}{2} dV \tag{7.24}$$

dissipates much faster than H_m.

From these facts, the Taylor relaxation state was derived under the condition that K_m is minimized for constant H_m; namely, we have

$$\nabla \times \mathbf{B} = \mu \mathbf{B}, \tag{7.25}$$

with μ related to the Lagrange multiplier. The essence of Taylor's argument is that MHD turbulence is strong enough to have a correlation length comparable to the system size. This condition allows us to choose μ as a common value in the entire region of plasmas. As a result, μ is determined by the global parameters such as the toroidal magnetic flux and the total plasma current. In fluid dynamics, the enstrophy

$$K_\omega = \int \boldsymbol{\omega}^2 dV, \tag{7.26}$$

to which the dissipation rate is proportional, decays faster than H_u. The minimum-enstrophy state under the quasi-conserved flow helicity satisfies [7/14]

$$\nabla \times \boldsymbol{\omega} = \mu \boldsymbol{\omega}. \tag{7.27}$$

The foregoing discussions may give useful insights to understanding of the magnetic dynamo. When a large-scale turbulence exists, that is, the turbulence has a long correlation length, the coefficient ratios such as α/β may be taken to be constant in the wide region that a mixing length of turbulence covers. Once α/β is taken to be constant, the resultant structure can be deduced by solving the equation of the mean filed, which is a linear differential equation, as is given in Eq. (7.25). As a result, α/β could be rewritten in terms of boundary conditions or global quantities.

In turbulent plasmas, the coupling between the flow and field is essential. The importance of the cross-helicity effect has been stressed in this review. One method for incorporating such an effect is to minimize the total energy

$$K_t = \int \frac{\mathbf{u}^2 + \mathbf{B}^2}{2} dV, \tag{7.28}$$

under the conservation of the cross helicity H_C [7/15]. With this variational principle, we have

$$\mathbf{u} = \mu \mathbf{B} \quad \text{and} \quad \mathbf{B} = \mu \mathbf{u}, \tag{7.29}$$

resulting in $\mu = \pm 1$.

The alignment between **u** and **B** was pointed out for the cross-helicity dynamo, as is described by Eq. (5.39) and others. The complete identity between **u** and **B** like Eq. (7.29), however, holds only for Alfven waves. Then Eq. (7.29) is too stringent to describe the dynamo state. This result might be owing to the fact that only H_C is considered with H_m and H_u ignored.

The variational principle has been extended to the two-fluid MHD framework [7/16, 7/17]. There the enstrophies of electron and ion fluids are minimized under constant electron and ion helicities as well as constant K_t. Then we have

$$(\nabla \times -\mu_1)(\nabla \times -\mu_2)\mathbf{u} = 0, \tag{7.30}$$

$$\mathbf{B} = \mu_3(\mathbf{u} - \mu_4 \nabla \times \mathbf{B}), \tag{7.31}$$

where coefficients μ_n $(n = 1-4)$ are related to Lagrange multipliers.

How to choose minimizers and constraints in an appropriate manner is still an on-going subject. It is worth while recalling that Lagrange multipliers can be considered to be constant within the range of a coherence turbulence length. In many examples associated with the flow dynamo in toroidal plasmas, structures such as transport barriers appear owing to the steep spatial variation of turbulence properties. The improved-confinement states are usually associated with the reduced correlation length of turbulence, as is discussed in § 7.2.1. This fact implies that different approaches other than, e.g., Eqs. (7.25) and (7.27), are necessary for examining improved confinements in the form of variational principle.

8. Summary

In this article, we presented a review of the mean-field approaches to electrically conducting turbulent flows. For the turbulent fluxes playing a central role there, the heuristic explanation was preferred to the statistical method based on turbulence theories. With the full use of those fluxes, we discussed on the following three themes:

(i) Magnetic dynamo or magnetic-field generation mechanism with special attention to a spherical-shell dynamo;

(ii) Flow dynamo or flow generation mechanism by electromagnetic forces;

(iii) Electromagnetic effects on turbulent transports.

In the first, the fundamental processes of magnetic-field generation were discussed in light of some macroscopic features of the geomagnetic and solar fields. In the second, flow generation was discussed through the investigations into the generation of bipolar jets from an accretion disk and into the occurrence of plasma rotation in the improved-confinement modes of tokamaks. In the third, the suppression of turbulence and transports was discussed in close relation to the improved-confinement modes of tokamaks. Dynamo problems were reviewed from the viewpoint of structure formation, but the temporal variation of field polarity was not addressed.

In this article, the structure formation by the dynamo mechanism was discussed with an emphasis on the self-consistent determination of the mean-field flow. This point first became possible through the introduction of the turbulent cross-helicity effect. Examples are the geomagnetic field, solar magnetic field and magnetic fields associated with accretion disks. The primary results are summarized in Table 2.4.

The governing equation of the mean magnetic field depends strongly on the magnitude of the coefficient ratio γ / β. In light of this parameter, it might be possible to characterize the form of established magnetic fields through the self-consistent treatment of the associated flow structure. The final goal of the mean-field approach should be the simultaneous determination of the turbulent transport coefficients and established structures as functions of nondimensional parameters such as R_a, T_a, R_e, etc. as well as geometrical parameters. This task is a future direction of research in understanding of the dynamo phenomena in nature.

In the present discussions, we also gave a brief review of the other analytical and numerical methods intrinsic to each phenomenon and attempted to elucidate the features

of the mean-field method as well as its theoretical limitation. We showed that by the inclusion of proper turbulence effects into turbulent fluxes, the mean-field method can capture some of macroscopic properties common to apparently different phenomena.

In short, we attempted to illustrate that the progress of plasma physics leads to the further development in understanding of evolution in nature.

Acknowledgments

One of the authors (KI) acknowledges the discussions with Prof. P H. Diamond, Prof. D. Hughes and Prof. E. Vishniak and other members on occasion of Festival Theorie (Aix-en-Provence, July 2003) in completing this article.

This work is partly supported by the Grant-in-Aid for Scientific Research of Ministry of Education, Culture, Sports, Science and Technology Japan, by the collaboration program of National Institute for Fusion Science and by the collaboration program of the Research Institute for Applied Mechanics of Kyushu University.

Part of this work was performed when one of the authors (AY) was a visiting professor at National Institute for Fusion Science.

Appendix A: Derivation of Correlation Functions

1. Constant Magnetohydrodynamic Flows.

1.1. Turbulent electromotive force

We write the turbulent electromotive force $\mathbf{E}_T$ [Eq. (4.35)] as

$$E_{Ti} = \varepsilon_{inn}\langle u_m' B_n' \rangle \tag{A.1}$$

(ε_{ijl} is the alternating tensor). Then we have

$$\frac{D}{Dt}\langle u_m' B_n' \rangle = -\langle u_l' B_n' \rangle \frac{\partial \overline{u}_m}{\partial x_l} + \langle u_m' B_l' \rangle \frac{\partial \overline{u}_n}{\partial x_l}$$

$$+\langle B_l' B_n' \rangle \frac{\partial \overline{B}_m}{\partial x_l} - \langle u_m' u_l' \rangle \frac{\partial \overline{B}_n}{\partial x_l} + \left(\left\langle B_n' \frac{\partial B_m'}{\partial x_l} \right\rangle + \left\langle u_m' \frac{\partial u_n'}{\partial x_l} \right\rangle \right) \overline{B}_l$$

$$-\left\langle B_n' \frac{\partial \varpi'}{\partial x_m} \right\rangle - \left\langle u_l' B_n' \frac{\partial u_m'}{\partial x_l} \right\rangle + \left\langle B_l' B_n' \frac{\partial B_m'}{\partial x_l} \right\rangle$$

$$-\left\langle u_l' u_m' \frac{\partial B_n'}{\partial x_l} \right\rangle + \left\langle u_m' B_l' \frac{\partial u_n'}{\partial x_l} \right\rangle - (\nu + \lambda_B) \left\langle \frac{\partial u_m'}{\partial x_l} \frac{\partial B_n'}{\partial x_l} \right\rangle$$

$$+\frac{\partial}{\partial x_l}\left(\nu \left\langle B_n' \frac{\partial u_m'}{\partial x_l} \right\rangle + \lambda_B \left\langle u_m' \frac{\partial B_n'}{\partial x_l} \right\rangle \right). \tag{A.2}$$

In the first two terms on the right-hand side, we assume the isotropy of the correlation between $\mathbf{u}'$ and $\mathbf{B}'$, and write

$$\langle u_i' B_j' \rangle \cong \frac{1}{3} W \delta_{ij}, \tag{A.3}$$

where W is the turbulent cross helicity defined by Eq. (4.48). There the two terms are reduced to

$$-\langle u_l' B_n' \rangle \frac{\partial \overline{u}_m}{\partial x_l} + \langle u_m' B_l' \rangle \frac{\partial \overline{u}_n}{\partial x_l} = \frac{1}{3} W \left(\frac{\partial \overline{u}_n}{\partial x_m} - \frac{\partial \overline{u}_m}{\partial x_n} \right). \tag{A.4}$$

In the third and fourth terms of Eq. (A.2), we similarly make the isotropic approximation

$$\langle u_i' u_j' \rangle \cong \frac{2}{3} K_u \delta_{ij}, \tag{A.5}$$

$$\langle B_i' B_j' \rangle \cong \frac{2}{3} K_B \delta_{ij}, \tag{A.6}$$

where K_u and K_B are the kinetic and magnetic energies defined by

$$K_u = \left\langle \frac{1}{2} \mathbf{u}'^2 \right\rangle, \tag{A.7}$$

$$K_B = \left\langle \frac{1}{2} \mathbf{B}'^2 \right\rangle. \tag{A.8}$$

Then those two terms are rewritten as

$$\langle B_\ell' B_n' \rangle \frac{\partial \overline{B}_m}{\partial x_\ell} - \langle u_m' u_\ell' \rangle \frac{\partial \overline{B}_n}{\partial x_\ell} = -\frac{2}{3} K_u \frac{\partial \overline{B}_n}{\partial x_m} + \frac{2}{3} K_B \frac{\partial \overline{B}_m}{\partial x_n}. \tag{A.9}$$

In the fifth term of Eq. (A.2), we rewrite

$$\frac{\partial u_n'}{\partial x_\ell} = \frac{1}{2}\left(\frac{\partial u_n'}{\partial x_\ell} - \frac{\partial u_\ell'}{\partial x_n} \right) + \frac{1}{2}\left(\frac{\partial u_n'}{\partial x_\ell} + \frac{\partial u_\ell'}{\partial x_n} \right) = \frac{1}{2} \varepsilon_{\ell np} \omega_p' + \frac{1}{2}\left(\frac{\partial u_n'}{\partial x_\ell} + \frac{\partial u_\ell'}{\partial x_n} \right), \tag{A.10}$$

$$\frac{\partial B_n'}{\partial x_\ell} = \frac{1}{2} \varepsilon_{\ell np} J_p' + \frac{1}{2}\left(\frac{\partial B_n'}{\partial x_\ell} + \frac{\partial B_\ell'}{\partial x_n} \right). \tag{A.11}$$

We assume the isotropy of the correlations between $\mathbf{u}'$ and $\boldsymbol{\omega}'$ and between $\mathbf{B}'$ and $\mathbf{J}'$; namely, we write

$$\langle u_i' \omega_j' \rangle \cong \frac{1}{3} H_u \delta_{ij}, \tag{A.12}$$

$$\langle B_i' J_j' \rangle \cong \frac{1}{3} H_B \delta_{ij}, \tag{A.13}$$

where H_u and H_B are called the turbulent kinetic and current helicities, respectively, which are defined by

$$H_u = \langle \mathbf{u}' \cdot \boldsymbol{\omega}' \rangle, \tag{A.14}$$

$$H_B = \langle \mathbf{B}' \cdot \mathbf{J}' \rangle. \tag{A.15}$$

From Eqs. (A.12) and (A.13), the fifth term is reduced to

$$\left(\left\langle B_n' \frac{\partial B_m'}{\partial x_\ell} \right\rangle + \left\langle u_m' \frac{\partial u_n'}{\partial x_\ell} \right\rangle \right) \overline{B}_\ell = \frac{1}{6} \left(H_u \varepsilon_{\ell nm} + H_B \varepsilon_{\ell mn} \right) B_\ell. \tag{A.16}$$

Here we discarded

$$\left\langle u_m'\left(\frac{\partial u_n'}{\partial x_\ell}+\frac{\partial u_\ell'}{\partial x_n}\right)\right\rangle,\quad \left\langle B_n'\left(\frac{\partial B_m'}{\partial x_\ell}+\frac{\partial B_\ell'}{\partial x_m}\right)\right\rangle, \tag{A.17}$$

in comparison with H_u and H_B.

We summarize Eqs. (A.4), (A.9), and (A.16), and combine them with Eq. (A.1). The final result is given by Eq. (4.37).

1.2. Reynolds stress

The primary mathematical feature of the Reynolds stress R_{ij} is derived in entirely the same manner for $\mathbf{E}_T$. The equation for R_{ij} is

$$\begin{aligned}
\frac{DR_{ij}}{Dt} &= -\left(\langle u_j' u_\ell'\rangle+\langle B_j' B_\ell'\rangle\right)\frac{\partial \overline{u}_i}{\partial x_\ell}-\left(\langle u_i' u_\ell'\rangle+\langle B_i' B_\ell'\rangle\right)\frac{\partial \overline{u}_j}{\partial x_\ell}\\
&+\left(\langle u_j' B_\ell'\rangle+\langle u_\ell' B_j'\rangle\right)\frac{\partial \overline{B}_i}{\partial x_\ell}+\left(\langle u_i' B_\ell'\rangle+\langle u_\ell' B_i'\rangle\right)\frac{\partial \overline{B}_j}{\partial x_\ell}\\
&+\left(\left\langle B_j'\frac{\partial u_i'}{\partial x_\ell}\right\rangle+\left\langle B_i'\frac{\partial u_j'}{\partial x_\ell}\right\rangle-\left\langle B_j'\frac{\partial u_i'}{\partial x_i}\right\rangle-\left\langle B_i'\frac{\partial u_j'}{\partial x_i}\right\rangle\right)\overline{B}_\ell\\
&+\left\langle \varpi'\left(\frac{\partial u_j'}{\partial x_i}+\frac{\partial u_i'}{\partial x_j}\right)\right\rangle-2\left(\nu\left\langle\frac{\partial u_i'}{\partial x_\ell}\frac{\partial u_j'}{\partial x_\ell}\right\rangle-\lambda_B\left\langle\frac{\partial B_i'}{\partial x_\ell}\frac{\partial B_j'}{\partial x_\ell}\right\rangle\right)\\
&+\frac{\partial}{\partial x_\ell}\Big(-\langle u_i' u_j' u_\ell'\rangle+\langle u_\ell' B_i' B_j'\rangle+\langle \varpi' u_i'\rangle\delta_{j\ell}+\langle \varpi' u_j'\rangle\delta_{i\ell}\\
&\qquad+\nu\frac{\partial}{\partial x_\ell}\langle u_i' u_j'\rangle-\lambda_B\frac{\partial}{\partial x_\ell}\langle B_i' B_j'\rangle\Big)\\
&+\left\langle u_j' B_\ell'\frac{\partial B_i'}{\partial x_\ell}\right\rangle+\left\langle u_i' B_\ell'\frac{\partial B_j'}{\partial x_\ell}\right\rangle-\left\langle B_j' B_\ell'\frac{\partial u_i'}{\partial x_\ell}\right\rangle-\left\langle B_i' B_\ell'\frac{\partial u_j'}{\partial x_\ell}\right\rangle.
\end{aligned} \tag{A.18}$$

The first four terms on the right-hand side of Eq. (A.18) are written as

$$\begin{aligned}
&-\left(\langle u_j' u_\ell'\rangle+\langle B_j' B_\ell'\rangle\right)\frac{\partial \overline{u}_i}{\partial x_\ell}-\left(\langle u_i' u_\ell'\rangle+\langle B_i' B_\ell'\rangle\right)\frac{\partial \overline{u}_j}{\partial x_\ell}\\
&+\left(\langle u_j' B_\ell'\rangle+\langle u_\ell' B_j'\rangle\right)\frac{\partial \overline{B}_i}{\partial x_\ell}+\left(\langle u_i' B_\ell'\rangle+\langle u_\ell' B_i'\rangle\right)\frac{\partial \overline{B}_j}{\partial x_\ell}
\end{aligned}$$

$$= -\frac{2}{3} K\overline{s}_{ij} + \frac{1}{3} W\overline{m}_{ij}, \tag{A.19}$$

where the mean magnetic-field-strain tensor $\overline{m}_{ij}$ is defined by

$$\overline{m}_{ij} = \frac{\partial \overline{B}_j}{\partial x_i} + \frac{\partial \overline{B}_i}{\partial x_j}. \tag{A.20}$$

We substitute Eq. (A.10) into the fifth term linearly dependent on $\overline{\mathbf{B}}$. The contribution from $\langle \mathbf{B}' \cdot \boldsymbol{\omega}' \rangle$ vanishes identically owing to the symmetry condition. We assume that the physical importance of

$$\left\langle B_j' \left(\frac{\partial u_i'}{\partial x_t} + \frac{\partial u_t'}{\partial x_i} \right) \right\rangle \tag{A.21}$$

is small, compared with Eqs. (A.3), (A.5), (A.6), (A.12) and (A.13). We discard it, as is for expression (A.17). Then the fifth term in Eq. (A.18) does not contributes to R_{ij}.

We summarize the above findings and have Eq. (4.38).

2. Nonneutral variable-density flows

In electrically-conducting constant-density flows, the correlation functions represented by the Reynolds stress have been modelled with the aid of two methods. One is the heuristic method in § 4.1 [4/5, 4/8, A/1]. The other is the theoretical method based on the extension of isotropic to inhomogeneous turbulence theories [4/3, 4/7, A/2-A/4], These two methods supplement each other and contribute to the enlargement of the applicability of mathematical expressions or models for the Reynolds stress etc.

The equation for the turbulent flux $\mathbf{P}$ [Eq. (4.83)] linked with the turbulent heat flux $\mathbf{H}_{M\theta}$ [Eq. (4.85)] is complicated, compared with Eqs. (4.4) and (4.28) in the constant-density case. It is difficult to abstract a definite information about the mathematical structure of $\mathbf{P}$ with the aid of the heuristic method in § 4.1. Then we examine Eqs. (4.82)-(4.84) by using the turbulence theory based on the mass-weighted averaging [4/18, 4/19].

2.1. Introduction of mass-weighted fluctuations

The essence of the mass-weighted velocity is the use of the momentum as the definition of the mean velocity. This fact indicates that the use of the momentum-related velocity fluctuation is more proper than $\mathbf{u}''$ itself. Then we introduce the mass-weighted velocity fluctuation by

$$\mathbf{v}' = \frac{\rho \mathbf{u}''}{\overline{\rho}}. \tag{A.22}$$

It should be noted that this new velocity fluctuation obeys $\langle \mathbf{v}' \rangle = 0$, as for the constant density case. From Eq. (A.22), $\mathbf{u}''$ is expressed as

$$\mathbf{u}'' = \frac{1}{1+(\rho'/\overline{\rho})}\mathbf{v}' = \left(1 - \frac{\rho'}{\overline{\rho}} + \cdots\right)\mathbf{v}'. \tag{A.23}$$

On the other hand, the decomposition based on the ensemble averaging is applied to p and ρ_e. As a result, we adopt the following decomposition:

$$f = F + f', \tag{A.24}$$

where

$$f = (\rho, \mathbf{u}, p, \rho_e), \quad F = (\overline{\rho}, \hat{\mathbf{u}}, \overline{p}, \overline{\rho}_e), \quad f' = \left(\rho', \frac{\overline{\rho}}{\rho}\mathbf{v}', p', \rho_e'\right). \tag{A.25}$$

In the use of Eq. (A.23), Eq. (4.82) is written as

$$R_{Mij} = \langle v_i' v_j' \rangle - \frac{1}{\overline{\rho}}\langle \rho' v_i' v_j' \rangle + \cdots \cong \langle v_i' v_j' \rangle, \tag{A.26}$$

where the correlation of the second order based on $\mathbf{v}'$ was retained preferentially. The other correlation functions may be written as

$$\mathbf{P} = \langle p' \mathbf{v}' \rangle - \frac{\overline{p}}{\overline{\rho}}\langle \rho' \mathbf{v}' \rangle, \tag{A.27}$$

$$\overline{\mathbf{u}''} = -\frac{1}{\overline{\rho}}\langle \rho' \mathbf{v}' \rangle. \tag{A.28}$$

A system of equations for the fluctuations is given by

$$\frac{D\rho'}{Dt} + \overline{\rho}\frac{\partial v_i'}{\partial x_i} = -v_i'\frac{\partial \overline{\rho}}{\partial x_i} - \rho'\frac{\partial \hat{u}_i}{\partial x_i}. \tag{A.29}$$

$$\frac{Dv_i'}{Dt} + \frac{\partial}{\partial x_j}v_i' v_j' + \frac{1}{\overline{\rho}}\frac{\partial p'}{\partial x_i} = -v_j'\frac{\partial \hat{u}_i}{\partial x_j} + \rho_e'\frac{\overline{E}_i}{\overline{\rho}} - \frac{\rho'}{\overline{\rho}}\frac{D\hat{u}_i}{Dt} - v_i' v_j'\frac{1}{\overline{\rho}}\frac{\partial \overline{\rho}}{\partial x_j}, \tag{A.30}$$

$$\frac{Dp'}{Dt} + v_i'\frac{\partial p'}{\partial x_i} + \gamma p'\frac{\partial v_i'}{\partial x_i} + \gamma \overline{p}\frac{\partial v_i'}{\partial x_i} = -v_i'\frac{\partial \overline{p}}{\partial x_i} - \gamma p'\frac{\partial \hat{u}_i}{\partial x_i}, \tag{A.31}$$

$$\frac{D\rho_e'}{Dt}+\frac{\partial}{\partial x_i}\rho_e' v_i'+\rho_e'\frac{\partial v_i'}{\partial x_j}=-v_i'\frac{\partial\overline{\rho}_e}{\partial x_i}-\rho_e'\frac{\partial\hat{u}_i}{\partial x_i}. \tag{A.32}$$

One prominent feature of this system lies in the mathematical simplicity comparable to the constant-density case. It is entirely due to the use of the mass-weighted fluctuations, which paves the way for the straightforward application of a constant-density turbulence theory, for instance, the two-scale direct-interaction theory (TSDIA) [4/3, 4/7], to the variable-density case.

2.2. Two-scale direct-interaction approximation

The key mathematical procedures of the TSDIA may be summarized as follows. We first introduce a small-scale parameter δ for distinguishing the fast spatial and temporal variation of the fluctuation f' from the slow variation of the mean field F, as

$$\boldsymbol{\xi}\,(=\mathbf{x}),\ \tau\ (=t);\ \mathbf{X}\ (=\delta\mathbf{x}),\ T\ (=\delta t), \tag{A.33}$$

and write

$$F=F(\mathbf{X};T),\quad f'=f'(\boldsymbol{\xi},\mathbf{X};\tau,T). \tag{A.34}$$

We use Eqs. (A.33) and (A.34) and rewrite Eqs. (A.29)-(A.32). For instance, Eq. (A.29) is reduced to

$$\frac{D\rho'}{D\tau}+\overline{\rho}\frac{\partial v_i'}{\partial\xi_i}=\delta\left(-v_i'\frac{\partial\overline{\rho}}{\partial X_i}-\rho'\frac{\partial\hat{u}_i}{\partial X_i}-\frac{D\rho'}{DT}-\overline{\rho}\frac{\partial v_i'}{\partial X_i}\right), \tag{A.35}$$

where $D/D\tau=\partial/\partial\tau+\hat{u}_i\partial/\partial\xi_i$ and $D/DT=\partial/\partial T+\hat{u}_i\partial/\partial X_i$. We should note that effects of spatial and temporal inhomogeneity occur in the combination of the parameter δ, as is seen from the right-hand side.

For the fast spatial variation due to $\boldsymbol{\xi}$, we adopt the Fourier representation

$$f'(\boldsymbol{\xi},\mathbf{X};\tau,T)=\int f'(\mathbf{k},\mathbf{X};\tau,T)\exp\left(-i\mathbf{k}\cdot(\boldsymbol{\xi}-\hat{\mathbf{u}}\tau)\right)d\mathbf{k}. \tag{A.36}$$

We apply Eq. (A.36) to Eq. (A.35) etc. and perform the scale-parameter expansion

$$f'(\mathbf{k},\mathbf{X};\tau,T)=\sum_{n=0}^{\infty}\delta^n f_n'(\mathbf{k},\mathbf{X};\tau,T). \tag{A.37}$$

As a result, the lowest-order part f_0' obeys the equation of the same form as for homogeneous turbulence. There the inhomogeneity of field occurs implicitly through the dependence on the slow spatial variable $\mathbf{X}$.

The higher-order parts f_n' $(n \geq 1)$ are expressed in terms of f_0'. Then any correlation functions such as Eqs. (A.27), (A.28), etc. may be evaluated with the aid of the statistical properties concerning f_0'. As the specifically important properties, we adopt

$$\left\langle v_{0i}'(\mathbf{k},\mathbf{X},\tau,T)v_{0j}'(\mathbf{k}',\mathbf{X},\tau',T)\right\rangle = Q_{vij}(\mathbf{k},\mathbf{X},\tau,\tau',T)\delta(\mathbf{k}+\mathbf{k}'), \tag{A.38}$$

$$\left\langle \rho'(\mathbf{k},\mathbf{X},\tau,T)\rho'(\mathbf{k}',\mathbf{X},\tau',T)\right\rangle = Q_{\rho}(\mathbf{k},\mathbf{X},\tau,\tau',T)\delta(\mathbf{k}+\mathbf{k}'). \tag{A.39}$$

The equations for the lowest-order part f_0' explicitly contain no mean-field gradients that are the primary generators of statistical anisotropy, as is understood from Eq. (A.35). Then it is plausible to assume the isotropy of Eqs. (A.38) and (A.39) with the implicit inhomogeneity expressed through $\mathbf{X}$; namely, we write

$$Q_{vij}(k,\mathbf{X},\tau,\tau',T) = D_{ij}(\mathbf{k})Q_{vS}(k,\mathbf{X},\tau,\tau',T) + \Pi_{ij}(\mathbf{k})Q_{vC}(k,\mathbf{X},\tau,\tau',T), \tag{A.40}$$

$$Q_{\rho}(\mathbf{k},\mathbf{X},\tau,\tau',T) = Q_{\rho}(k,\mathbf{X},\tau,\tau',T), \tag{A.41}$$

where

$$D_{ij}(\mathbf{k}) = \delta_{ij} - \frac{k_i k_j}{k^2}, \quad \Pi_{ij}(\mathbf{k}) = \frac{k_i k_j}{k^2}, \tag{A.42}$$

and subscripts S and C denote solenoidal and compressible parts of the $\mathbf{v}_0'$ energy spectrum. From the isotropy of the lowest-order part, the transport of scalars does not occur; namely, we may write

$$\left\langle w'(\mathbf{k},\tau,)\mathbf{v}_0'(\mathbf{k}',\tau')\right\rangle = 0, \tag{A.43}$$

with $w' = (\rho_0', p_0', \rho_{e0}')$.

In the evaluations of correlation functions, we retain the contributions up to the first order in the scale parameter δ in general. The effects of the mean electric field $\overline{\mathbf{E}}$ on the turbulent heat flux, however, occur as the terms of the second order in δ. They are specifically retained in light of their importance in investigating into the transport effects in nonneutral plasmas. The scale parameter δ disappears automatically through the replacement $\mathbf{X} \to \delta\mathbf{x}$ and $T \to \delta t$.

From the foregoing procedures, the correlation functions such as Eqs. (4.83), (4.84), etc. may be expressed in terms of Eqs. (A.40) and (A.41) characterizing the lowest-order properties of inhomogeneous turbulence. We introduce the characteristic time scale τ_e and simplify the two-time representations, obtaining Eqs. (4.88)-(4.91).

Appendix B. Nondimensional form of Magnetohydrodynamic Equations

As a typical instance of MHD equations, we consider Eqs. (5.2)-(5.4) with a spherical shell kept in mind. We put

$$\hat{\mathbf{g}} = \frac{\mathbf{g}}{|\mathbf{g}|}, \quad \hat{\boldsymbol{\omega}}_F = \frac{\boldsymbol{\omega}_F}{|\boldsymbol{\omega}_F|}. \tag{B.1}$$

We take the reference length and the velocity

$$\ell_R = d, \quad u_R = \frac{\chi_\theta}{d}, \tag{B.2}$$

where d denotes the shell thickness.

We use Eq. (B.2), and make the nondimensionalization

$$\frac{\mathbf{x}}{d} \to \mathbf{x}, \quad \frac{t}{d^2/\chi_\theta} \to t, \quad \frac{\mathbf{u}}{\chi_\theta/d} \to \mathbf{u}, \quad \frac{\mathbf{B}}{\chi_\theta/d} \to \mathbf{B},$$

$$\frac{\mathbf{j}}{\chi_\theta/d^2} \to \mathbf{j}, \quad \frac{p}{(\chi_\theta/d)^2} \to p, \quad \frac{\theta-\theta_R}{\Delta\theta} \to \theta. \tag{B.3}$$

Then Eqs. (5.2)-(5.4) are converted to

$$\frac{\partial u_i}{\partial t} + \frac{\partial}{\partial x_j} u_j u_i = -\frac{\partial p}{\partial x_i} + P_r \nabla^2 u_i + (\mathbf{j}\times\mathbf{B})_i + P_r T_a^{1/2} (\mathbf{u}\times\hat{\boldsymbol{\omega}}_F)_i - P_r R_a \hat{g}_i, \tag{B.4}$$

$$\frac{\partial \theta}{\partial t} + \nabla\cdot(\theta\mathbf{u}) = \nabla^2\theta. \tag{B.5}$$

$$\frac{\partial \mathbf{B}}{\partial t} = \nabla\times(\mathbf{u}\times\mathbf{B}) + \frac{P_r}{P_M}\nabla^2\mathbf{B}. \tag{B.6}$$

From Eq. (B.4), we may see that the relative importance of the buoyancy to Coriolis effects is measured by $R_a/T_a^{1/2}$.

Appendix C. Magneto-Rotational Instability

Both the dynamo magnetic field and the anomalous viscosity arise from some kind of turbulence. At this moment, a plausible candidate that induces the turbulence in an accretion disk is the magneto-rotational instability [2/30, 2/35, 6/1, 6/2, 6/10]. A brief description is given here.

When disk plasmas are magnetized, the plasmas on the same magnetic field line rotate with the same angular frequency. When the radial displacement of plasmas takes place along the field line, plasmas at different radii on a magnetic field line move with the same angular frequency since the elements on the same field line are connected each other. Then the motion deviates from the Keplerian motion, resulting in the release of energy.

We denote the radius and the rotation frequency by σ and ϖ, respectively. When a small volume of plasmas is on an equilibrium orbit with σ_0 and ϖ_0, it is subject to the balance between the gravitational attraction and the centrifugal force. The former changes as σ^{-2} and the latter as $\varpi^2\sigma$. We consider the change of energy associated with the deviation of radial location, $\Delta\sigma$. If the angular momentum is conserved, as in the case without any interaction, the centrifugal force behaves $\varpi_0^{\,2}\sigma_0^{\,4}\sigma^{-3}$. The sum of the gravitational and centrifugal forces gives

$$F_\sigma = -\varpi_0^{\,2}\Delta\sigma, \tag{C.1}$$

which shows that the net force is against the displacement. In contrast, the centrifugal force behaves as $\varpi_0^{\,2}\sigma$ in the case of constant ϖ . Then the net force in the direction of the displacement is

$$F_\sigma = 3\varpi_0^{\,2}\Delta\sigma. \tag{C.2}$$

A part of this force is compensated to enhance the kinetic energy os rotation, but resultant force is in the direction to increase the displacement $\Delta\sigma$. This displacement is associated with the bending of the magnetic field line. The restoring force associated with the field-line bending is

$$F_{\sigma.A} \cong -V_A^{\,2}k_{//}^{\,2}\Delta\sigma, \tag{C.3}$$

where V_A is the Alfven velocity, and $k_{//}$ is the wavenumber in the direction of $\mathbf{B}$. From this consideration, we are led to an instability in the presence of the magnetic field obeying

$$0 < V_A^{\,2}k_{//}^{\,2} < \varpi_0^{\,2}. \tag{C.4}$$

Table C.1. Analogy of magneto-rotational instability (c_S: sound velocity, L_p and L_M: gradient scale lengths of pressure and magnetic field, respectively).

	Magneto-rotational instability	Interchange instability
Energy source	Motion in the direction of $-\nabla\Phi$	Motion in the direction of $-\nabla p$
Constraint	Constant ϖ	Magnetic flux conserved
Stabilization	Bending of magnetic field line	←
Instability condition	$0 < V_A < \varpi k_{//}^{-1}$	$V_A < c_S / \left(k_{//}\sqrt{L_p L_M}\right)$

Table C.1 shows an analogy between the magneto-rotational instability and the interchange instability in toroidal plasmas.

We express the temporal dependence of linear modes in the form $\exp(-i\lambda t)$. The quantitative investigation into the dispersion relation shows that the growth rate of the instability can be as large as

$$\gamma_{\mathrm{MRI}} = \mathrm{Im}\,\lambda \cong \varpi . \tag{C.5}$$

Appendix D. Countergradient Diffusion in Turbulent Combustion

The problem of burning could be important with the improvement of plasma confinement. There fuel mixing is a central issue. In this context, we refer to the turbulent transport in the interface of burning.

We consider the diffusion of chemical reactants in a turbulent premixed flame illustrated in Fig. D1. We adopt the coordinate system with a flame region fixed. There fresh (unburned) gases come into the region, and burned gases go out from it. The instantaneous surface of the flame is very thin, but it highly fluctuates in time and space. In the statistical sense based on the ensemble averaging, the flame region characterized by $0 < \hat{Y} < 1$ becomes much thicker than the width of the instantaneous flame, where Y denotes the concentration of chemical reactants.

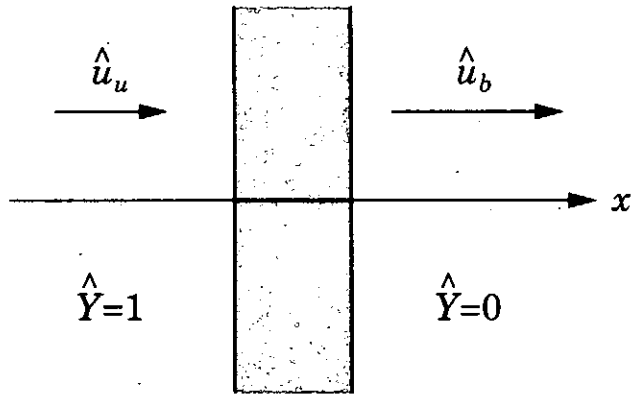

Fig. D.1. Flame region in a turbulent premixed flame.

In a turbulent premixed flame, we often encounter the situation that the reactants are transported from the low-concentration to high-concentration regions [7/11, D/1]. The elucidation of this countergradient-diffusion mechanism has long been one of the central themes in the study of turbulent combustion. The comprehensive reviews are given in [D/2, D/3].

The countergradient diffusion may be explained as follows. The turbulent flux of reactants is expressed by the familiar gradient-diffusion term and some other ingredient(s) opposing it. Then the countergradient diffusion arises from the dominance of the latter over the former.

We make full use of the statistical method detailed in § 4.3 and Appendix A.2, and investigate into a mechanism of the countergradient diffusion. In Fig. D.1, the mean field $(\overline{\rho}, \hat{\mathbf{u}}, \overline{p}, \hat{Y})$ may be expressed as

$$\hat{\mathbf{u}} = (\hat{u}(x),0,0),\ \ \overline{\rho} = \overline{\rho}(x),\ \ \overline{p} = \overline{p}(x)\,,\ \hat{Y} = \hat{Y}(x). \tag{D.1}$$

The flame zone where the countergradient diffusion may occur is characterized by

$$\frac{d\hat{u}}{dx} > 0,\ \ \frac{d\overline{p}}{dx} < 0,\ \ \frac{d\overline{\rho}}{dx} < 0,\ \ \frac{d\,\hat{Y}}{dx} < 0, \tag{D.2}$$

resulting in

$$\frac{D\hat{u}}{Dt} = \hat{u}\frac{d\hat{u}}{dx} > 0,\ \ \frac{D\hat{Y}}{Dt} = \hat{u}\frac{d\hat{Y}}{dx} < 0. \tag{D.3}$$

Under Eq. (D.1), the turbulent reactant flux may be expressed as [7/12]

$$\Gamma_{Yx} \equiv \{Y''u''\}_M = -C_{\Gamma 1}K_M\tau_{CO}\frac{d\hat{Y}}{dx} + C_{\Gamma 2}\tau_{CO}{}^2\frac{K_\rho}{\overline{\rho}^2}\frac{D\hat{u}}{Dt}\frac{D\hat{Y}}{Dt}, \tag{D.4}$$

where u'' is the velocity fluctuation in the x direction, $C_{\Gamma 1}$ and $C_{\Gamma 2}$ are positive numerical coefficients, and τ_{CO} is the time scale characterizing the transport in turbulent combustion.

In the gradient-diffusion model given by the first term in Eq. (D.4), Γ_{Yx} is always positive. From the computer experiments of countergradient diffusion [D/4, D/5], however, Γ_{Yx} becomes negative under a favorable pressure gradient ($d\overline{p}/dx < 0$), and the usual gradient-diffusion model breaks down completely. The second term is the combination of the Lagrange acceleration and the streamwise $\hat{Y}$ variation. From the situation (D.3), this term is negative and contributes to the turbulent transport of Y'' in the negative x direction, which paves the way for the countergradient transport. The magnitude of $D\hat{u}/Dt$ is an indicator of the strength of thermal-expansion effects due to the heat released by the chemical reaction.

The conclusion here is that the acceleration in the direction of a mean-scalar gradient may affect the turbulent flux in such a direction. This mechanism is quite similar to the suppression mechanism of the turbulent heat-flux due to the poloidal plasma rotation that is discussed in § 7.2.2.2.

References

[2/1] Moffatt H K 1978 *Magnetic Field Generation in Electrically Conducting Fluids* (Cambridge: Cambridge University Press)

[2/2] Parker E N 1979 *Cosmical Magnetic Fields* (Oxford: Clarendon)

[2/3] Krause F and Rädler K-H 1980 *Mean-Field Magnetohydrodynamics and Dynamo Theory* (Oxford: Pergamon)

[2/4] Parker E N 1979 *Cosmical Magnetic Fields* (Oxford: Clarendon)

[2/5] Ruzmaikin A A, Shukurov A M and Sokoloff D D 1988 *Magnetic Fields of Galaxies* (Dordrecht: Kluwer)

[2/6] Roberts P H 1993 *Astrophysical Fluid Dynamics* ed J-P Zahn and J Zinn-Justin (Amsterdam: Elsevier) p 229

[2/7] Widrow L M 2002 *Rev. Mod. Phys.* **74** 776

[2/8] Yoshizawa A, Itoh S-I and Itoh K 2003 *Plasma and Fluid Turbulence: Theory and Modelling* (Bristol: Institute of Physics)

[2/9] Diamond P H, Hughes D W and Kim E-J 2003 "Self-consistent mean field electrodynamics in two and three dimensions," in *The Fluid Mechanics of Astrophysics and Geophysics* ed A M Soward and M Ghil Vol 12 (London: Taylor and Francis)

[2/10] Bogenal F 1992 *Annu. Rev. Earth Planet. Sci.* **20** 289

[2/11] Cravens T H 1997 *Physics of Solar System Plasmas* (Cambridge: Cambridge University Press)

[2/12] Miner E D 1990 *Physics Today* **43** 40

[2/13] Melchior P 1986 *The Physics of the Earth's Core* (Oxford: Pergamon)

[2/14] Merrill R T, McElhinny M W and McFadden P L 1996 *The Magnetic Field of the Earth* (London: Academic)

[2/15] Priest E R 1982 *Solar Magnetohydrodynamics* (Dordrecht: Reidel)

[2/16] Wilson P R 1994 *Solar and Stellar Activity Cycles* (Cambridge: Cambridge University Press)

[2/17] Schrijver C J and Zwaan C 2000 *Solar and Stellar Magnetic Activity* (Cambridge: Cambridge University Press)

[2/18] Lang K R 2001 *The Cambridge Encyclopedia of the Sun* (Cambridge: Cambridge University Press)

[2/19] Stix M 2002 *The Sun* (Berlin: Springer)

[2/20] Bodin H A B and Newton A A 1980 *Nuclear Fusion* **20** 1255

[2/21] Taylor J B 1986 *Rev. Mod. Phys.* **58** 741

[2/22] Miyamoto K 1976 *Plasma Physics for Nuclear Fusion* (Cambridge: The MIT Press)

[2/23] Wesson J 1997 *Tokamaks* (Oxford: Clarendon)

[2/24] Bickerton R D, Connor J W and Taylor J B 1971 *Nature Physical Science* **229** 110.

[2/25] Kikuchi H and Azumi M 1995 *Plasma Phys. Contr. Fusion* **37** 1215.

[2/26] Roberts P H 1972 *Phil. Trans. Roy. Soc.* **A 271** 411

[2/27] Yoshimura H 1975 *Astrophys. J.* **201** 740

[2/28] Begelman M C, Blandford R D and Rees M J 1984 *Rev. Mod. Phys.* **56** 256

[2/29] Balbus S A and Hawley J F 1998 *Rev. Mod. Phys.* **70** 1

[2/30] Kato S, Fukue J and Mineshige S 1998 *Black-Hole Accretion Disks* (Kyoto: Kyoto University Press)

[2/31] Colgate S A, Li H and Pariev V 2001 *Phys. Plasmas* **8** 2425

[2/32] Taylor G B and Perley R A 1993 *Astrophys. J.* **416** 554

[2/33] Ferrari A 1998 *Annu. Rev. Astron. Astrophys.* **36** 539.

[2/34] Shakura N J and Sunyaev R A 1973 *Astron. Astrophys.* **24** 337

[2/35] Vishniac E 2003 "Dynamos and Accretion in Accretion Disks - A tutorial for the plasma physicists" presented at Festival Theorie (Aix-le-Provence, July 2003)

[2/36] Wagner F *et al* 1982 *Phys. Rev. Lett.* **49** 1408

[2/37] Itoh K and Itoh S-I 1996 *Plasma Phys. Control. Fusion* **38** 1

[2/38] Burrell K H 1997 *Phys. Plasmas* 4 1499

[2/39] Ida K 1998 *Plasma Phys. Control. Fusion* **40** 1429

[2/40] Itoh K, Itoh S-I and Fukuyama A 1999 *Transport and Structural Formation in Plasmas* (Bristol: Institute of Physics Publishing)

[2/41] Itoh S-I *et al.* 1995 *J. Nucl. Materials* **220-222** 117.

[2/42] Synakovski E J 1998 *Plasma Phys. Control. Fusion* **40** 581

[2/43] Kamada Y 2000 *Plasma Phys. Control. Fusion* **42** A65

[2/44] Fujita T 1997 *J. Plasma Fusion Res.* **73** 549

[2/45] Carreras B A 1997 *IEEE Trans* **25** 1281

[2/46] Connor J W and Wilson H R 2000 *Plasma Phys. Control. Fusion* **42** R1

[2/47] Terry P W 2000 *Rev. Mod. Phys.* **72** 109

[2/48] Wolf R C 2003 *Plasma Phys. Control. Fusion* **45** R1

[2/49] Diamond P H, Itoh K, and Itoh S-I, and Halm T S in preparation for the topical review of *Plasma Phys. Control. Fusion*

[2/50] Landau L D and Lifshitz E M 1960 *Electrodynamics of Continuous Media* (Oxford: Pergamon Press) § 25

[3/1] Freidberg J P 1987 *Ideal Magnetohydrodynamics* (New York: Plenum)

[4/1] Tennekes H and Lumley J L 1972 *A First Course in Turbulence* (Cambridge: The MIT Press)

[4/2] Townsend A A 1976 *The Structure of Turbulent Shear Flow* (Cambridge: Cambridge University Press)

[4/3] Yoshizawa A 1998 *Hydrodynamic and Magnetohydrodynamic Turbulent Flows* (Dordrecht: Kluwer)

[4/4] Pope S B 2000 *Turbulent Flows* (Cambridge: Cambridge University Press)

[4/5] Launder B and Sandham N 2002 *Closure Strategies for Turbulent and Transient Flows* (Cambridge: Cambridge University Press)

[4/6] Melling A and Whitelaw J H 1976 *J. Fluid Mech.* **78** 289

[4/7] Yoshizawa A 1984 *Phys. Fluids* **27** 1377

[4/8] Speziale C G 1987 *J. Fluid Mech.* **178** 450

[4/9] Nisizima S 1990 *Theoret. Comput. Fluid Dynamics* **2** 61

[4/10] Yoshizawa A 1988 *J. Fluid Mech.* **195** 541

[4/11] Tavouralis S and Corrsin S 1985 *J. Heat Mass Transfer* **28** 265

[4/12] Yoshizawa A 1990 *Phys. Fluids* **B 2** 1589

[4/13] Hamba F 1992 *Phys. Fluids* A **4** 441

[4/14] Parker E 1955 *Astrophys. J.* **122** 293

[4/15] Pouquet A, Frisch Y and Léorat J 1976 *J. Fluid Mech.* **77** 321

[4/16] Blackman E G 2000 *Astrophys. J.* **529** 138

[4/17] Chassaing P et al 2002 *Variable Density Fluid Turbulence* (Dordrecht: Kluwer)

[4/18] Yoshizawa A 2003 *Phys. Fluids* **15** 585

[4/19] Yoshizawa A and Yokoi N 2003 *Phys. Plasmas* **10** 1371

[5/1] Gilman P A 1977 *Geophys. Astrophys. Fluid Dynamics* **8** 93

[5/2] Gilman P A 1983 *Astrophys. J. Suppl.* **53** 243

[5/3] Glatzmaier G A 1985 *Astrophys. J.* **291** 300

[5/4] Glatzmaier GA and Roberts P H 1995 *Nature* **377** 203

[5/5] Glatzmaier GA and Roberts P H 1995 *Phys. Earth Planet. Inter.* **31** 137

[5/6] Roberts P H 2000 *Rev. Mod. Phys.*. **72** 1081

[5/7] Pedlosky J 1979 *Geophysical Fluid Dynamics* (New York: Springer-Verlag)

[5/8] Landau L D and Lifshitz E M 1960 *Electrodynamics of Continuous Media* (Oxford: Pergamon Press) § 55

[5/9] Gilman P A 2000 *Geophysical and Astrophysical Convection* ed P A Fox and R M Kerr (Australia: Gordon and Breach) p 37

[5/10] Busse F H 1970 *J. Fluid Mech.* **44** 441

[5/11] Christensen U R *J. Fluid Mech.* **470** 115

[5/12] Zhang K-K and Schubert G 2000 *Annu. Rev. Fluid Mech.* **32** 409

[5/13] Kasagi N and Shikazono N 1995 *Proc. Roy. Soc. Lond.* **A 451** 257

[5/14] Moin P and Mahesh K 1997 *Annu. Rev. Fluid Mech.* **30** 539

[5/15] Kageyama A and Sato T 1995 *Phys. Plasmas* **2** 1421

[5/16] Katayama J S, Matsushima M and Honkura Y 1999 *Phys. Earth Planet. Inter.* **111** 141

[5/17] Olson P, Christensen U R and Glatzmaier G A 1999 *J. Geophys. Res.* **104** 10383

[5/18] Ishihara N and Kida S 2002 *J. Fluid Mech.* **465** 1

[5/19] Ochi M M, Kageyama A and Sato T 1999 *Phys. Plasmas* **6** 777

[5/20] Glatzmaier G A et al 1999 *Nature* **401** 885

[5/21] Schou J *et al* 1998 *Astrophys. J.* **505** 390

[5/22] Gruzinov A V and Diamond P H 1994 *Phys. Rev. Lett.* **72** 1651

[5/23] Vishniac E T and Brandenburg A 1997 *Astrophys. J.* **475** 263

[5/24] Field G B, Blackman E G and Chou H 1999 *Astrophys. J.* **513** 638

[5/25] Blackman E G and Brandenburg A 2002 *Astrophys. J.* **579** 359

[5/26] Brandenburg A, Dobler W and Subramanian K 2002 *Astron. Nachr.* **323** 99

[5/27] Mininni P D, Gómez D O and Mahajan S M 2003 *Astrophys. J.* **587** 472

[5/28] Urpin V 2002 *Phys. Rev.* **E 65** 026301

[5/29] Gimblett C G and Watkins M L 1975 *Proceedings of the Seventh European Conference on Controlled Fusion and Plasma Physics* (Ecole de Polytechnique Fédéral de Lausanne, Lausanne) Vol I p 103

[5/30] Yoshizawa A, Yokoi N and Kato H 1999 *Phys. Plasmas* **6** 4586

[5/31] Yoshizawa A, Kato H and Yokoi N 2000 *Astrophys. J.* **537** 1039

[6/1] Velikov E P 1959 *Soviet Phys. JETP* **36** 995

[6/2] Chandrasekhar S 1961 *Hydrodynamic and Hydromagnetic Stability* (Oxford: Clarendon Press)

[6/3] Uchida Y and Shibata K 1985 *Publ. Astron. Soc. Jpn.* **37** 515

[6/4] Shibata K and Uchida Y 1986 *Publ. Astron. Soc. Jpn.* **38** 631

[6/5] Shibata K and Uchida Y 1986 *Publ. Astron. Soc. Jpn.* **42** 39

[6/6] Stone J M and Norman M L 1994 *Astrophys. J.* **433** 746

[6/7] Matumoto *et al* 1996 *Astrophys. J.* **461** 115

[6/8] Kudoh T, Matsumoto R and Shibata K 1998 *Astrophys. J.* **508** 186

[6/9] Turner N J, Bodenheimer P and Rózyczka M 1999 *Astrophys. J.* **524** 129

[6/10] Balbus S A and Hawley J F 1998 *Rev. Mod. Phys.* **70** 1

[6/11] Kuwabara T, Shibata K, Kudoh T and Matsumoto R 2000 *Publ. Astron. Soc. Jpn.* **52** 1109

[6/12] Yoshizawa and Yokoi N 1993 *Astrophys. J.* **407** 540

[6/13] Nishino S and Yokoi N 1998 *Publ. Astron. Soc. Jpn.* **50** 653

[6/14] Li L-X 2002 *Astrophys. J.* **564** 1108

[6/15] Asada A *et al* 2002 *Publ. Astron. Soc. Jpn.* **54** L39

[6/16] Yoshizawa A, Yokoi N and Kato H 2000 *Phys. Plasmas* **7** 2646

[6/17] Shibata K *et al* (ed) 1999 Active Universe (Tokyo: Shokabo) (in Japanese)

[6/18] Description in this subsection depends on the discussion at Festival Theorie (Aix-en-Provence, July 2003) Courtesy to Prof. Diamond and Prof. Vishniak

[6/19] Itoh S-I and Itoh K 1988 *Phys. Rev. Lett.* **60** 2276

[6/20] Shaing K C and Crume E C Jr 1988 *Phys. Rev. Lett.* **63** 2369

[6/21] Itoh K, S-I Itoh, Yagi M and Fukuyama A 1998 *Phys. Plasmas* **5** 4121

[6/22] Hinton F L *et al* 1994 *Phys. Rev. Lett.* **72** 1216

[6/23] Diamond P H and Kim Y-B 1991 *Phys. Fluids* **B 3** 1626

[6/24] Diamond P H, Liang Y-M, Carreras B A and Terry P W 1994 *Phys. Rev. Lett.* **72** 2565

[6/25] Kim E-J and Diamond P H 2003 *Phys. Plasmas* **10** 1698

[6/26] Champeaux S and Diamond P H 2001 *Phys. Lett.* A **288** 214

[6/27] Yoshizawa A, Yokoi N, Itoh S-I and Itoh K 1998 *Phys. Plasmas* **6** 3194

[6/28] Fujita T *et al* 2001 *Phys. Rev. Lett.* **87** 245001

[7/1] Gurzinov A V and Diamond P H 1996 *Phys. Plasmas* **3** 1853

[7/2] Zeldovich Ya B 1957 *Sov. Phys. JETP* **4** 460

[7/3] Staebler G M 1998 *Plasma Phys. Control. Fusion* **40** 569

[7/4] Biglari H, Diamond P H and Terry P W 1989 *Phys. Fluids* **B 2** 1

[7/5] Itoh S-I, Itoh K, Fukuyama A and Yagi M 1994 *Phys. Rev. Lett.* **72** 1200

[7/6] Ware A S, Terry T W, Carreras B A and Diamond P H 1998 *Phys. Plasmas* **5** 173

[7/7] Yoshizawa A 2003 *Phys. Plasmas* **10** 329

[7/8] Yoshizawa A and Yokoi N 2003 *Phys. Plasmas* **10** 1371

[7/9] Inutake M 2001 J. Plasma Fusion Res. Series **4** 75

[7/10] Yoshinuma M *et al* 1999 *Physics Letters* A **255** 301

[7/11] Peters N 2000 *Turbulent Combustion* (Cambridge: Cambridge University Press)

[7/12] Yoshizawa A 2003 *Phys. Fluids* **15** 538

[7/13] Biskamp D *Nonlinear Magnetohydrodynamics* (Cambridge: Cambridge University Press) Chap. 2

[7/14] Yoshizawa A *et al* 2001 *Phys. Fluids* **13** 2309.

[7/15] Burlage L F and Turner J M1976 *J. Geophys. Res.* **81** 73

[7/16] Mahajan S M and Yoshida Z 1998 *Phys. Ref. Lett.* **81** 4863

[7/17] Yoshida Z and Mahajan S M 2002 *Phys. Rev. Lett.* **88** 095001

[A/1] Speziale C G 1991 *Annu. Rev. Fluid Mech.* **23** 107

[A/2] Hamba F 1987 *J. Phys. Soc. Jpn.* **56** 79

[A/3] Rubinstein R and Barton M 1990 *Phys. Fluids* **A 2** 1472

[A/4] Okamoto M 1994 *J. Phys. Soc. Jpn.* **63** 2102

[D/1] Libby P A and Bray K N C 1981 *AIAA J.* 19, 205

[D/2] Libby P A and Williams F A 1994 *Turbulent Reacting Flows* ed. P A Libby and F A Williams (London: Academic) p 1

[D/3] Bray K N C 1995 *Proc. Roy. Soc. Lond.* **A 451** 231

[D/4] Veynante D, Trouvé A, Bray K N C and Mantel T 1997 *J. Fluid Mech.* **332** 26

[D/5] Nishiki K, Hasegawa T, Borghi R and Himeno R 2002 *J. Combust. Soc. Jpn.* **44** 47

Recent Issues of NIFS Series

NIFS-764 NIFS Contributions to 19th IAEA Fusion Energy Conference (Lyon, France, 14-19 October 2002)
Nov. 2002

NIFS-765 S. Goto and S. Kida
Enhanced Stretching of Material Lines by Antiparallel Vortex Pairs in Turbulence
Dec. 2002

NIFS-766 M. Okamoto, A.A. Maluckov, S. Satake, N. Nakajima and H. Sugama
Transport and Radial Electric Field in Torus Plasmas
Dec. 2002

NIFS-767 R. Kanno, N. Nakajima, M. Okamoto and T. Hayashi
Computational Study of Three Dimensional MHD Equilibrium with m/n=1/1 Island
Dec. 2002

NIFS-768 M. Yagi, S.-I. Itoh, M. Kawasaki, K. Itoh and A. Fukuyama
Multiple-Scale Turbulence and Bifurcaion
Jan. 2003

NIFS-769 S.-I. Itoh, K. Itoh and S. Toda
Statistical Theory of L-H Transition and its Implication to Threshold Database
Jan. 2003

NIFS-770 K. Itoh
Summary: Theory of Magnetic Confinement
Jan. 2003

NIFS-771 S.-I. Itoh, K. Itoh and S. Toda
Statistical Theory of L-H Transition in Tokamaks
Jan. 2003

NIFS-772 M. Stepic, L. Hadzievski and M.M. Skoric
Modulation Instability in Two-dimensional Nonlinear Schrodinger Lattice Models with Dispersion and Long-range Interactions
Jan. 2003

NIFS-773 M.Yu. Isaev, K.Y. Watanabe, M. Yokoyama and K. Yamazaki
The Effect of Hexapole and Vertical Fields on α-particle Confinement in Heliotron Configurations
Mar. 2003

NIFS-774 K. Itoh, S.-I. Itoh, F. Spineanu, M.O. Vlad and M. Kawasaki
On Transition in Plasma Turbulence with Multiple Scale Lengths
May 2003

NIFS-775 M. Vlad, F. Spineanu, K. Itoh, S.-I. Itoh
Intermittent and Global Transitions in Plasma Turbulence
July 2003

NIFS-776 Y. Kondoh, M. Kondo, K. Shimoda, T. Takahashi and K. Osuga
Innovative Direct Energy Conversion Systems from Fusion Output Thermal Power to the Electrical One with the Use of Electronic Adiabatic Processes of Electron Fluid in Solid Conductors.
July 2003

NIFS-777 S.-I. Itoh, K. Itoh and M. Yagi
A Novel Turbulence Trigger for Neoclassical Tearing Modes in Tokamaks
July 2003

NIFS-778 T. Utsumi, J. Koga, T. Yabe, Y. Ogata, E. Matsunaga, T. Aoki and M. Sekine
Basis Set Approach in the Constrained Interpolation Profile Method
July 2003

NIFS-779 Oleg I. Tolstikhin and C. Namba
CTBC A Program to Solve the Collinear Three-Body Coulomb Problem: Bound States and Scattering Below the Three-Body Disintegration Threshold
Aug. 2003

NIFS-780 Contributions to 30th European Physical Society Conference on Controlled Fusion and Plasma Physics (St.Petersburg, Russia, 7-11 July 2003) from NIFS
Aug. 2003

NIFS-781 Ya. I. Kolesnichenko, K. Yamazaki, S. Yamamoto, V.V. Lutsenko, N. Nakajima, Y. Narushima, K. Toi, Yu. V. Yakovenko
Interplay of Energetic Ions and Alfvén Modes in Helical Plasmas
Aug. 2003

NIFS-782 S.-I. Itoh, K. Itoh and M. Yagi
Turbulence Trigger for Neoclassical Tearing Modes in Tokamaks
Sep. 2003

NIFS-783 F. Spineanu, M. Vlad, K. Itoh, H. Sanuki and S.-I. Itoh
Pole Dynamics for the Flierl-Petviashvili Equation and Zonal Flow
Sep. 2003

NIFS-784 R. Smirnov, Y. Tomita, T. Takizuka, A. Takayama, Yu. Chutov
Particle Simulation Study of Dust Particle Dynamics in Sheaths
Oct. 2003

NIFS-785 T.-H. Watanabe and H. Sugama
Kinetic Simulation of Steady States of Ion Temperature Gradient Driven Turbulence with Weak Collisionality
Nov. 2003

NIFS-786 K. Itoh, K. Hallatschek, S. Toda, H. Sanuki and S.-I. Itoh
Coherent Structure of Zonal Flow and Nonlinear Saturation
Dec. 2003

NIFS-787 S.I. Itoh, K. Itoh, M. Yagi and S. Toda
Statistical Theory for Transition and Long-time Sustainment of Improved Confinement State
Dec. 2003

NIFS-788 A. Yoshizawa, S.-I. Itoh, K. Itoh and N. Yokoi
Dynamos and MHD Theory of Turbulence Suppression
Dec. 2003